EAU TERRE ENVIRONNEMENT

MONITORING OF POROUS ASPHALT AND ITS UNDERGROUND RESERVOIR AS A STORMWATER MANAGEMENT STRUCTURE FOR A PARKING LOT

Par

Arthur Ebenezer Oko

Mémoire présenté pour l'obtention du grade de

Maître ès Sciences (M.Sc.)

En sciences de l'eau

Jury d'évaluation

Président du jury et examinateur interne	Alain N. Rousseau INRS-ETE
Examinateur externe	Jean-Pascal Bilodeau Université Laval
Directrice de recherche	Sophie Duchesne INRS-ETE
Codirectrice de recherche	Geneviève Pelletier Université Laval

ACKNOWLEDGEMENTS

I am deeply grateful to everyone whose support made this research possible. First, I would like to thank the officials at the Ministère des Transports et de la Mobilité durable du Québec (MTMD) and the City of Québec, whose collaboration with INRS was instrumental to the success of this project.

I extend my sincere appreciation to Professor Sophie Duchesne, my supervisor, for her unwavering patience, guidance, and encouragement throughout my work. I am also thankful to Professor Geneviève Pelletier, my co-supervisor and the examiners, Professor Alain N. Rousseau and Professor Jean-Pascal Bilodeau, for sharing their valuable insights and providing direction for this project.

Finally, I would like to express my heartfelt gratitude to my wife, Nancy Freeman-Arthur, for her steadfast support, prayers, and love. I also extend my sincere thanks to my research team colleagues for making my graduate studies an immensely enriching experience.

SUMMARY

This study assessed porous asphalt (PA) as a sustainable alternative to conventional impervious asphalt (CA) in stormwater management. The studied PA site was constructed in 2020 at the bibliothèque Le Tournesol parking lot located in the Lac Saint-Charles area, in Quebec City. The monitoring process began immediately after construction and continued for two years until 2022. Following this period, a second monitoring phase, which is the subject of this thesis, was conducted to evaluate 4-year hydrological and water quality performances of the PA. Over a 12-month monitoring period across 2023 and 2024, key parameters including surface infiltration rates, runoff volumes, flow rates, and water quality, were assessed, for both the CA and PA surfaces.

It was found that the average infiltration rate (IR) declined substantially, from 6000 mm/hr in 2021 to 68 mm/hr in 2024, resulting in water accumulation and surface ponding during all storm events. In 2024, restorative maintenance of the PA was conducted using three cleaning trucks (CityFant 6000, Elgin Whirlwind, and Ravo 5) which were used on different areas of the PA. The CityFant 6000 increased IR by 137 %, 753 %, and 14 % across three tested locations. The Elgin Whirlwind truck resulted in an 85 % increase in IR following cleaning, while the Ravo 5 led to a 153 % increase. However, despite these improvements, the maintenance practice failed to restore the IR to levels sufficient for effective stormwater management, largely due to the high degree of clogging present before maintenance.

During the study period, flow rates and volumes were estimated for 23 rainfall events for the CA and PA portions of the study site. In 9 of these events, the water height in the PA's outfall pipe exceeded the weir's maximum measurable height. Similarly, for the weir collecting CA outflows, the water height surpassed the maximum during 11 events. As a result, for 11 of the 23 events, it was not possible to determine the volume or flow rate reduction provided by PA. For the other 12 studied rainfall events, volume reductions ranged from 9 % to 99 % and peak flow reductions ranged from 2 % to 78 % depending on the rainfall event. Results suggest that, compared to the 2020-2022 period, the PA pavement has become less effective in managing stormwater.

Water quality monitoring from PA and CA provided insights into contaminants removal effectiveness. During three rainfall events, water samples revealed that the PA system still improved stormwater quality moderately despite reduced infiltration rates, as water continued to filter through the underlying aggregate layers, though less effectively than expected. TSS reduction varied, with two samples showing negative removal rates (-72 %, -40 %) and one

sample achieving an 86 % reduction. Electrical conductivity in the three PA-outlet water samples were elevated by 324 %, 552 %, and 392 % compared to the CA outlet samples, highlighting leaching of de-icing salts from the porous aggregate layers. Despite partial clogging, the PA reduced runoff temperature effectively, keeping water cooler than that from CA, with potential for further improvement if infiltration can be restored. Overall, these findings highlight the need for more frequent and efficient maintenance strategies to restore infiltration rates, ensuring the long-term benefit for stormwater management.

Keywords: Low impact development; porous asphalt; stormwater management; hydrological perfomance; water quality perfomane

RÉSUMÉ

Un suivi expérimental d'un asphalte poreux (AP) comme alternative à l'asphalte conventionnel imperméable (AC) pour la gestion des eaux pluviales a été réalisé. Le site d'AP étudié a été construit en 2020 dans le stationnement de la bibliothèque Le Tournesol, situé dans le secteur du lac Saint-Charles, à Québec. Le suivi expérimental a commencé immédiatement après la construction et s'est poursuivi pendant deux ans jusqu'en 2022. Après cette période, une deuxième phase de suivi, qui est l'objet de ce mémoire, a été menée afin d'évaluer les performances hydrologique et environnementale à long terme de l'AP. Pendant la période de suivi de douze mois, qui a eu lieu en 2023 et 2024, des paramètres clés incluant les taux d'infiltration de l'asphalte, le volume de ruissellement, les débits et la qualité de l'eau ont été évalués pour les zones du site d'étude en AP et AC.

Il a été constaté que le taux d'infiltration moyen a considérablement diminué, passant de 6 000 mm/hr en 2021 à 68 mm/hr en 2024, ce qui a entraîné une accumulation d'eau en surface lors de tous les événements pluvieux. En 2024, un entretien curatif de l'AP a été réalisé à l'aide de trois camions aspirateurs (CityFant 6000, Elgin Whirlwind et Ravo 5), qui ont été utilisés sur différentes parties de l'AP. Le CityFant 6000 a permis d'augmenter le taux d'infiltration de 137 %, 753 % et 14 % sur les sites testés. Le camion Elgin Whirlwind a entraîné une augmentation de 85 % du taux d'infiltration après nettoyage, tandis que le Ravo 5 a entraîné une augmentation de 153 %. Cependant, malgré ces améliorations, les pratiques d'entretien n'ont pas permis de rétablir le taux d'infiltration à des niveaux suffisants pour une gestion efficace des eaux pluviales, en grande partie en raison du fort degré de colmatage présent avant l'entretien.

Au cours de la période d'étude, le débit et le volume ont été estimés pour 23 événements pluvieux. Lors de 9 de ces événements, la hauteur d'eau dans la conduite drainant les eaux de l'AP a dépassé la hauteur maximale mesurable du déversoir. De même, pour le déversoir collectant les débits sortants de la zone en AC, la hauteur d'eau a dépassé cette limite lors de 11 événements. Par conséquent, pour 11 des 23 événements, il n'a pas été possible de déterminer le volume ou le débit. L'analyse des 12 événements autres événements pluvieux) a révélé une réduction du volume de ruissellement de 9 % à 99 %, et une réduction du débit de pointe de 2 % à 78 %, en fonction de l'événement. Les résultats suggèrent que, par rapport à la période 2020-2022, la chaussée en AP est devenue moins efficace pour gérer les eaux pluviales.

Le suivi de la qualité de l’eau des zones en AP et en AC a permis de mieux comprendre l’efficacité du système en matière d’élimination des polluants. Lors de trois épisodes pluvieux, des échantillons d'eau ont révélé que l‘AP améliorait modérément la qualité des eaux pluviales malgré une diminution des taux d'infiltration. L’eau continuait de s’infiltrer à travers les couches d'agrégats sous-jacentes, mais avec une efficacité moindre que prévu. L’enlèvement des matières en suspension était varié, deux échantillons présentant des taux de réduction négatifs (-72 %, -40 %), alors qu’un échantillon a présenté une réduction de 86 %. La conductivité électrique dans les trois échantillons d'eau de sortie de l'AP était élevée de 324 %, 552 % et 392 % par rapport aux échantillons de sortie de l'AC, mettant en évidence le lessivage du sel de déglaçage des couches d’agrégats. Malgré un colmatage partiel, l’AP a réduit efficacement la température des eaux de ruissellement, gardant l’eau plus fraîche que celle provenant de la zone imperméable, avec un potentiel d’amélioration supplémentaire si l’infiltration était rétablie. Dans l’ensemble, ces résultats soulignent la nécessité de mettre en place des stratégies d’entretien plus fréquentes et plus efficaces afin de rétablir les taux d’infiltration et de garantir les avantages à long terme de la gestion des eaux de ruissellement.

Mots-clés : Développement à faible impact ; asphalte poreux ; gestion des eaux pluviales ; performance hydrologique ; performance environnementale

TABLE OF CONTENTS

LIST OF FIGURES

LIST OF TABLES

LIST OF ABBREIATIONS

CA: Conventional asphalt

COD: Chemical oxygen demand

EC: Electrical conductivity

INRS : Institut National de la Recherche Scientifique

IR: Infiltration rate

LID: Low impact development

MTMD : Ministère des Transports et de la Mobilité durable du Québec

PA: Porous asphalt

PP: Permeable pavement

SWMM : Storm Water Management Model

TSS: Total suspended solids

TN: Total nitrogen

TP: Total phosphorous

1 INTRODUCTION

In natural, undeveloped landscapes, stormwater runoff is regulated by inherent processes such as surface detention, soil infiltration, and the formation of drainage networks along natural flow paths (Minnesota Stormwater, 2023). However, urban development, characterized by the construction of roads, parking lots, and other impervious surfaces, significantly disrupts these processes. The removal of vegetation, tree clearing, and surface leveling reduce the land's natural infiltration capacity (Støvring et al., 2018), leading to increased runoff volumes and faster flow rates. This alteration in hydrological behavior can contribute to downstream flooding, accelerate channel erosion, reduce groundwater recharge (Xie et al., 2017) and lead to the need for larger, more robust stormwater drainage systems, particularly under the influence of climate variability (Houle et al., 2013). The challenges posed by urbanization extend beyond just increased runoff quantity. Runoff from parking lot contains many contaminants, ranging from vehicular oils and grease to fertilizers, pesticides, and pet waste, that are washed away into receiving water bodies during rainfall events (Boving et al., 2008; Collins et al., 2008.). Consequently, the quality of stormwater is compromised, adversely affecting the health of rivers and other aquatic ecosystems.

Maintaining a naturalized water balance within urban environments where stormwater is allowed to infiltrate into the subsurface, recharge groundwater, or evaporate is critical for mitigating these adverse effects (Qin, 2015; Selbig & Buer, 2018). This concept is widely supported by engineers, urban planners, policy makers, and other stakeholders. In response, stormwater management systems have evolved rapidly, driven by new regulations aimed at reducing the hydrological and environmental footprints of urban areas. For example, in Quebec, the Environment Quality Act (*Loi sur la Qualité de l'Environnement*; section 22, 3º) mandates that projects authorized after January 1, 2012, incorporate stormwater best management practices (BMPs). This regulatory framework has particularly impacted the *Ministère des Transports et de la Mobilité durable du Québec* (MTMD), which manages transportation infrastructure where runoff from roads and parking lots is a significant concern.

One promising stormwater management system is PA. PA reduces runoff volume and peak flow by enhancing water infiltration, thereby promoting groundwater recharge and minimizing erosion. Additionally, it improves water quality by filtering contaminants through a combination of physical, chemical, and biological processes (Azad et al., 2024; Dierkes et al., 2002). The design of PA also contributes to cooling stormwater runoff through mechanisms such as infiltration cooling and

evaporative cooling (Qin, 2015; Tota-Maharaj & Scholz, 2010), making it a sustainable and multifunctional solution for urban stormwater management.

Despite PA potential benefits, its widespread adoption in cold climates such as Quebec remains uncertain. While studies conducted by Drake (2013), Brattebo & Booth (2003), Drake et al. (2010), Fassman & Blackbourn (2010), Muttuvelu et al. (2024) and Roseen et al. (2012) have examined its performance, uncertainties persist regarding long-term benefit under conditions of winter plowing activities. For example, research such as that by Drake et al. (2010) has indicated that the infiltrate from porous concrete (PC) and permeable interlocking concrete paver (PICP) can contain higher levels of dissolved ions and heavy metals not detected in the runoff from conventional asphalt (CA) after almost 5 years of implementation. Brattebo & Booth (2003) also raised a similar water quality issue on three types of 6-year-old permeable pavement (PP) installed in Renton, Washington. In their study, Zn concentrations in the PP exfiltrate were higher as compared to what was observed when the PP was newly installed. Moreover, using PA in parking lots alongside an underground reservoir introduces additional structural risks such as settlement of the foundation layer from prolonged water saturation (Selbig & Buer, 2018). Vehicle movement and traffic also expediate transport and accumulation of particulate contaminants (e.g., sediments) which can clog the voids, reducing infiltration capacity and diminishing the system's effectiveness (Danz et al., 2020) in managing stormwater runoff. In some cases, the pavement clogging is irreversible even after cleaning (Van Duin et al., 2008). These uncertainties, coupled with the unknown effective lifespan under harsh winter conditions, complicates the broader adoption of PA as a sustainable Low Impact Development (LID) practice in cold climates. Addressing these long-term issues through research is essential to validate the sustained performance and environmental benefits of PA, ensuring its viability as a stormwater management solution.

1.1 Project history

The study site for this research project is the parking lot of the Le Tournesol library, located at 530 rue Delage in Quebec City. The parking lot was formally made of 2300 m^2 CA. However, for the purpose of this study, it was rebuilt in 2020 by the MTMD and the Québec city. After the reconstruction, the study area was divided into two sections: one section featured CA covering 854 m², and the other utilized PA over an area of 529 m². The PA pavement is drained by a perforated pipe. The portion of the studied CA, is drained via a catch basin. Both pavements are hydraulically separated to prevent inter-mixing of flows. The native soil has a good permeability

with an infiltration rate (IR) between 26 mm/hr and 61 mm/hr ensuring that the PA system was not hindered by poor infiltration in the underlying soil.

The work presented herein, referred to as phase 2 of the project, follows the study (phase 1) conducted by Duchesne et al. (2022) from INRS, after the initial reconstruction of the site in 2020. The overall objective of the initial research study, conducted between October 15, 2019, and November 15, 2022, was to evaluate the environmental and hydrological performances of PA and reservoir pavements as stormwater management structures…

1.1.1 Findings from the phase 1 (Duchesne et al., 2022)

The IR of the PA measured on November 7, 2020, was high, ranging from 4700 mm/hr to 6720 mm/hr, but decreased over the 17 months of the study from 728 mm/hr to 4452 mm/hr on April 13, 2022, possibly due to sediment accumulated in the pores of the PA.

The PA was found to reduce runoff volumes consistently for the 13 rainfall events studied in 2021-2022, despite the decline of IR. Relative to the CA, the PA was able to reduce the runoff volumes by 68 % to 100 % and the runoff peak flow rates by 91 % to 100 %, depending on the rainfall events. For 10 out of the 13 studied flow events, 100 % volume and flow rate reductions were achieved. In fact, the PA completely infiltrated all rainfall events less than 21 mm, which correspond to a return period of less 2 years.

A total of 4 samples were collected from the outlets of the PA and CA in 2021-2022. The PA effluents leaving the reservoir (i.e., through the underdrain) had lower concentrations of most studied contaminants relative to CA runoff. Maximal reductions in concentrations reached 75 % for total suspended solids (TSS), 93 % for petroleum hydrocarbon C_{10}-C_{50}, 98 % for zinc (Zn), 99 % for copper (Cu), 58 % for aluminum, 40 % for total phosphorous (TP). and 54 % for total nitrogen (TN). On the other hand, electrical conductivity measured from the PA was from 276 % to 913 % higher than the one from the CA runoff.

Despite these promising outcomes, phase 1 of the project also highlighted several limitations and recommendations that warranted further investigations. The performance of the PA was affected by partial clogging. The decline of the PA IR over the period was rapid but the author attributed this performance to the PA receiving sediment from construction activities happening 30 m away from the study site. It was therefore uncertain if this could have negatively impacted water quality from the PA. Also, it was hoped that seasonal spring cleaning conducted by the City of Quebec

could improve the IR and the overall performance of the PA, but this could not be verified during phase 1. Moreover, the short study period of phase 1 (18 months) could not fully capture the long-term durability and stormwater management performance of the PA under repeated seasonal stresses.

Building on the outcomes and addressing the challenges from phase 1, the second phase of the study began on May 1, 2023, and continued until August 31, 2024, with the aim to extend the monitoring period and enhance data collection. In doing so, phase 2 sought to offer a more comprehensive assessment of the long-term behavior of PA, including its resilience against clogging and performance under a broader spectrum of weather conditions. The extended monitoring was expected to refine maintenance practices and support design improvements, ultimately contributing to more sustainable urban stormwater management practices. At the beginning of phase 2, the study site had no form of physical deterioration to the pavement surfaces and the drainage network infrastructure.

The monitoring program of phase 2 included collecting rainfall data using an on-site rain gauge, measuring the IR of the PA at three points in 2023 and six points in 2024 during the different seasons of the year, measuring outflow from the PA and CA, and laboratory analysis of water quality parameters (TSS, chemical oxygen demand (COD), petroleum hydrocarbons C_{10}-C_{50}, electrical conductivity (EC), total phosphorous (TP), total nitrogen (TN), pH, and heavy metals) and runoff temperature from the PA and the CA. Additionally, phase 2 examined the effectiveness of three different types of vacuum cleaning trucks. This study, together with phase 1, contributes to 4 years of continuous field monitoring of the PA and provides good guide to evaluate its performance for stormwater management.

1.2 Main objective and specific objectives of the project

The main objective of this project was to monitor and evaluate the environmental and hydrological performance of the PA and its reservoir structure for source control stormwater management.

To achieve this, the following specific objectives were set:

I. Monitor and evaluate the IR of the PA over the seasons.
II. Compare the performance of the PA and the CA in terms of reduction of runoff rate and volume.
III. Compare the quality of runoff water from the PA and the CA.

IV. Characterise the runoff temperature from the PA and the CA.
V. Develop a hydrological model of the experimental site using the Storm Water Management Model (SWMM) software.

The thesis is organized into five chapters, each contributing to a comprehensive exploration of the research objectives. Chapter 1 presents the research topic, detailing the study's objectives, and outlining the overall thesis structure. In Chapter 2, a review of pertinent literature on PP establishes the theoretical foundation for the study. Chapter 3 outlines the methodology used to assess the environmental and hydrological performances of the pavements, detailing both the data collection processes and the analytical techniques employed. In Chapter 4, performance metrics including reduction of runoff volume and flow rate, water quality, and runoff temperature from the PA parking lot are detailed and compared against those of the CA. The analysis also offers a critical evaluation of the overall pavement performance. Finally, Chapter 5 summarizes the main findings, presents the study's conclusions, and offers recommendations for future research.

2 LITERATURE REVIEW

2.1 Permeable pavements

Permeable pavements (PP) are stormwater source control infrastructure and are among the LID systems which help to decrease surface runoff to the sewer network, majorly through infiltration and storage. Runoff infiltrates through the pavement surface or joints of the pavement (in the case of interlocking concrete pavement) to an underlying temporary (i.e., vertical column) reservoir of high porosity packed materials and later infiltrates into the soil with or without geomembrane. PP are deemed sustainable not only for their structural, economic, and road-user advantages but also for their application in stormwater management (Singer et al., 2022). PP are suitable for residential roadways and parking lots and can be utilised on low traffic roads. Nevertheless, long-term performance as well as technical difficulties in installation and maintenance can hamper their full consideration as effective stormwater management systems for longer durations (Singer et al., 2022). They can be composed of different surface materials which define their permeability, such as concrete, asphalt, pavers, or grids, and can have various benefits and drawbacks depending on the context and design. In the context of this literature review, pervious asphalt (or permeable porous pavement), pervious concrete (or permeable concrete), and permeable interlocking pavement will be discussed. The surface pavement type or material for the different types of pavements is shown in Figure 2.1, taken from Selbig & Buer (2018).

2.1.1 Types of permeable pavement

1. **Porous asphalt (PA):** PA has a composition quite like that of CA, only with much less fines, thus creating a material with large porosity that allows water to infiltrate. PA has a higher void and porosity ratio than CA. Ahmad & Hafeez (2021) found that PA has a void space ranging from 15 % to 25 %, as opposed to 2 % for CA, and can provide additional water storage. However, the pores in PA are more prone to frost damage for some site conditions (Candra et al., 2020) and require careful design and maintenance.

2. **Permeable interlocking concrete paver (PICP):** This is made of interlocking concrete blocks or cobblestones with joints filled with porous media such as graded sand or gravel. Surface water infiltrates through the granular joints to an adjacent storage or soil beneath the pavement. This type of pavement is majorly used for driveways, walkways, parking areas, and low-traffic roads. It normally has a stone reservoir base that stores water and

allows infiltration and/or drainage. The recommended void content of PICP joint media is between 5 % to 15 %.

3. **Pervious or porous concrete (PC):** PC is prepared with mixtures of cement and engineered coarse aggregates allowing for sufficient permeability, which guarantees stormwater to infiltrate to the underlying soil or reservoir layer. According to the Virginia Department of Environmental Quality (Virginia DEQ, 2011), the void created in the pavement is 15 % to 25 % of the total volume of the material.

Figure 2-1 Different types of permeable pavements (Selbig & Buer, 2018)

The structure of the pavement and the underground reservoir may vary depending on the type of PP, but they all share a common feature: a permeable surface layer made of paving materials, and a stone aggregate layer beneath that acts as a reservoir. Some PP also have a geomembrane at the bottom of the reservoir layer to prevent contamination of the native soil.

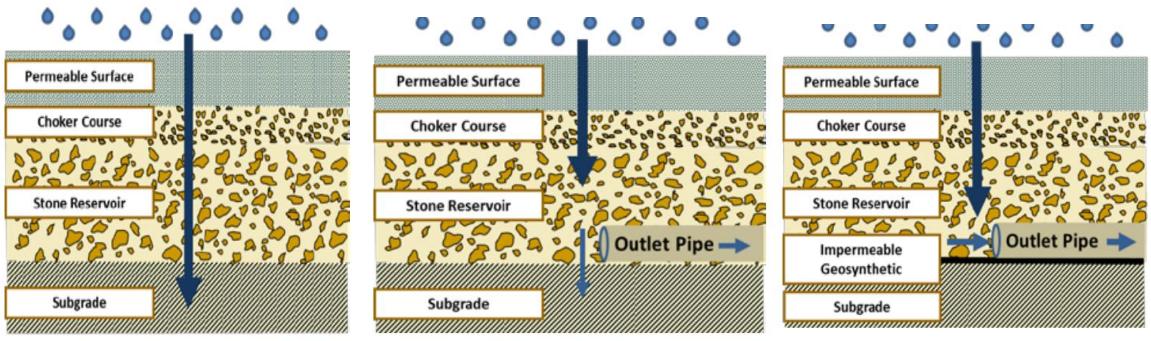

(a) (b) (c)

Figure 2-2 Design adaptation based on characteristics of the native soil: (a) full infiltration, (b) partial infiltration, and (c) low infiltration (Ndon, 2017)

Figure 2.2 illustrates typical PA systems that have a surface layer that let water pass through to a base/subbase layer of open-graded aggregates, which is a reservoir layer that stores water before it exits the pavement. Some designs have drainage pipes for water that cannot infiltrate low permeability underlaying soils (see Figure 2.2b), while some other PPs can let stormwater infiltrate fully into (high infiltration) soils below, without underdrains (see Figure 2.2a). Others may use a geomembrane (a waterproof liner) to prevent water from reaching unsuitable soils or structures nearby. These pavements have an outlet pipe for storage and flow control and can also collect water for reuse. This is called a low infiltration design (see Figure 2.2c). The system filters the water and traps the particles in the layers of bedding and aggregates. Stormwater runoff and traffic load are two factors that affect the design of PA pavements. The design process requires to estimate the thickness of all layers based on structural and hydrological analyses (Virginia DEQ, 2011). The structural analysis considers the strength and durability of the pavement under the traffic load, while the hydrological analysis considers the stormwater storage and infiltration capacity of the pavement (ASCE, 2015).

2.1.2 Hydrological and structural considerations for permeable pavement

In vehicle-heavy areas like parking lots, PPs are engineered with layers capable of supporting the anticipated traffic loads. Moreover, the hydrological and structural designs are tailored to the specific type of PP system being used. General considerations for hydrological and structural designs as stipulated by Virginia DEQ (2011) are:

1. Total traffic.
2. In-situ soil strength and IR.
3. Designed storm volume, water quality, and flood control volumes and rate.
4. Bedding and reservoir layer design.

2.1.3 Design considerations

The design of PPs differs from several regional guidelines based on climatic and geological conditions. For example, technical design guidelines including material specifications, mixture proportioning, etc., are outlined by the American Concrete Institute (ACI) for PC, the National Asphalt Pavement Association (NAPA) for PA and the American Association of State Highway and Transportation Official (AASHTO). The choice of type of PP is also influenced by the intended use of the pervious surface. Credit Valley Conservation & Toronto Region Conservation Authority

(2010) and other researchers specify common considerations that should be considered in the design and construction of PP structures, such as.

1. Limitations: Heavy traffic can damage PP, so they are not suitable for such surfaces. PPs are not recommended to treat runoff from stormwater hotspots (e.g., high sediment load like construction sites, vehicle maintenance areas, petrol/gas stations etc.). PA is easier to install than other pavement types, but it is limited by its higher cost and lower strength.
2. Site topography: The slope of the PP should be between 1 % and 5 %. If it also receives runoff from nearby impermeable surfaces, those surfaces should not have a slope higher than 20 %.
3. Water table: The bottom of the reservoir layer in the pavement structure must be at least 1 meter above the highest seasonal water level.
4. Soil infiltration: Native soil conditions do not limit the use of PPs though the IR of the soil is very important and must be measured for any pavement design. If the soil IR is less than 15 mm/hr, a perforated drain is needed. Virginia DEQ (2011) prescribed that native soil with hydrological soil groups A and B may not require underdrain.
5. Drainage area and runoff volume: The impervious surface area that drains into the PP should not be more than 1.2 times the area of the PP. The design runoff reduction volume must not stay within the reservoir layer of the PP for more than 36 h.
6. Temperature conditions: Pervious asphalt and pervious concrete are sensitive to low temperatures. They should not be installed when the air temperature is below 16°C.

2.1.4 Cold climate conditions and winter performance

In regions with cold climates and harsh winter conditions like that of Quebec, freeze-thaw cycles can undermine the integrity of PP systems. In these circumstances, incorporating specific design modifications can help mitigate such adverse effects. The Virginia DEQ (2011) and Credit Valley Conservation & Toronto Region Conservation Authority (2010) recommend some guidelines for such conditions including:

1. To prevent freeze damage, water pooling on the PP surface should be eliminated. The surface should be engineered to drain completely within 24 hours after any rainfall event.
2. It is recommended that large snow storage piles be situated next to grass areas, allowing sediments and contaminants in the melting snow to be partially filtered before reaching the PP.

3. Fine sand should not be used for winter traction on PP or on conventional pavements that channel water toward permeable surfaces because the fine sand tends to clog the drainage system rapidly.
4. Application of chloride-based de-icers on PP should be limited as these salts are likely to leach into the groundwater.

2.1.5 Construction, maintenance and life-cycle cost consideration

Studies such as those of Dempsey & Swisher (2004), Schaefer & Wang (2006) and Xie et al. (2017) have noted that the initial construction cost of PP is generally higher than CA. This is largely due to the construction of the underlaying infiltration cell which increases labor and material expenses. Despite this higher initial cost, Brattebo & Booth (2003) argued that the added benefits of enhanced stormwater management and environmental sustainability can offset these initial expenditures over time. For example, Brattebo & Booth (2003), Roseen et al. (2012) and Azad et al. (2024) suggested other benefits, including the drainage infrastructure area that is replaced or reduced because of the infiltration and storage provided by a PP system. Additionally, Roseen et al. (2012) showed that under reduced winter de-icing practices, PA can achieve lower winter maintenance costs. Cahill (2003) reported that PA parking lots require less plowing and that snow and ice melt faster on these than on regular parking lots. Azad et al. (2024) suggest that PP, at the end of its useful life, provide a benefit from the use of the recycled aggregate to manufacture newer one, because of the higher volume of dense coarse aggregate.

Maintenance costs for PA represent another important cost consideration. While traditional asphalt typically requires less frequent maintenance, PP surfaces are more susceptible to clogging from sediment accumulation. This necessitates regular cleaning to maintain surface permeability, thereby affecting long-term operational costs (Hu et al., 2020). Roseen et al. (2012) suggested that, when maintenance is conducted using optimized protocols, the performance of PA can be sustained effectively. However, the absence of standardized maintenance practices often complicates cost predictions (Drake, 2013).

Life cycle analysis is therefore critical for acceptance of a PP system over a conventional impervious asphalt (Roseen et al., 2012; Xie et al., 2017). The life cycle costs include initial cost, annual operation and maintenance costs, and salvage value (Xie et al., 2017). A study by Xie et al. (2017) used lifecycle cost analysis to assess the long-term benefits of PPs relative to traditional alternatives. In Xie et al. (2017), and other reported cases such that of NRMCA (2004) and ASCE (2015), the cost difference is reduced or eliminated when the total life cycle costs of PP over its

lifespan is considered. Nonetheless, these savings are highly context-dependent, varying with factors such as local climate, traffic patterns, LID type and specific site conditions (Roseen et al., 2012; Montalto et al., 2007). Specific maintenance costs depend on the PP type, the site, and the area that contributes runoff to the facility. For example, Drake (2013), Danz et al. (2020) and Vaillancourt et al. (2019) reported that cost and time associated with maintenance is anticipated to be higher for PICP than PA and PC. This is because the joint materials of the PICP need to be replaced after each intensive cleaning. Table 2.1 shows the construction cost of the three typically used PPs. The construction cost of PA is anticipated to be lower than PICP and PC. This advantage is attributed to the simplicity of its installation process, in contrast to PC and PICP which respectively require extended drying times and more complex installation procedures (ASCE, 2015). Vaillancourt et al. (2019) revealed that constructing a PICP system with an underground reservoir typically costs around 200 CAD/m^2, covering both materials and labor. This estimate includes expenses for the pavers, bedding layer, foundation, sub-foundation, borders, and geotextile.

Table 2.1 Construction cost of the three typical permeable pavement

Porous asphalt (PA)	Porous concrete (PC)	Permeable interlocking concrete paver (PICP)	Source
28 to 51 \$/m^2	21.53 to 96.96 \$/m^2	53.82 to 107.64 \$/m^2	WERF (2005) (updated by NVRA, 2007)
28 to 51 \$/m^2	87 to 145 \$/m^2	72 to 130 \$/m^2	ASCE (2015)

2.1.6 Maintenance requirements of permeable pavement

Maintenance of PAs, like any other PPs, helps to prolong the useful life and benefits of the system. The dual purpose of PA system, i.e. for stormwater management (infiltration, storage, and treatment) and transportation, requires maintenance activities that address both functionalities. In terms of stormwater management, sediment accumulation in the pores of the PA from stormwater runoff is inevitable and, therefore, regular monitoring and maintenance is needed. Sediment loads

can also increase when winter abrasives are used to maintain traction during and after snowstorm. By far, maintenance of PA is primarily linked to the restoration of the pavement permeability (Danz et al., 2020). Improper maintenance leads to a higher incidence of premature failure (Van Duin et al., 2008) because clogging materials are not removed in a timely and regular manner and become embedded within the pavement. Some of the maintenance practices that have been explored in previous studies include pressure washing, power brushing, milling, commercial street sweepers, and combinations of these (Van Duin et al., 2008) under variable pavement conditions such as pavement age, degree of clogging, and land use. Studies such as Danz et al. (2020), which examined six maintenance practices on PC, PICP, and PA test plots under the same environmental conditions, gave a good understanding of different maintenance efficacy. Table 2.2 shows a summary of findings related to maintenance techniques on PA. Particularly, limited studies have been carried out with PA. Maintenance practices such as push broom, vacuum sweeping with shop-vac, power washing, etc., have been found not to be effective for PC and PA (Danz et al., 2020; Henderson & Tighe 2011), largely because of solidity of the interconnected pores created during manufacturing (Kia et al., 2017). Sediments penetrate the solid matrix of the PA, making maintenance practices using a high-pressure wash (either by air or water followed by high-suction vacuum) the most effective (Danz et al., 2020). Studies by Selbig & Buer (2018) and Winston et al. (2016b) further indicated that maintenance practices that penetrate deeper into a permeable surface will have a greater likelihood of restoring the infiltrative capacity. Frequent maintenance is widely accepted as an effective operational plan to prolong the usefulness of PA. A study by Al-Rubaei et al. (2013) in northern Sweden observed that the average infiltration rate at one PA residential street recovered from 30 to 209 cm/h after pressure washing and vacuuming. However, they observed little to no improvement at a second PA street, the difference potentially being due to regular maintenance at the first site but little-to-no maintenance at the other. Developing a maintenance plan to regularly restore infiltration capacity is a critical step in the planning process for PP design (Danz et al., 2020).

Table 2.2 Summary findings of restorative maintenance techniques for porous asphalt

Study	Age (years)	Maintenance practice	Results
Van Duin et al. (2008)	1	Schwarze A8000 Regenerative-air truck (single dry pass)	Maintenance decreased measured IR
		Schwarze A8000 regenerative-air truck (three wet passes)	Pavement appeared to be irreversibly clogged
Chopra et al. (2010)	n.a.	Loading of sand followed by vacuum truck	The first pass of the vacuum sweeper improved IR but repeated passes decreased infiltration
		Loading of limestone followed by vacuum truck	No significant effect
Danz et al. (2020)	Within 2 years	Vacuum assisted street cleaner-Elgin Whirlwind.	16 % average IR change in post maintenance
Danz et al. (2020)	< 7 months	Compressed air and vacuuming	40 % average IR change in post maintenance
Roseen et al. (2012)	3	Combination of an Elgin Whirlwind MV vacuum sweeper and pressure-washing	An overall decline in IR was observed throughout the study

Assessing the impact of maintenance procedures is essential for PP longevity. The maintenance practices outlined in Table 2.2 emphasize the effectiveness of certain interventions, while overlooking uncertainties introduced by site conditions. This makes it difficult to adopt a specific maintenance practice. For instance, Danz et al. (2020) evaluated six maintenance practices on an isolated test plot, but did not account for the impact of moving vehicles compacting sediment deeper into the PA layers. Overall, none of the reviewed studies provided any estimates of the effective life of the studied PP systems, most likely because the reported results are inconclusive. General trends from the above-mentioned studies show that:

1. The degree to which the surface is restored is dependent on multiple variables such as pavement age, usage intensity, pavement void ratio, etc.
2. The effectiveness of maintenance practices decreases with repeated exposure to clogging materials.
3. Maintenance practices are likely to provide partial restoration, but not full restoration of surface IR.
4. There is a lack of standard cleaning maintenance for PA.

Other maintenance practices are required to repair any cracks, potholes, or settlements that may occur on the pavement surface or the underlying layers. NAPA (2008) suggested that conventional, nonporous patching materials can be used to repair PA, if the total area is less than 10 % of the paved area. However, if the total area of patching exceeds 10 %, approved permeable patching material should be used instead. In cases when the surface of the PP experienced severe distresses, such as raveling, which is the loss of aggregate from the surface, Bruinsma et al. (2017) suggested grinding the surface and overlaying with new permeable material especially for PA with a stabilized base layer. They noted that ensuring that fine material does not enter the underlying permeable material remained difficult and that permeability of the remaining material would need to be verified. Drainage structures that are associated with PA, such as underdrains, catch basins, or outlets, also need to be inspected occasionally to ensure proper functioning, especially after major rain events.

2.2 Evaluation of hydrological and water quality performances of permeable pavement

2.2.1 Runoff volume mitigation potential

The potential of PPs to reduce stormwater volume depends on how fast the subsoil can infiltrate water and how much water the retention layer can store. PPs with thicker subsurface layers can hold more stormwater, while the surrounding soils with high IRs can drain the subsurface layers faster, also increasing the storage capacity. The design of PPs has been subjected to many considerations based on intended outcomes. Site location, soil type, geometric and structural soundness, among many design characteristics, influence the runoff volume reduction of PA.

As seen in Table 2.3, PPs have demonstrated stormwater reduction effectiveness from 24 % to 100 %, reflecting the range of design approaches and site conditions. PA slightly outperforms the

other two types of PP in terms of runoff volume reduction potential; this is due to its high IR, as mentioned earlier

Table 2.3 Summary of design characteristics and performances for permeable pavements aged installed for at least 22 months

Reference	Type of PP	Design characteristics	Location	Max. rain/ duration	Runoff volume reduction	Runoff peak flow/time reduction
Kwiatkowski et al. (2007)	PC	Silty sand	Pennsylvania, USA	NA 2.5 years	100% infiltration achieved for rainfall < 50 mm	
Legret et al. (1999)	PA	Porous pavement with reservoir structure	Loire-Atlantique, France	NA 4 years	Averaged 96.7%	
Barrett (2008)	PA (overlay)			117 mm 2.5 years	Increased surface runoff	Minimal lag between peak rainfall and runoff
Drake & Bradford (2012)	PICP	Silty clay with underdrains	Ontario, Canada	51.6 mm 22 months	No direct runoff observed	Hydrograph lag ranged between 45 min and 57.5 h
Drake & Bradford (2012)	PC	Silty clay with underdrains		51.6 mm 22 months	UEV was 57 % of SRV	PF reductions averaged 92 %

Reference	Type of PP	Design characteristics	Location	Max. rain/ duration	Runoff volume reduction	Runoff peak flow/time reduction
Pratt et al. (1995)	PICP	Impermeable liner with underdrains		22.6 mm 2 years	UEV averaged 24-47 % of SRV	
Rushton (2001)	PP	Sandy soil		NA 2 years	UEV was 35 % of SRV	Reduction was more pronounced for small rain events
TRCA (2008)	PICP	Impermeable liner with underdrains		72 mm, 2.5 years	No runoff observed during the summer except for 1 large rain event (72 mm)	

PF = peak flow; RV = rainfall; SIR = surface IR; SRV = surface runoff volume, UEV = underdrain exfiltrated volume

One significant limitation of recent research is that most monitoring studies have evaluated PA performance for less than 2.5 years. This short duration may be due to perceptions that PA performance does not justify prolonged monitoring. Moreover, PA has been used sparingly in cold-climate regions, highlighting the need for additional demonstration projects and long-term testing in these areas.

2.2.2 Potential to improve water quality

Stormwater quality can be modified through physical, chemical, and biological processes when it infiltrates through the PPs, such as filtration, adsorption, precipitation, decomposition, and biodegradation (Houle et al., 2013). Effectiveness for PPs to remove contaminants depends on many factors, such as the type and design of the pavement, runoff and contaminants features, pavement condition and maintenance, and site climate and hydrology (Roseen et al., 2012). PP design that allows all the rainfall to infiltrate (no drain) is recommended because almost no effluent or contaminants will leave to the sewer system or the receiving water course. Effluent from partial infiltration PP systems need to be studied to analyze the performance of the structure in removing contaminants. Sandy soils infiltrate more stormwater but have less treatment capability (Dover, 2015). Clay soils can hold and capture more contaminants, but they infiltrate less. This implies that most of the contaminants are captured in the surface pores and underlying granular base of PP. Some studies (see Table 2.4) have examined the quality of stormwater effluent. In these studies, the quality of the effluent was also used to measure the potential for groundwater contamination.

A study by Drake et al. (2010) on PICP installed in a college parking lot in King City, Ontario, showed that stormwater that infiltrated through a granular reservoir layer and 1 meter of native soil had significantly lower concentrations of several contaminants typical of parking areas compared to surface runoff from adjacent CA. This observation is consistent with research on effluent water quality from pervious pavements in Washington (Brattebo & Booth, 2003) and Pennsylvania (Kwiatkowski et al., 2007). As with all stormwater infiltration practices, the risk of groundwater contamination from infiltration of roadway runoff laden with de-icing salt constituents (typically sodium and chloride) is a significant concern. Chloride ions are highly mobile in soil and are readily transported by water percolation to aquifers.

Table 2.4 Summary of selected PA stormwater effluent quality performance evaluations for systems that have been in operation for at least 1 year

Study	Mass/ concentration	Duration	Average removal (%)						
			TSS	Zn	Cu	Pb	Cd	TP	TN
Legret et al. (1999)	Mass	4 yr	59	73	-	84	77	-	-
Barrett (2008)	Concentration	2.5 yr	93	79	52	88	-	-	-
Rushton et al. (2001)	Mass	2 yr	91	75	81	85	-	-	-
Roseen et al. (2012)	EMC	1-4 yr	NC	NC	-	-	-	42	-
Huang et al. (2012)	Concentration	1 yr	91	55	68	65		78	5.6
Roseen et al. (2009)	Concentration	1-2 yr	83	94	92	-	-	-	70

NC = nearly complete, EMC = event mean concentration.

2.2.3 Urban heat and stormwater temperature mitigation

Suitable temperature is vital for survival of aquatic species. Aquatic plants and animals which are sensitive to temperature changes could be affected by a sudden rise in waterbody temperature from stormwater discharges. Research has shown that PPs generally exhibit lower pavement temperatures compared to CA (Wang et al., 2023; Asaeda & Ca, 2000; Qin, 2015). This suggests that the use of PP could help alleviate urban and stormwater temperatures. Heat retained in both permeable and impermeable pavements disrupt the normal thermal condition of the natural land surface (Wang et al., 2023). During rainfall, the retained heat is absorbed by the rain upon contact with the impervious pavement and/or as it infiltrates through PP layers. This modifies the heat balance of receiving water bodies (Qin at al., 2025). However, unlike impervious asphalt pavement, heat absorption in PPs is less (Wang et al., 2023; Asaeda & Ca, 2000). Asaeda & Ca (2000) examined the surface and internal temperatures of PPs during summer conditions in Tokyo. They found that pervious ceramic pavement and PICP generated lower temperatures than impervious asphalt. PP initial surface temperature and their distinct properties such as pore size

were found to influence stormwater temperatures. Asaeda & Ca (2000) observed that the smaller pore size of the pervious ceramic pavement kept more water near the surface aiding evaporative cooling during the day and keeping the pavement cool. A laboratory scaled test determination of thermal pollution reduction of PPs by Wang et al. (2023) saw a temperature increasing from 28.5 to 31.1 °C at the start of runoff and from 26 to 27.3 °C for the final runoff temperature, when the initial surface temperature of the permeable brick pavement was changed from 35 to 47 °C.

2.3 Conclusion

Although PPs have been studied as LID components for decades, they remain underutilized across certain parts of Canada. This limited adoption suggests that developers, designers, engineers, and planners lack the necessary tools and knowledge to embrace this technology. Because stormwater engineering must account for uncertain risks, long-term performance data on PPs are essential to demonstrate that they can match the safety and reliability of conventional stormwater management solutions. This review, by summarizing current understanding, serves as a resource to promote both comprehension and acceptance of PPs. As attention in PP expands, it becomes increasingly important to rigorously assess their performance practicality, and, in certain cases, their limitations. This review has highlighted existing research gaps and identified areas for future investigation, which can be summarized as follows:

1. Long-term investigations remain essential to evaluate how PPs perform and function across diverse climatic conditions and usage scenarios.
2. The mechanisms driving reductions in permeability are not well understood, preventing the formulation of reliable estimates for effective lifespan.
3. It is necessary to conduct more rigorous evaluations and tests of maintenance procedures. Commercially available equipment must undergo thorough testing to ensure consistent, reproducible outcomes. Since various PP types probably demand distinct upkeep methods, these differences still need to be explored in depth.

The PP types reviewed here have demonstrated a strong ability to counteract many adverse impacts of urbanization. By dramatically reducing runoff volumes, slowing the rate of flow, and lowering peak flow rates, PPs relieve pressure on downstream surface waters. During minor precipitation events, PPs can capture and infiltrate all incoming water, greatly reducing how often urban runoff occurs. These systems also enhance urban water quality by trapping

suspended sediments and heavy metals before they enter receiving bodies of water. Additionally, PPs remove and treat hydrocarbons and, under certain circumstances, encourage beneficial nutrient removal. To date, substantial improvements in surface water quality have been observed for most contaminants, although chloride reduction in cold climates remains less effective.

3 METHODOLOGY

3.1 Description of study site

The site, the municipal parking lot of Le Tournesol library, was initially fully CA. In October 2020, the site was reconstructed partially with PA by the MTMD. With this reconstruction, the 2300 m^2 CA lot was partitioned to create a drainage area of 854 m^2 made of PA (red perimeter in Figure 3.1) and 529 m^2 made of CA (yellow perimeter in Figure 3.1), together referred to as the study zone. The remaining portion of the CA, with an area of 917 m^2, shown by the green perimeter in Figure 3.1, is drained independently and not considered in this study.

Figure 3-1 Parking lot specification: porous asphalt (red), conventional asphalt (yellow), and conventional asphalt not considered in this study (green)

As shown in Figure 3.2 and Table 3.1, the cross-section of the PP shows three layers including a 80 mm thick PA, an engineered soil/foundation layer of 200 mm thick (10-20 mm diameter crush stone), and a 600 mm deep reservoir layer made of crush stones (20-40 mm diameter) with a 150 mm diameter slotted PVC underdrain pipe. There was no lining between the subgrade (native soil) and the storage/reservoir layer allowing infiltration to the native soil. According to the hydro-geotechnical study conducted by Stantec (Godé, 2018), the native soil is made of silty sand and sandy silt with an IR between 26 and 61 mm/hr. Since this was an experimental site, the reservoir

layer with an underdrain pipe was opted to let the water in the reservoir layer infiltrate into the in-situ soil while the excess water could flow through the underdrain.

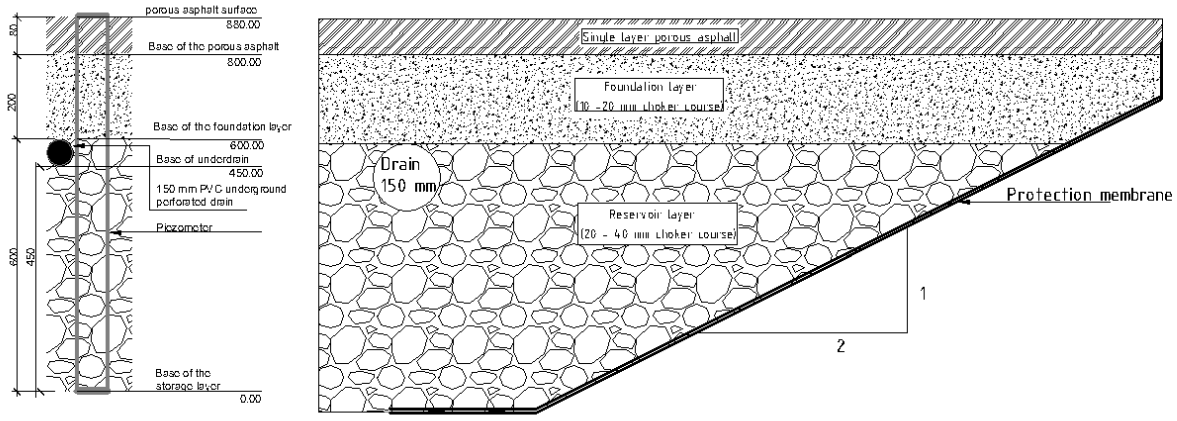

Figure 3-2 Cross-section of the studied PA showing the various layers with their material composition

Table 3.1 Characteristics of the porous pavement

Layer	Material	Thickness (mm)	Function
PA layer	Like CA with fewer finer aggregates	80	Infiltrate the surface water
Engineered soil layer	Coarse aggregate of 10-20 mm diameter stones	200	Foundation for the PA layer
Reservoir/storage layer	Coarse aggregate of 20-40 mm diameter stones	600	Temporary store infiltrated water from upper layer

*150 mm diameter underdrain perforated pipe, perforation width of 2-3 mm, surface area of perforation > 32 cm^2/m, Polyethylene type 2 (High-Density Polyethylene) material.

It should be noted that no sand was spread on the study zone during winter. However, Figure 3.3 shows a trace of winter abrasives at the entrance and drive lane of the PA. Unfortunately, part of the unstudied CA was used to store snow and thus, during the transport of snow from the

neighbouring public parking lot and streets, traces of winter abrasives were left behind the main driveway of the parking area.

Figure 3-3 Signs of road salt or winter abrasives on the main driveway of the parking area (March 20, 2024)

3.2 Characterization of the infiltration rate

The infiltration process forms part of the key mechanism of every PP ensuring the runoff reduction. Additionally, it is the infiltration capability of the PP that distinguishes the PA from the CA. As such, it is important to quantify the IR of the PA at different moments.

The surface IR was measured using the C1781/C1781M-17a standard of the American Society of Testing and Material (ASTM, 2015). In the 2023 season, the IR of the PA was determined on May 26, 2023, before summer cleaning/maintenance, and again on June 13, 2023, after cleaning. The IR tests were performed at the same discrete points as in Duchesne et al., 2022 (points 1, 2, and 3 in Figure 3.4) to compare the results over successive years. However, to adequately account for the spatial fluctuation of the IR, during the 2024 monitoring period, the tests were conducted in three more discrete points (see points 4, 5, and 6 in Figure 3.4) on May 21, 2023 and June 13, 2024. Points 2 and 4 are on local lanes, point 3 is on a parking lane, and points 1, 5, and 6 are situated along the main driveway leading to the parking lot. In addition, supplementary infiltration tests were performed at all six discrete points on July 19, 2024 and August 27, 2024 to further examine the clogging issue of the PA.

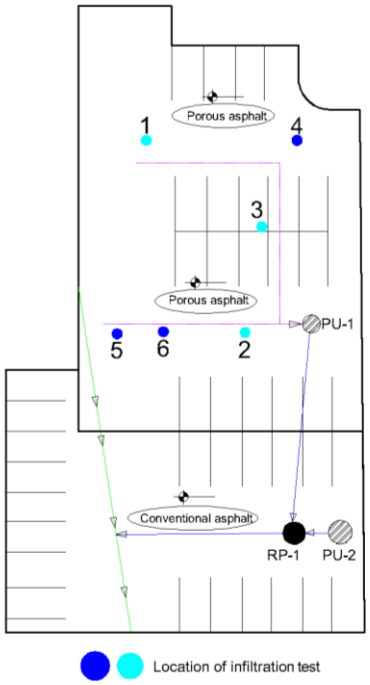

Figure 3-4 Layout of surface infiltration test locations. Points 1 to 3 are test locations for 2023 year and points 4 to 6 are the additional test locations during the 2024 year

Figure 3-5 Measurement of infiltration rate of the porous asphalt according to ASTM C1781/C1781M-17a method

Following the C1781/C1781M-17a method, IR was determined by introducing 3.6 kg of water in a sealed tube of 275 mm in diameter and a minimum height of 50 mm infiltrate to the pavement surface (Figure 3.5). If this initial (pre-wetting) infiltration occurred within 30 s, a second test (main

test) was conducted using 0.25 kg of water for a precise evaluation of the infiltration rate. For each test, the time required for the total infiltration was recorded and the IR was computed using Eq. (3.1). In some instances, when the time taken for one third of the 3.6 kg water exceeded 60 min to infiltrate, the prewetting test was terminated and the prewetting IR was used as the final observed IR of that point (Danz et al., 2020; Winston et al., 2016a; Al-Rubaei et al., 2013).This indication implies an IR lower than 20.2 mm/hr. Sehgal et al. (2023) used a water mass less than 3.6 kg on clogging areas when evaluating the IR.

$$I = K\frac{m}{d^2\, t} \qquad 3.1$$

where *I* is the IR (mm/hr), *m* is the water mass (kg), *d* is the internal diameter of the infiltration cylinder (mm), t is the infiltration time (s), and *K* is the unit conversion factor equal to 4.283×10^9 $mm^3 \cdot s / kg \cdot h$.

3.3 Rainfall monitoring

An ONSET S-RGB-M002 heating tipping bucket rain gauge (Figure 3.6) was calibrated at the beginning of every monitoring period at the laboratory of Institut National de la Recherche Scientifique (INRS). For the calibration, 373 ml of potable water was allowed to drip from the bottom of a plastic container through the mesh area of the rain gauge. As stipulated by the device manual, a successful calibration is attained when the poured water produces 100 ± 1 tick (1 tick = 0.2 mm), in one hour. After the calibration, the rain gauge was installed on the rooftop of the library, located next to the site with a configuration to record data at a 5-minute interval. The data was transmitted wirelessly by a HOBO MicroRX station data logger. Rainfall data collection gaps were experienced throughout the monitoring period due to the rain gauge system malfunction and intermittent electrical breakdowns. Data were collected up until the beginning of the winter (November) and resumed at the end of winter (May). During the winter season, since most of the precipitation fell as snow, de-icing activities on the watershed were monitored instead.

Figure 3-6 ONSET S-RGB-M002 heating tipping bucket rain gauge and the HOBO micro station data logger installed on the roof of the Le Tournesol library

3.3.1 Rainfall data pre-processing and validation

A 5-minute rainfall time series was extracted from the HOBO MicroRX station data logger and verified for errors that may have arisen due to technical malfunctions. Prior to separating the rainfall data into a series of storm events, the data was validated to ensure that precipitation recorded on the site is not over- or under-estimated, which would affect the data analysis process. The validation process was divided into two steps:

1. Validating the raw rainfall time series by comparing the projected number of steps to the actual rainfall duration. A value less than the theoretical number of steps indicates missing data, which must be addressed while analysing the rainfall time series. A number greater than the theoretical number of steps indicates duplicates that must be removed.

2. Comparing the monthly precipitation data collected from the site to the Jean-Lesage Airport rain gauge operated by Environment and Climate Change Canada (ECCC), located 11.6 km south of the site. Although there may be some discrepancies between the rainfall data collected daily at the two rain gauges due to the spatial heterogeneity of rainfall, the monthly data should be comparable. Furthermore, a systematic underestimation or overestimation of the daily rainfall observed at the Le Tournesol library rain gauge compared to the ECCC rain gauge may be a sign of malfunction.

3.3.2 Rainfall event classification

In hydrological modeling, rainfall event classification helps to categorize different types of rainfall based on their characteristics that impact the hydrological system. Shahed Behrouz et al. (2020) found that rainfall event characteristics such as low and high intensity affect the model calibration and post-calibration assessment. The rainfall event classification and assessment of the hydrological performance requires separating the observed rainfall data series into hydrologically significant events. For this purpose, three separation criteria were used:

1. Any time step with less than 0.2 mm of rain was considered dry weather.
2. Events separated by 6 hours or more of dry weather were considered independent. This duration corresponds to the upper limit of the time required for the water retained in the storage reservoir of the PP to be evacuated by the underground drain (Duchesne et al., 2022).
3. A minimum cumulative rainfall depth threshold of 5 mm was considered. Based on a previous study on the site, events with cumulated rain depth less than 5 mm generate little to no flow from both surfaces.

3.4 Overview of the site's drainage network and infrastructure

The drainage area consists of two subcatchments with the PA and CA. According to the technical specification, the subcatchments have surface slopes varying from 1.4 % to 1.8 % allowing runoff to drain into their respective catch basin. As illustrated in Figure 3.7, surface runoff from the CA area is first routed to the catch basin PU-2 and then to manhole RP-1 by an underground 200 mm diameter, high-density, PVC pipe routing water to the municipal drainage network. This flow routing facilitates flow measurement and water quality sampling at RP-1 and PU-2, respectively.

On the PA, rainfall infiltrates through the PA layers to the storage layer and the native soil. When the infiltrated water within the storage layer reaches the underdrain level, it is transported by the 150 mm perforated underdrain pipe to the catch basin PU-1, which is also directed to the manhole RP-1 by a 200 mm diameter, high-density, PVC pipe. The water in the RP-1 is finally routed to the municipal network. Some field visits during rainfall events revealed that pounding occurred on the PA surface resulting in surface runoff entering directly into the catch basin PU-1 through the manhole cover without infiltrating through the PA. This condition resulted in flow recorded at the monitoring location (RP-1) for all rain events on the site. As such, flow measured from the PA at the exit of the pipe at manhole RP-1 is a sum of underdrain flow (if any is observed or measured) and surface runoff.

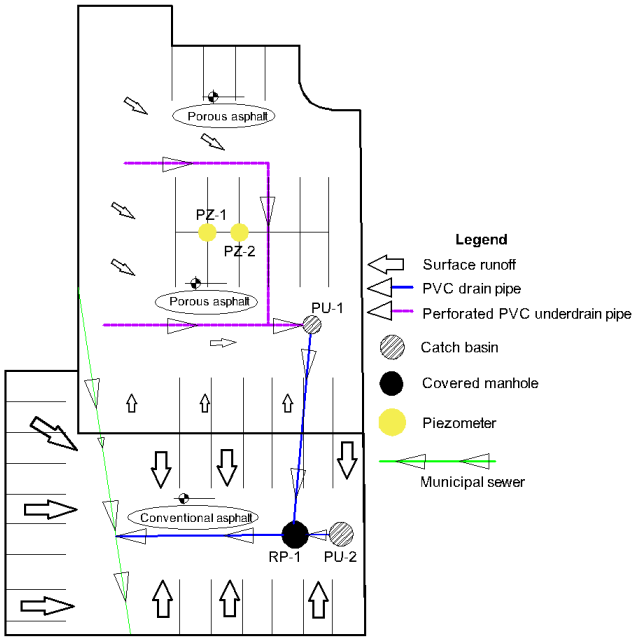

Figure 3-7 Hydraulic diagram and flow routing on the study zone

3.5 Monitoring of the hydrological performance of the porous asphalt

3.5.1 Runoff monitoring

Figure 3.8 shows that outflows from the CA, and the sum of surface runoff and underdrain flow (subsurface flow) of the PA, were measured respectively in the two incoming pipes of manhole RP-1. The underdrain flow (subsurface flow) was also measured upstream of catch basin PU-1. Two 8-inch and one 6-inch Thel-Mar weirs (compound rectangular-triangular weir) (Figure 3.9) were installed at the outlet pipes (C1 and C2) of the subcatchments to estimate their flows from measured water levels (see below). The maximum flow that can be measured by the 8-inch weir is 5.44 L/s at a height of 99 mm from the top of the triangular notch. Note that water height below 30 mm (measured from the weir) is within the dead pool or the threshold height, which means there is no outflow, while water heights above the maximum weir height were not considered. Flows from the catchment outlet pipes were considered to begin and terminate when the water height was above the dead pool.

Wireless Bluetooth HOBO MX2001 pressure probes (Figure 3.9) were installed approximately 20 cm upstream of the weirs to measure pressure (barometric and absolute) and temperature at 1-minute intervals. During each rainfall, the water height in the pipes were estimated by relating the

barometric pressure and water pressure readings with water density. Prior to the installation of the pressure probes in the field, they were calibrated in the INRS laboratory at the beginning of each monitoring period. Each HOBO MX2001 was calibrated using water in a container, and the probe was inserted at a precise known level. Readings for the calibration were taken once the water in the container had stabilized. During the analysis of field data in 2023, an error was noted in the barometric pressure reading. The barometric pressure readings were at some points higher than the absolute water pressure readings during flow events. As a result, runoff volumes and rates prior to August, 2023 could not be computed with certainty and were omitted from the analysis. The error due to this condition was corrected by calibrating and installing a HOBO U20L-04 pressure probe to measure barometric pressure, which was used for the subsequent (August 2023 to July 2024) water depth computations.

During the 2024 monitoring period, high runoff volumes were observed from the PA outlet (C1), which was inferred to be excess surface runoff which flowed directly into catch basin PU-1. To verify this hypothesis, a 6-inch weir and a MX2001 probe were installed at the outlet of the PA underdrain (Figure 3.8, pipe C3) to estimate the flowrate from the drain. The 6-inch weir had a maximum height of 69 mm, measured from the top of the V-notch, and could measure flows up to 2.02 L/s with a dead pool height of 17 mm. Table 3.2 provides an overview of the equipment installed in the catchment area to monitor flows, along with the specific locations where each instrument is placed.

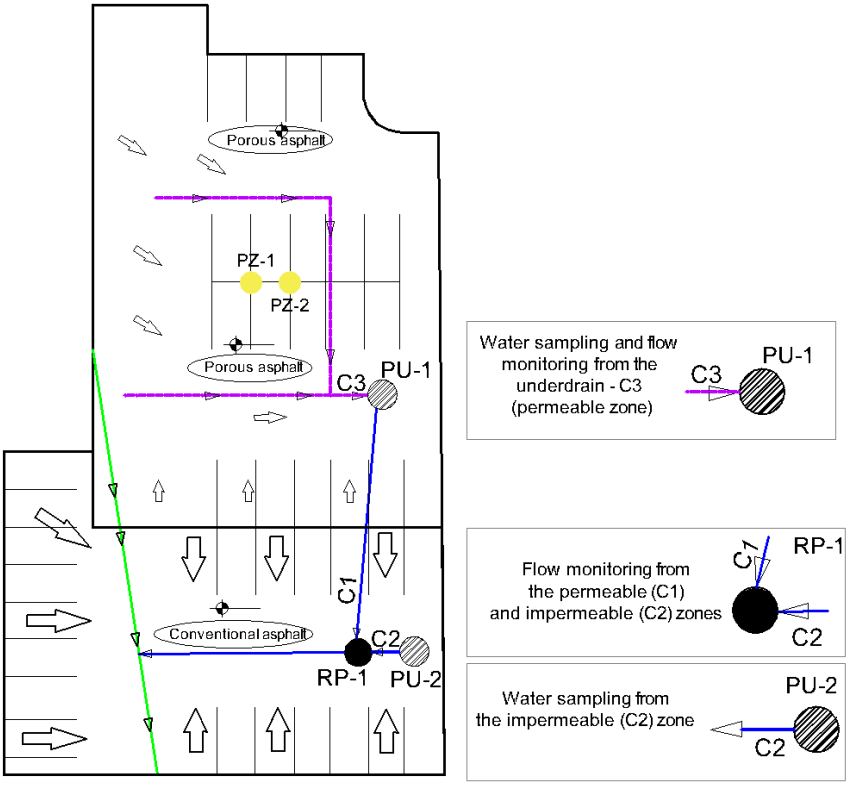

Figure 3-8 Location for the Thel-Mar weirs, HOBO MX2001 pressure probes, and ISCO 3700 sampling equipment for flow and water sampling monitoring

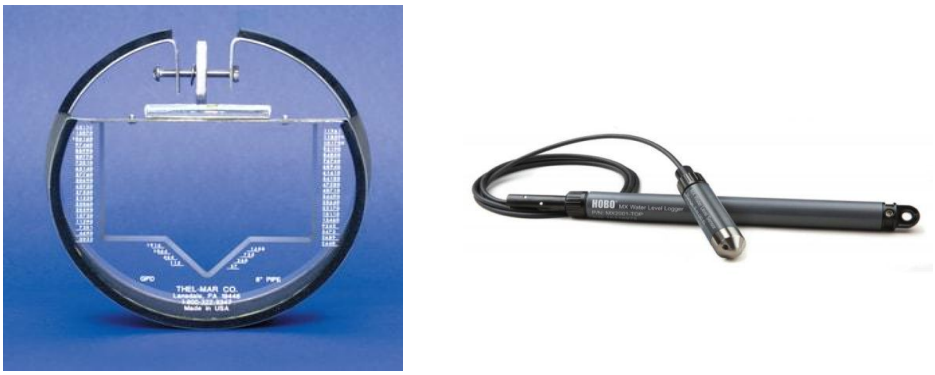

Figure 3-9 Thel-Mar weir (left) and HOBO MX2001 pressure probes (right) for flow monitoring

Table 3.2 List of equipment installed to monitor water flow and level in the structure

Use	Instrument	Location
Measuring the height of water in the underground reservoir	• 1 HOBO MX2001 pressure sensor	PZ-1
Measuring water level and atmospheric pressure in catch basin PU-1	• 2 ONSET U20L-04 pressure sensor	PU-1
Measurement of water flow and temperature in permeable and impermeable zones	• 2 HOBO MX2001 pressure and temperature probes • 2 Thel-Mar weirs (8-inch weir)	RP-1
Measurement of permeable zone water flow and temperature from drain (2024 only)	• 1 HOBO MX2001 pressure and temperature sensor • 1 Thel-Mar weir (6-inch weir)	PU-1

3.5.2 Flow computation from the weir and the HOBO data.

Both the 8-inch and 6-inch Thel-Mar weirs have manufacturer's manuals that correlate the water height upstream from the weirs (mm) with the associated flow rate (L/s), as shown in Figures 3.10 and 3.11. Water height was measured using a HOBO MX2001 sensor for absolute pressure and a HOBO U20L sensor for barometric pressure. The differential pressure, calculated as the difference between the absolute and barometric pressures (see Eq 3.2) was then used to compute the water height (see Eq 3.3). Finally, the flow rate is determined by interpolating the computed water height using the graphs in Figures 3.10 and 3.11.

$$P_{diff} = P_{abs} - P_{baro} \qquad 3.2$$

where P_{diff} is the differential pressure (kPa), P_{abs} is the absolute pressure (kPa), and P_{baro} is the atmospheric pressure (kPa).

$$H_w = \frac{P_{diff}\,(10 \times 10^6)}{\rho g} \qquad 3.3$$

where H_w is the water height through the weir (mm), P_{diff} is the differential pressure (kPa), ρ is the density of water taken as 997 kg/m^3, and g is acceleration due to gravity taken as 9.81 m/s^2.

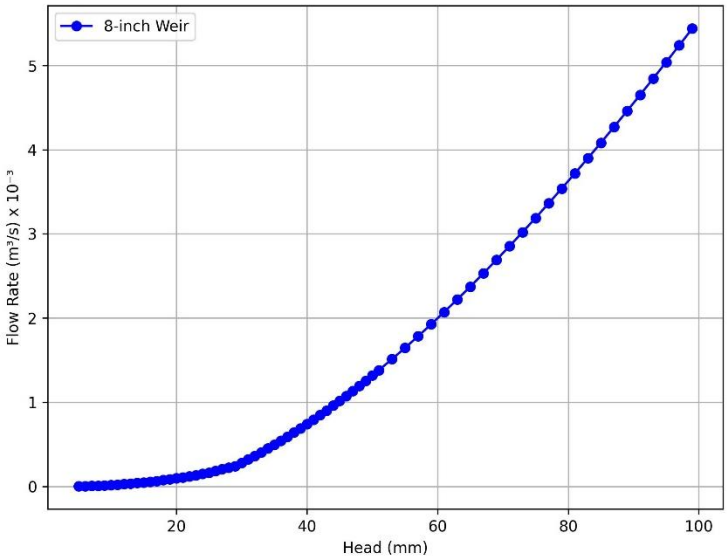

Figure 3-10 Rating curve for the 8-inch Thel-Mar weirs

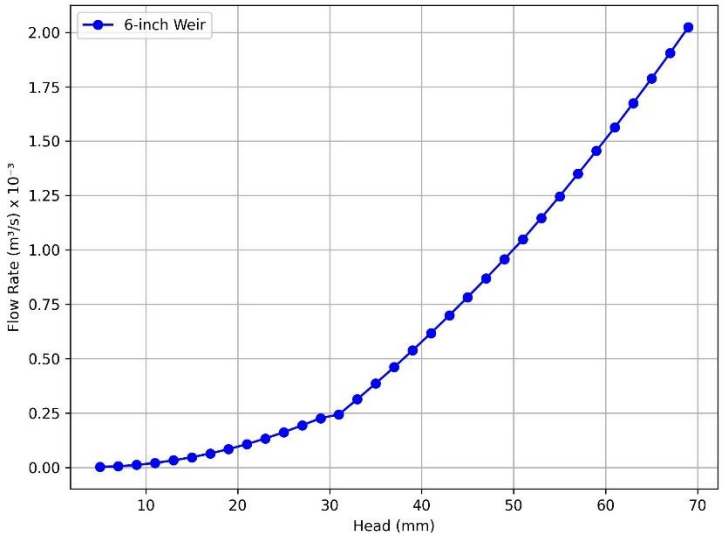

Figure 3-11 Rating curve for the 6-inch Thel-Mar weir

3.6 Monitoring of the environmental performance of the porous asphalt

Physico-chemical contaminants in runoff water was monitored for both pavements by undertaking sampling campaigns spreading over two consecutive years (April to November 2023 and 2024). During this period, one sample was collected in 2023 (September 18) and two samples in 2024 (June 23 and August 10). Winston et al. (2016a) found that water quality performance of PP could

lead to conservative results, because sampling tends to represent storms of high depth, which generate more contaminants.

3.6.1 Sampling methods and protocols

A composite sampling method was adopted to sample runoff from the CA. This was achieved by installing an ISCO 3700 automatic sampler (Figure 3.12) in catch basin PU-2. After laboratory calibration of the automatic sampler at INRS, it was configured to sample 150 ml of water in each of the 24 bottles (Figure 3.13) at every 10 minutes. The automatic sampler had a moisture detector and suction line which were placed about 1 m upstream of catch basin PU-2 in pipe C2. Before the start of each sampled rainfall event, the 24 bottles in the automatic samplers were manually emptied, washed and placed in their positions. During rainfall, when water was detected by sensor in the pipe C2, the automatic sampler was triggered to collect water samples by the help of the suction tube. The collected samples were stored in the 24 bottles inside the automatic sampler. After mixing the contents of the 24 bottles, a single composite sample was taken to be analysed. All sampling bottles were cleaned prior to use to prevent external contamination.

Figure 3-12 Autosampler installed in catch basin PU-2

Figure 3-13 Automatic sampling from the conventional asphalt during a flow event

As for the PA, the sample taken on the rainfall event of September 18, 2023, was collected as a single sample from the outlet of the PA underdrain (in catch basin PU-1) as shown in Figure 3.14, which was assumed to be representative of the water quality leaving the reservoir towards the municipal drainage system. Only one sample was collected during season 2023 due to absence of flow from the PA underdrain (except for September 18, 2023). This condition continued during the 2024 monitoring season even after surface cleaning of the asphalt. To compare the water quality of the PA and CA, for the event on June 23, 2024, samples were collected from the piezometer PZ-2 (see Figure 3.8) using a peristaltic pump (Geotech Geopump 2 model), as shown in Figure 3.15. For the August 10, 2024 event, the PA sample was collected in a depression located at the outlet of the underground drain. During this event, for which 81 mm of rain was recorded by the ECCC rain gauge, it is possible that water flowed through the drain. The water collected for the sample, after the end of the rain, is therefore most likely water that accumulated in this location during the rain.

Figure 3-14 Manual sampling of water from the underdrain

Figure 3-15 Sampling from the observation well (piezometer PZ-2) using a Geopump peristaltic pump from Geotech Environmental Equipment Inc

After each campaign, samples were stored in their respective bottles (Figure 3.16), where they were labeled, and placed in coolers for same-day transport for analysis. Pre-washed plastic 50 ml and 1 L tinted glass bottles were used to store samples for heavy metals and C_{10}-C_{50} hydrocarbons analysis, respectively, while plastic 1 L bottles were used for TSS, TN, TP and COD. The samples were analysed at INRS laboratory and Université Laval's Laboratory of water and environment headed by Prof. Paul Lessard. Table 3.3 shows the analysis protocols for the various water quality parameters.

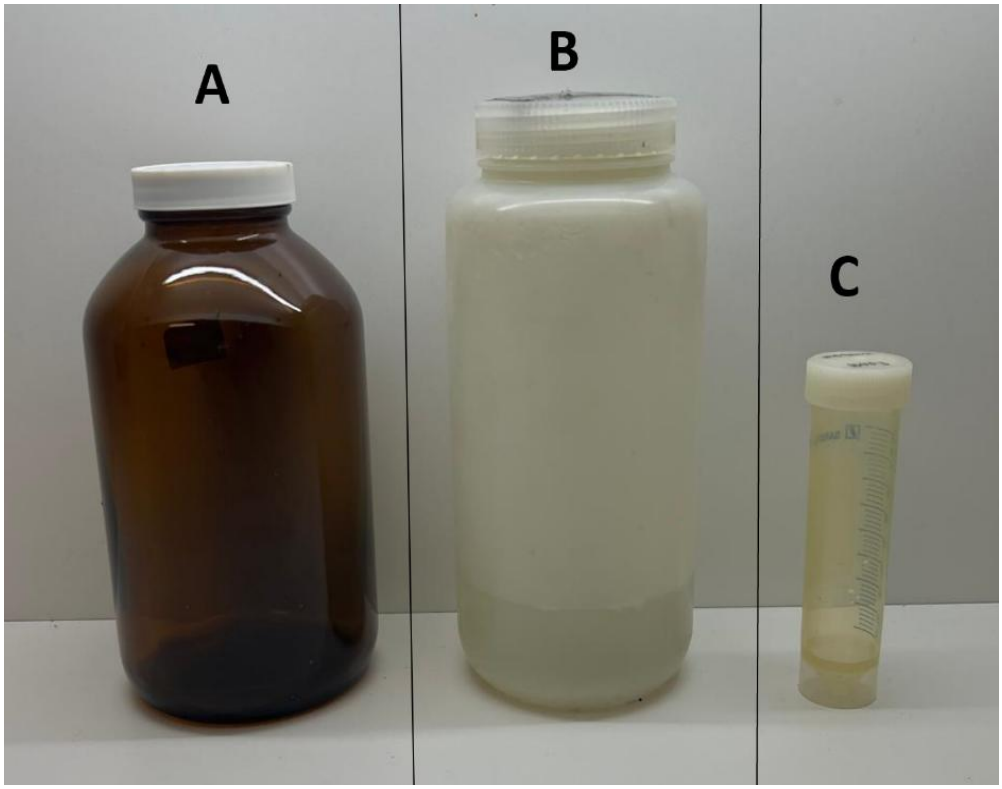

Figure 3-16 Samples bottles used for the different water quality analysis. A – glass bottle used to store samples for total petroleum hydrocarbons C_{10}-C_{50}; B – plastic bottle used to store samples for TSS, TN, TP, and COD analysis; C – plastic bottle used to store samples for total cations

Table 3.3 Parameters analysis for runoff water quality, sampling protocol and laboratories for analysis

Parameters	Sample storages	Analysis protocols	Laboratory
TSS	4 °C	MA 115-SS protocol. 1.2	Université Laval

Parameters	Sample storages	Analysis protocols	Laboratory
Total major cations	Collect 40 ml of well-mixed unfiltered sample, add 0.4 ml of HNO_3, add 0.2 ml of HCl, heat at 100°C for 2 h, make up the volume to 50 ml with ultrapure water	Analysis by ICP-AES Agilent 5110 Dual View. US EPA Method #200.7	INRS
Total trace cations	Collect 40 ml of well-mixed unfiltered sample, add 0.4 ml of HNO_3, add 0.2 ml of HCl, heat at 100°C for 2 h, make up the volume to 50 ml with ultrapure water	Analysis by ICP-MS Thermo X series. US EPA Method #200.8	INRS
TP	4 °C, H_2SO_4	Hach TNT 826	Université Laval
TN	4 °C, H_2SO_4	Hach TNT 826	Université Laval
Total petroleum hydrocarbons	Unfiltered, 4 °C	Liquid-liquid extraction using the ampoule with hexane.	INRS
		Purification with silica gel.	
		Assay by gas chromatography coupled with a flame ionization detector (GC-FID Agilent 7890B).	
		Based on the “MA.400-Hyd 1.1” method from the Center of Expertise in Environmental	

Parameters	Sample storages	Analysis protocols	Laboratory
		Analysis of Quebec (CEAEQ).	
COD	4 °C	Hash 8000	Université Laval
pH	4 °C	-	Université Laval
EC	4 °C	-	Université Laval and INRS

3.6.2 Temperature monitoring

Analyzing the temperature reduction of runoff from permeable and impermeable pavement is important because it helps to evaluate the impact of runoff on aquatic ecosystems and general pavement surface heat. During each rainfall event, water temperature data were recorded at one-minute intervals at manhole RP-1 using HOBO MX2001 sensors. These measurements captured the temperature of runoff from the impermeable zone pipe (C2) and the flow from the permeable zone pipe (C1). Similarly, the water temperature in PZ-1 was monitored by installing a HOBO MX2001 sensor at the bottom of the storage layer of the PA, providing continuous temperature readings for that layer.

3.7 Hydrological modeling of the site

The numerical hydrological model of the site was built using the Personal Computer Storm Water Management Model (PCSWMM) software (https://www.pcswmm.com/). This software uses the computational engine of the Storm Water Management Model (SWMM 5) (https://www.epa.gov/water-research/storm-water-management-model-swmm). SWMM 5 is a dynamic rainfall-runoff simulation model that can simulate runoff generation, routing, and treatment in urban drainage systems. SWMM can also incorporate various LID practices, such as PP (PA), to evaluate their effects on the hydrological cycle and water quality.

In the SWMM LID module, the pavement is modeled as a rectangular subcatchment with a constant slope (S) and width (W), which drains either to a catch basin or to another subcatchment. The PA is conceptualized in the LID module by solving a set of continuity equations through four layers. As shown in Figure 3.17, vertical water movement occurs within and between layers of the PA. By considering the water balance of each individual layer, the rate of water transferring between the layers over time, expressed in mm/hr, is determined. The inflow, which is the precipitation hydrograph to the LID unit (plus runoff from an upstream subcatchment if present) is thus transformed into a combination of runoff, infiltration, storage, and drainage into the nearby native soil by numerically solving the continuity equation at each time step.

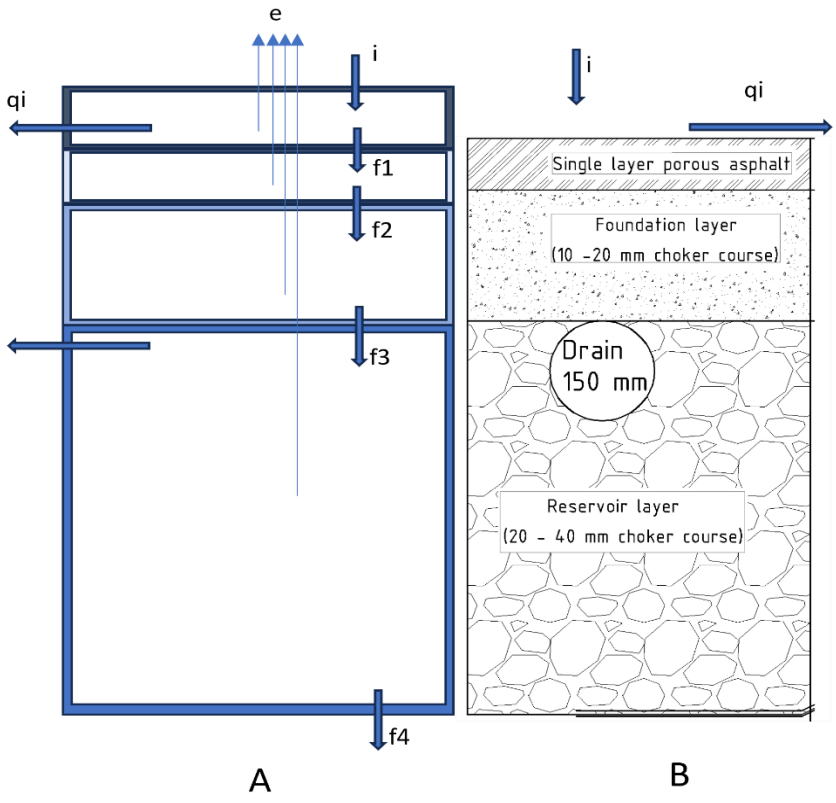

Figure 3-17 PCSWMM conceptualised model representation (A) and the cross section of the porous pavement (B)

For the PA, the overall water balance is modeled using the continuity equation (Eq. 3.4) by neglecting evaporation losses due to the relatively small size and the nature of the study zone.

$$\frac{\partial d}{\partial t} = i - f - q \qquad 3.4$$

where d (mm) is the head of ponded water on the surface, t is time (h), i is the rate of precipitation (mm/hr), f is the infiltration rate (mm/hr), and q is the runoff rate (mm/hr).

In the case of the CA, runoff is generated when the ponded surface water exceeds the depression storage. The depression storage depth was determined from visual/estimated measurement from the site. Runoff rate q is estimated using Eq. (3.5), d_s is the depth of depression storage, S is the slope of the subcatchment, W is the width of the catchment, n is Manning's roughness coefficient, and A is the area of the subcatchment. For a large catchment area like the study site, the flow width can be estimated to be very large compared to the flow depth making this equation applicable. However, the study does not include a formal derivation or analysis to establish the specific conditions under which this assumption may be invalid.

$$q = \frac{WS^{\frac{1}{2}}}{An} (d - d_s)^{\frac{5}{3}} \qquad 3.5$$

3.7.1 SWMM inputs

The required data for the SWMM model are the input parameters that represent the physical characteristics and conditions of the study area, such as rainfall, land use, topography, and drainage network characteristics. These data are needed for building a reliable and representative SWMM model that can simulate the hydrological and hydraulic processes of urban runoff. According to Rossman (2015), the input parameters for SWMM can be divided into three types: subcatchment data, node data, and link data. Subcatchment data describe the properties of the land surface that receives precipitation and generates runoff, such as area, slope, width, imperviousness, roughness, depression storage, and infiltration parameters. Node data describe the points where runoff is collected, stored, or discharged, such as junctions, outfalls, storage units, and diversion structures. Link data describe the conduits that transport runoff between nodes, such as pipes, channels, pumps, and weirs.

3.7.2 Revised representation of the study site in PCSWMM

Although the study area comprises two subcatchments, the PCSWMM model was developed with three subctachments comprising the CA, and the PA divided into two separate subcatchments (Figure 3.18): (a) clogged pavement area, which takes account of the non-infiltrating surface of the PA, and (b) pervious/infiltrating pavement area, which is simulated with the LID module (PA). The areas of (a) and (b) were determined by varying the area of each subcatchment for different rainfall events and surface conditions until the observed and simulated hydrolographs matched. The clogged pavement drains runoff directly into the catch basin PU-1 as direct inflow, which mimics the site runoff real conditions during rainfall events. Note that all dimensions for the manholes, pipe sizes, and subcatchment areas were taken from the plans provided by the MTTD, and were verified with site visits and field measurements. Inconsistent data identified in the plans, such as negative pipe slopes, were corrected, for example for pipes C2 and C3. The initial presence of water in the manholes was also accounted for by specifying the initial water depth in the nodes during modeling. For catch basins PU-1 and PU-2 and manhole RP-1, the initial water depth was taken as the invert of pipes C1, C2, and C3, respectively.

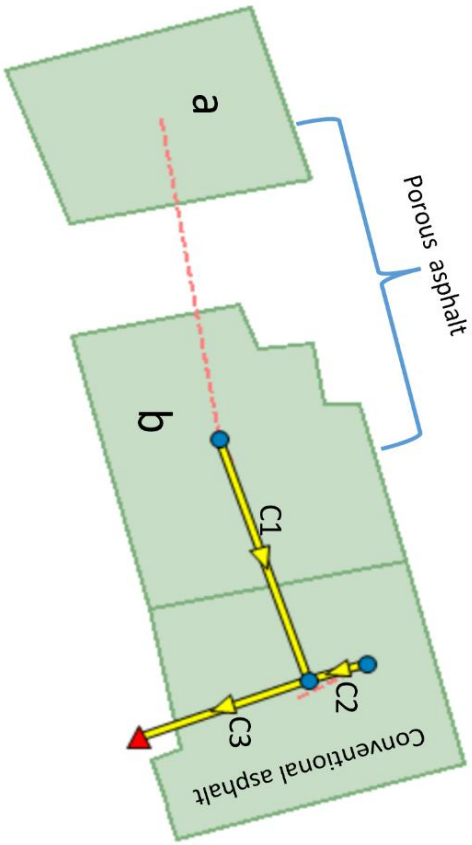

Figure 3-18 Modification to the porous asphalt subcatchment during the PCSWMM modeling; clogged porous asphalt area (a), and infiltrating porous asphalt area (b) which is modeled with the LID module

3.7.3 Underdrain Flow

The underdrain pipes of the LID module were modeled as PVC pipes and positioned 450 mm from the bottom of the reservoir layer. This configuration maximizes the reservoir layer's storage capacity and promotes optimal seepage into the native soil. In PCSWMM, flow from the underdrain pipe is estimated as a function of hydraulic head stored above its base as expressed in Eq. 3.6.

$$q = C\,(h - H_d)^n \qquad 3.6$$

where q (mm/hr) is the outflow from the underdrain, h (mm) is the head of stored water in the storage layer, H_d is the drain offset height taken as 450 mm here, C is the drain coefficient and n is the drain exponent. Thus, there is no flow through the underdrain pipe until the water in the storage layer reaches H_d. In the case of the study site, the full storage volume is achieved in the storage layer because the underdrain is placed at full storage height (Figure 3.7b). Since the underdrain consists of slotted pipes and each slot acts as an orifice, the drain exponent was taken as 0.5 and the drain coefficient was taken as 13.15 (Rossman, 2015) as computed with Eq. (3.7).

$$C = 60000 \times \frac{A_d}{A_{LID}} \qquad 3.7$$

where A_d is the total slotted area, taken as 1232 cm^2, and A_{lid} is the LID module area, taken as 562 m^2.

In practice, the PP occupies the full area of 854 m^2 but due to the modifications made in the model to consider the clogging effect (see Figure 3.18), the PP was modeled as an LID occupying 562 m^2. For this reason, the depth of each modeled LID layer in PCSWMM was altered to represent the available storage volume (Table 3.5), calculated by multiplying the actual depths by the total PP area of 854 m^2.

Table 3.4 Comparing the volume and depth of the LID layers in the field and when modeled in PCSWMM

LID layer	Volume (m^3)	In-situ depth (mm)	PCSWMM LID modeled depth (mm)
Pavement layer	68.32	80	120
Soil/Foundation layer	170.8	200	300
Storage layer	512.4	600	900

3.7.4 Calibration and validation of the model

3.7.4.1 Calibration

The purpose of calibrating the model is to adjust the values of the parameters such that the results of the model match as closely as possible the measured data. In other words, the parameters are adjusted to compensate for the unknown real conditions of the catchment. A combination of automatic and manual calibration methods was employed to determine the calibration values. In the first step, the PCSWMM SRTC tool was used to analyze the hydrograph response and then calibrate the model with total runoff volume as an objective function. During the second step, a manual calibration was performed to optimise the values obtained from the first step through an iterative process. This step is essential as it allows for adjustments to fine-tune the initial calibration results (step 1), ensuring the model accurately represents the detailed hydrograph characteristics for wider rainfall events. For the second step of calibration, the simulated flows were compared against the observed flows time series using the total runoff volume as benchmark. Parameters values were modified, and the model was resimulated multiple times to minimize discrepancies with observed total flow volumes at an accepted Nash-Sutcliffe model efficiency coefficient (NSE) value, computed with Eq. 3.8:

$$NSE = 1 - \frac{\sum_{i=1}^{n} \left(Q_{obs,i} - S_{sim,i}\right)^2}{\sum_{i=1}^{n} \left(Q_{obs,i} - Q_{obs}\right)^2} \qquad 3.8$$

where $S_{sim,i}$ is the simulated flowrate at time step *i*, $Q_{obs,i}$ is the observed flowrate at time step *i*, Q_{obs} is the mean of observed flowrate, and *n* is the total number of time steps. The NSE value varies between $-\infty$ and 1, the latter implying a perfect match between simulated and observed values. NSE values less than zero show a very poor model performance. The calibration of the model is considered satisfactory for the range 0.5 < NSE ≤ 0.7. NSE values between 0.7 and 0.8 are usually considered good, while values ≥ 0.8 are considered very good. NSE values below 0.5 are usually considered unsatisfactory (Rossman, 2015) and indicate a need for further calibration or data collection.

The model is said to have been calibrated when differences between simulated and observed hydrographs are reasonably small and the final calibrated parameters are within their acceptable thresholds (Rosa et al., 2015).

The criteria used to select the rainfall events for calibration were:

1. The event should reflect the typical storms experienced within the catchment.
2. The duration and total rainfall depth were sufficient for presenting a hydrograph curve suitable for calibration purposes.
3. The events characteristics, including the total rainfall depth, the average maximum 5 minutes rainfall intensities, etc., are not similar for each selected rainfall events.

To summarise, the steps for the calibration were as follows:

1. Identifying the subcatchment for which the model is calibrated (pervious or impervious).
2. Plotting the observed and simulated flowrates for the selected subcatchment.
3. Identifying the objective output (total runoff volume).
4. Adjusting each parameter independently to identify the changes in both simulated and observed hydrographs.
5. Adjusting all the parameters to maximize the NSE.

The model for the CA catchment was calibrated with the August 8, 2023, and October 7, 2023, rainfall events. The most sensitive parameter, which is the depression storage depth for the impervious surfaces (Dstore imperv), was first adjusted, followed by the impervious area without depression storage (zero imperv), the catchment width, the Manning roughness coefficient, and the slope, until satisfactory NSE coefficient is attained.

As for the model for the PA catchment, it was calibrated using the August 30, 2023, and June 7, 2024, rainfall events for the automatic and manual calibration, respectively. The parameters

adjusted during the calibration process were the IR of the pervious (unclogged subcatchment) and, for the clogged subcatchment, the catchment slope, the flow width, the Manning's roughness coefficient and the Dstore imperv.

3.7.4.2 Validation

The calibrated model was validated by running a simulation with one rainfall event each for PA (July 24, 2024) and CA (September 18, 2023). These events were selected to reflect typical rainfall experienced within the catchment. The simulated and observed hydrographs were assessed based on the NSE. The validation process was accepted, and the model was said to suitably represent the catchment hydrological performance, for NSE values higher than 0.5.

4 RESULTS AND DISCUSSION

4.1 Infiltration rate of the porous asphalt

Figure 4.1 presents the IR measured at each point before and after cleaning (2023 to 2024). Table 4.1 displays the average IR, including the measurements taken in July and August, 2024. Note that the IR at point 4 was not measured after clean-up because it was inaccessible to the vacuum truck.

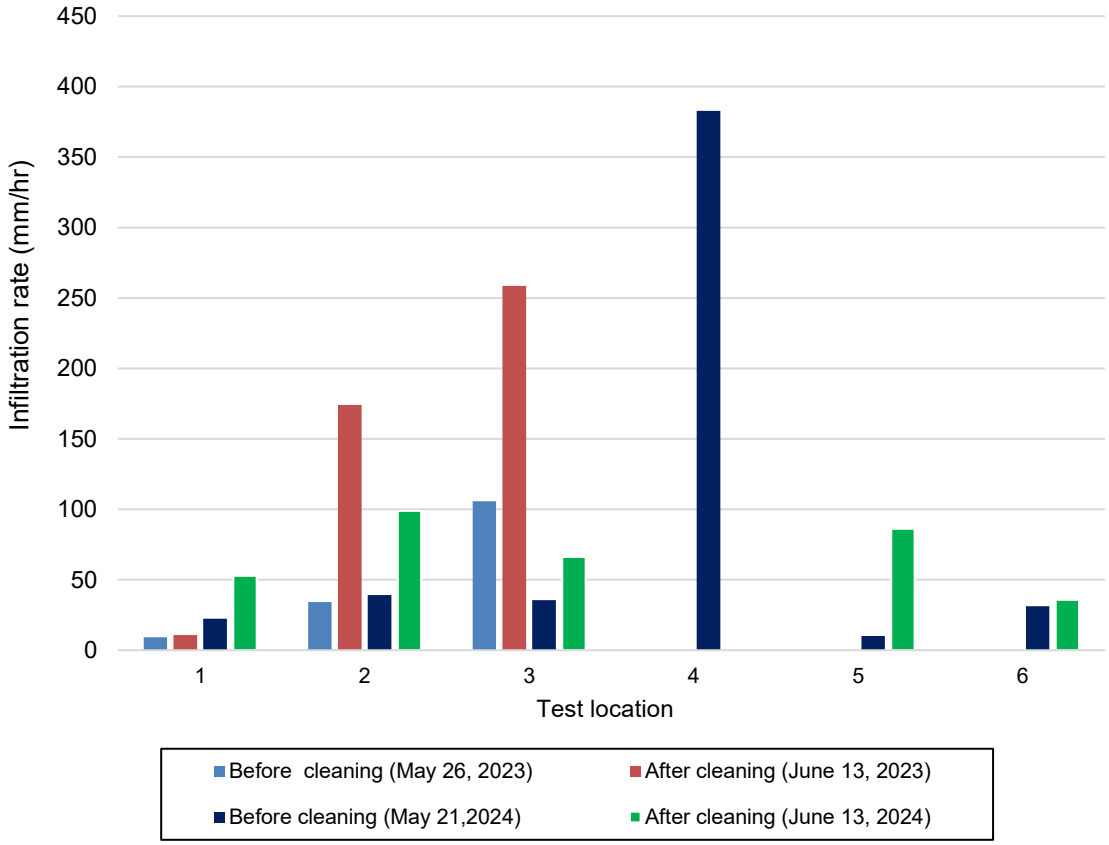

Figure 4-1 Infiltration rate (IR) for the various test points

In Quebec, and many other cold climate regions, winter abrasives (sand or gravel aggregates) are commonly used to improve safety conditions on public roads and parking lots during winter. The exposure of PA to sediment can lead to clogging of the porous spaces which reduces the infiltration of stormwater. These practises can result in diminishing the hydraulic and environmental performances of the system over time. The decision to clean PP by authorities is

when the IR has reduced to a threshold specified by standards. According to the Wisconsin Department of Natural Resources (WDNR, 2021) technical standard, an in-service PP should have an average IR of 254 mm/hr. A study by Danz et al. (2020) suggested that a surface IR less than 230 mm/hr is considered clogged as rainfall is not uniformly distributed on the surface.

Table 4.1 Descriptive statistics of the surface infiltration rates of the PA

Test date	Infiltration rate (mm/hr)		
	Range	Average	Standard deviation
May 26, 2023	9 - 106	50	41
June 13, 2023	11 - 259	148	103
May 21, 2024	10 - 383	87	133
June 13, 2024*	36 - 99	68	23
July 17, 2024	2 - 191	41	68
August 27, 2024	3 - 202	40	72

*One test location was not measured on this date.

All the test locations had varying IR but were all below the in-service criteria stipulated by Interlocking Concrete Pavement Institute (ICPI, 2008) and WDNR (2021). Measured surface IR on May 26, 2023 was in the range of 9 mm/hr to 106 mm/hr and the average rate was 50 mm/hr over the three test points (Table 4.1 and Figure 4.1). The low surface permeability observed could be caused by a lack of proper maintenance over the years. Physical observations showed that, though IR were low, the PA was able to infiltrate some of the rainfall prior to each cleaning.

After cleaning of the surface, IR ranged from 11 mm/hr to 383 mm/hr with an average rate of 148 mm/hr over the three test points. The average IR observed in 2023 (i.e., three years after construction) was significantly lower than the 2,540 mm/hr reported by Muttuvelu et al. (2024) in Denmark and by Selbig & Buer (2018) in Virginia for PA systems of similar age. In many other studies, average IR declined with time as the void space in the PA filled with sediment. By April 2022, approximately 17 months after construction was completed, the average IR of the PA on the study site was 2,237 mm/hr, reflecting a 63 % decrease of the average value in 2020, which was 1,409 mm/hr (Duchesne et al., 2022). However, in the subsequent 13 months (April 2022 to

May 2023), the average IR rate plummeted to 50 mm/hr, marking a drastic 98 % reduction of the value which was 2,237 mm/hr in April 2022. Following this sharp decline, the rate continued to decrease more gradually with minor fluctuations throughout the remainder of the monitoring period. This trend indicated the progression of asphalt clogging, which resulted in water accumulation on the surface of the PA, as illustrated in Figures 4.2 and 4.3. This suggests that the PA installed has not maintained its infiltrative capacity effectively over time. Selbig & Buer (2018) and Muttuvelu et al. (2024) revealed reductions in IR of 42 % and 92 % after three and nine years, respectively, following the initial construction.

Figure 4-2 Surface water pooling on permeable asphalt (photographed on September 18, 2023)

Figure 4-3 Pooling of water on the permeable asphalt surface (images captured on June 7 and 23, 2024, respectively)

Points 1, 2, 3, 5, and 6 were clogged at the beginning of 2023 according to the WDNR (2021) standard (min. 254 mm/hr). However, each successive cleaning of the pavement surfaces resulted in more than 50 % increases in the IR, except for points 1 and 6 which were below 14 % after the cleaning on June 13, 2023 and June 13, 2024. Point 4 maintained a high IR that periodically skewed the overall average IR as shown in Figure 4.1. Points 1, 5, and 6, which were within the main driving lanes of the parking lot, exhibited low IR. This could be due to a higher volume of vehicle movements compacting the sediment deeper into the porous media (Roseen et al., 2012) resulting in quicker and higher degree of clogging than for the remaining points. Moreover, even when less winter abrasives were applied on the PA lot during snowy periods, the driving lanes received additional amounts of sediments from the vehicles which used the lot and snow trucks that transported snow to the dumping site as seen in Figure 4.4. As expected, these areas began to clog and pond first and gradually transported sediment to other areas of the PA surface. The decline in IR was less noticed as distance increased from the main driving lanes; indeed, points 2, 3, and 4 had lower traffic, and thus showed relatively high IR on June 13, 2023 (point 2: 174 mm/hr; point 3: 259 mm/hr; point 4: 383 mm/hr), but then declined sharply on June 13, 2024, for points 2 (99 mm/hr) and 3 (66 mm/hr).

Figure 4-4 Sediment accumulation on the main driving lanes of the porous parking lot area

The significant reduction in IR for PA since autumn 2021 may be due to a combination of factors. On one hand, it is possible that the method of laying the PA has resulted in a lower void ratio than

that anticipated in the asphalt and/or that this void ratio has changed over time due to premature aging of the asphalt. On the other hand, it is possible that the clogging is due to the sediments that have clogged the asphalt pores. Although the use of sand as an abrasive in winter is prohibited on the study site, vehicles coming to the parking lot may have brought a certain amount of sediment to the study site (see Figure 4.4). Airborne or street-borne inputs are also possible.

Prior to June 2024, no standardised cleaning was done on the site from the time of initial construction in 2020. The use of the conventional street spring-cleaning method on the PA during the 2020-2022 period may have exacerbated the sharp decline of permeability. In evidence, the 2024 cleaning (see below) restored the average IR higher than the 51 % increase achieved by cleaning in the previous 2 years, from 2020 to 2022 (Duchesne et al., 2022). This confirms the need for proper cleaning as mentioned in many studies (e.g. Minnesota Stormwater, 2023; Støvring et al., 2018) to effectively restore IR of PP.

4.2 Restorative maintenance

Due to the clogging of the asphalt demonstrated by the results of infiltration tests in 2023, the deployment of cleaning trucks on the site on June 13, 2024, was considered as restorative maintenance. Additionally, this exercise helped to assess the efficiency of different types of cleaning trucks. These tests involved two passes of the vacuum trucks over the surface of the PA. Three different vacuum trucks - CityFant 6000, Ravo 5, and Elgin Whirlwind - were used on three different areas of the PA, as shown in Figures 4.5 and 4.6. The trucks all travelled at very low speed and maximum power, attempting to pass the suction nozzle over the entire area assigned to each. During the experiments, truck operators were encouraged to operate their vehicles in such a way to maximize the effectiveness of the maintenance. A small amount of water was used in each case, solely to control dust and prevent the equipment from overheating.

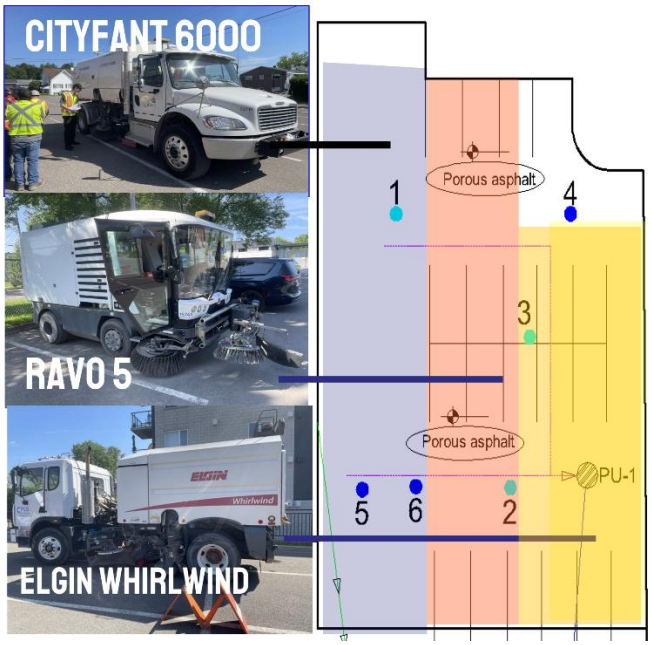

Figure 4-5 Areas covered by each vacuum truck during cleaning tests. The CityFant 600 covered the area shown in light blue, the Ravo 5 in orange, and the Elgin Whirlwind in yellow.

Figure 4-6 Site overview of the areas assigned to each vacuum truck during cleaning trials (left: Elgin Whirlwind; middle: Ravo 5; right: CityFant 6000)

Table 4.2 presents the measured pre- and post-cleaning IRs, and the calculated percent change. The CityFant 6000 passes resulted in 137 % and 753 % increases in IR at points 1 and 5 respectively, but only a 14 % increase at point 6. At point 3, located on the area vacuumed by the Elgin Whirlwind truck, the IR increased by 85 % following cleaning, from 36 to 66 mm/hr. As for the Ravo 5, at point 2, it led to a 153 % increase in the IR. However, although the improvements observed appear high when expressed in percentages, they are not sufficient to bring the IR above the 254 mm/hr threshold WDNR (2021), which is the minimum value for a well-maintained PP. In a study by Danz et al. (2020) on a PA nearly two years and 7-months after its initial construction, average IR increases of 16 % and 40 % were observed post-maintenance when a vacuum assisted street cleaner (Elgin Whirlwind) and compressed air and vacuuming were used, respectively.

Table 4.2 Infiltration test results for the restorative maintenance on June 13, 2024

Location	Truck	Infiltration rate (mm/hr)		% change
		Before cleaning	After cleaning	
1	CityFant 6000	22	53	137
2	Ravo 5	39	99	153
3	Elgin Whirlwind	36	66	85
4	n.a.	383	n.a.*	
5	CityFant 6000	10	86	753
6	CityFant 6000	31	36	14

* No infiltration test was carried out at this point after cleaning, as the vacuum truck did not cover this area.

4.3 Rainfall and hydrological characteristics of the study site

4.3.1 Evaluation of rainfall on the study site

The rain gauge installed on the roof of the library provided rainfall data for the period from May 2, 2023 to August 9, 2024 (with a break from October 19, 2023 to May 14, 2024). During the rainfall monitoring period, data loses were encountered due to technical problems with the rain gauge and data logger. Quebec City experiences a humid climate, with significant variations in monthly

precipitation. On average, the monthly precipitation can range from about 60 mm in the drier months (like February) to around 100 mm or more in the wetter months (like June and July). Annual precipitation in Quebéc City is in the range of 1261.1 to 1600 mm (Connolly et al., 2014). In 2023 and 2024, the annual precipitation recorded by Jean-Lesage Environment Canada rain gauge were 1262 mm and 1042 mm respectively (Environment and Climate Change Canada, 2025). The installation of the rain gauge was necessary to estimate the rainfall on site for modelling purposes. Table 4.3 compares the monthly rainfall measured by Jean-Lesage Airport rain gauge station and the rain gauge installed at the Le Tournesol library for the monitoring period.

Table 4.3 Monthly total rainfall depth recorded at the study site (bibliothèque Le Tournesol) during the monitoring period compared to the Jean-Lesage Environment Canada rain gauge data

Period	Total rainfall (mm)	
	Le Tournesol Library	Jean-Lesage Airport
2nd to 31 May, 2023	17	29
1st to 22 June, 2023	46	66
11 to 31 July, 2023	151	176
1st to 31 August, 2023	164	181
1st to 30 September, 2023	54	61
1st to 18 October, 2023	27	34
15 to 31 May, 2024	67	53
1st to 30 June 2024	162	164
11 to 31 July, 2024	59	59
1st to 5 August, 2024	3	7
3 to 6 and 24 to 30 September 2024	40	51
	Total = 790	**Total = 903**

Measured monthly rainfall on the study site was generally lower than those from Jean-Lesage airport except for May 15 to 31, 2024 where the rainfall was 14 mm higher. Differences between

the other measured periods at the study site and the Jean-Lesage rain gauge were between 4 mm to 25 mm, which could be due to spatial variability of rainfall. Results presented in Table 4.3 indicate that the rain gauge mounted on the roof of Le Tournesol Library provides a reliable measurement of the site's total rainfall.

4.3.2 Rainfall event characteristics

Summary of the main characteristics for all observed rainfall events with total depth greater than 5 mm are outlined in Table 4.4 including events runoff volumes and flowrates. The 5 mm threshold value was selected because it denotes the rainfall depth needed to produce significant surface runoff from the CA subcatchment. The minimum total rainfall depth, of 6.4 mm, was recorded on July 22, 2023 and the maximum, of 62.2 mm, was recorded on August 8, 2023. The event duration ranged from 1.2 to 33.4 hr. The analysis showed that the maximal 5-minute rainfall intensities varied between 4.8 mm/hr on July 11, 2024, and 69.6 mm/hr on June 26, 2024. Figure 4.7 presents the rainfall intensities and durations of the recorded events at the study site, overlaid with the 2-year, 5-year, and 10-year Intensity-Duration-Frequency (IDF) curves derived from the Charlesbourg Parc-Orléans rain gage (Mailhot & Talbot, 2025). Of the 35 rainfall events analyzed, 33 fall below the 2-year IDF curve, while only two events (#5 and #11) lie between the 2-year and 5-year curves.

Table 4.4 **Rainfall event and runoff characteristics**

Nº	Date (mm/jj/aa hh:mm:ss)	h total (mm)	I_{max} 5 min (mm/hr)	Antece-dent dry (h)	Rain duration (h)	Total outflow volume CA (l/m²)	Total outflow volume PA (l/m²)	Reduction total vol. (%)	Max. flow CA (l/s/ha)	Max. flow PA (l/s/ha)	Max. flow reduction (%)
1	05/20/23 23:40:00	15.2	9.6	103.5	10.6	-	-	-	-	-	-
2	06/13/23 13:15:00	9.8	16.8	70.1	10.6	-	-	-	-	-	-
3	06/14/23 08:05:00	9.0	16.8	8.3	1.4	-	-	-	-	-	-
4	06/15/23 02:25:00	7.0	16.8	16.9	9.8	-	-	-	-	-	-
5	07/13/23 20:15:00	38.8	45.6	39.9	3.6	-	-	-	-	-	-
6	07/16/23 10:40:00	24.6	36.0	58.8	4.3	-	-	-	-	-	-
7	07/21/23 11:45:00	7.8	16.8	57.1	10.7	-	-	-	-	-	-
8	07/22/23 06:35:00	6.4	7.2	8.2	5.3	-	-	-	-	-	-
9	07/31/23 04:05:00	13.2	62.4	58.2	10.4	-	-	-	-	-	-

Nº	Date (mm/jj/aa hh:mm:ss)	h total (mm)	I_{max} 5 min (mm/hr)	Antece-dent dry (h)	Rain duration (h)	Total outflow volume CA (l/m²)	Total outflow volume PA (l/m²)	Reduction total vol. (%)	Max. flow CA (l/s/ha)	Max. flow PA (l/s/ha)	Max. flow reduction (%)
10	08/03/23 09:55:00	28.8	31.2	67.4	27.5	> 27.5	4.9	n.a.	> 102.8	61.1	n.a.
11	08/08/23 00:40:00	62.2	33.6	83.3	24.5	58.3	32.0	45 %	99.1	43.5	56 %
12	08/10/23 19:25:00	20.0	57.6	42.3	9.5	> 16.9	> 5.9	n.a.	> 102.8	> 63.7	n.a.
13	08/13/23 00:05:00	6.6	24.0	43.2	6.9	> 5.6	1.6	n.a.	> 102.8	59.0	n.a.
14	08/13/23 18:20:00	8.4	21.6	11.3	5.0	7.3	1.6	78 %	87.9	45.6	48 %
15	08/18/23 08:40:00	15.4	52.8	19.1	8.8	> 12.5	> 5.4	n.a.	> 102.8	> 63.7	n.a.
16	08/30/23 10:55:00	10.0	24.0	12.6	6.3	5.8	1.9	67 %	63.6	29.6	53 %
17	09/18/23 09:55:00	45.2	9.6	85.0	33.4	32.3	8.1	75 %	23.7	9.3	61 %
18	10/07/23 19:20:00	23.8	7.2	114.8	24.5	21.7	2.2	90 %	23.7	5.3	78 %

Nº	Date (mm/jj/aa hh:mm:ss)	h total (mm)	I_{max} 5 min (mm/hr)	Antece-dent dry (h)	Rain duration (h)	Total outflow volume CA (l/m²)	Total outflow volume PA (l/m²)	Reduction total vol. (%)	Max. flow CA (l/s/ha)	Max. flow PA (l/s/ha)	Max. flow reduction (%)
19	05/17/24 20:20:00	25.6	33.6	54.7	10.8	> 42.7	> 16.06	n.a.	> 102.9	> 64.4	n.a.
20	05/23/24 04:25:00	12.2	36.0	117.3	7.6	> 11.5	> 6.35	n.a.	> 102.9	> 64.4	n.a.
21	05/27/24 09:20:00	8.2	16.8	71.3	5.5	-	-	-	-	-	-
22	05/27/24 21:25:00	14.4	36.0	6.6	12.3	-	-	-	-	-	-
23	06/07/24 03:35:00	18.6	16.8	223.9	7.0	34.4	12.9	62 %	63.6	39.8	37 %
24	06/07/24 18:50:00	18.4	14.4	8.3	17.3	25.1	9.5	62 %	39.2	31.8	19 %
25	06/09/24 10:30:00	13.2	43.2	22.4	11.3	> 14.0	> 7.1	n.a.	> 102.9	> 64.4	n.a.
26	06/10/24 14:50:00	8.0	19.2	17.1	6.7	6.7	6.1	9 %	53.9	52.8	2 %

Nº	Date (mm/jj/aa hh:mm:ss)	h total (mm)	I_{max} 5 min (mm/hr)	Antece-dent dry (h)	Rain duration (h)	Total outflow volume CA (l/m²)	Total outflow volume PA (l/m²)	Reduction total vol. (%)	Max. flow CA (l/s/ha)	Max. flow PA (l/s/ha)	Max. flow reduction (%)
27	06/14/24 01:30:00	13.0	33.6	7.2	1.8	> 13.7	> 6.5	n.a.	> 102.9	> 64.4	n.a.
28	06/23/24 07:25:00	42.0	9.6	220.1	13.8	84.1	> 20.0	76 %	47.8	19.5	59 %
29	06/26/24 04:55:00	8.4	69.6	42.7	7.8	> 5.0	3.0	n.a.	> 102.9	> 64.4	n.a.
30	06/26/24 23:50:00	17.6	45.6	11.0	7.2	> 25.7	> 10.4	n.a.	> 102.9	> 64.4	n.a.
31	06/29/24 13:50:00	20.0	7.2	48.3	13.1	24.4	2.8	88 %	24.9	7.6	70 %
32	07/11/24 11:25:00	7.8	4.8	13.6	2.6	7.3	0.1	99 %	15.0	9.4	37 %
33	07/16/24 03:00:00	8.6	33.6	9.1	1.2	> 6.8	> 5.1	n.a.	> 102.9	> 64.4	n.a.
34	07/24/24	16.8	12.0	95.3	14.3	25.5	6.0	76 %	77.2	29.9	61 %

Nº	Date (mm/jj/aa hh:mm:ss)	h total (mm)	I_{max} 5 min (mm/hr)	Antece-dent dry (h)	Rain duration (h)	Total outflow volume CA (l/m²)	Total outflow volume PA (l/m²)	Reduction total vol. (%)	Max. flow CA (l/s/ha)	Max. flow PA (l/s/ha)	Max. flow reduction (%)
	18:50:00										
35	07/31/24 10:40:00	14.0	55.2	130.8	8.4	-	-	-	-	-	-

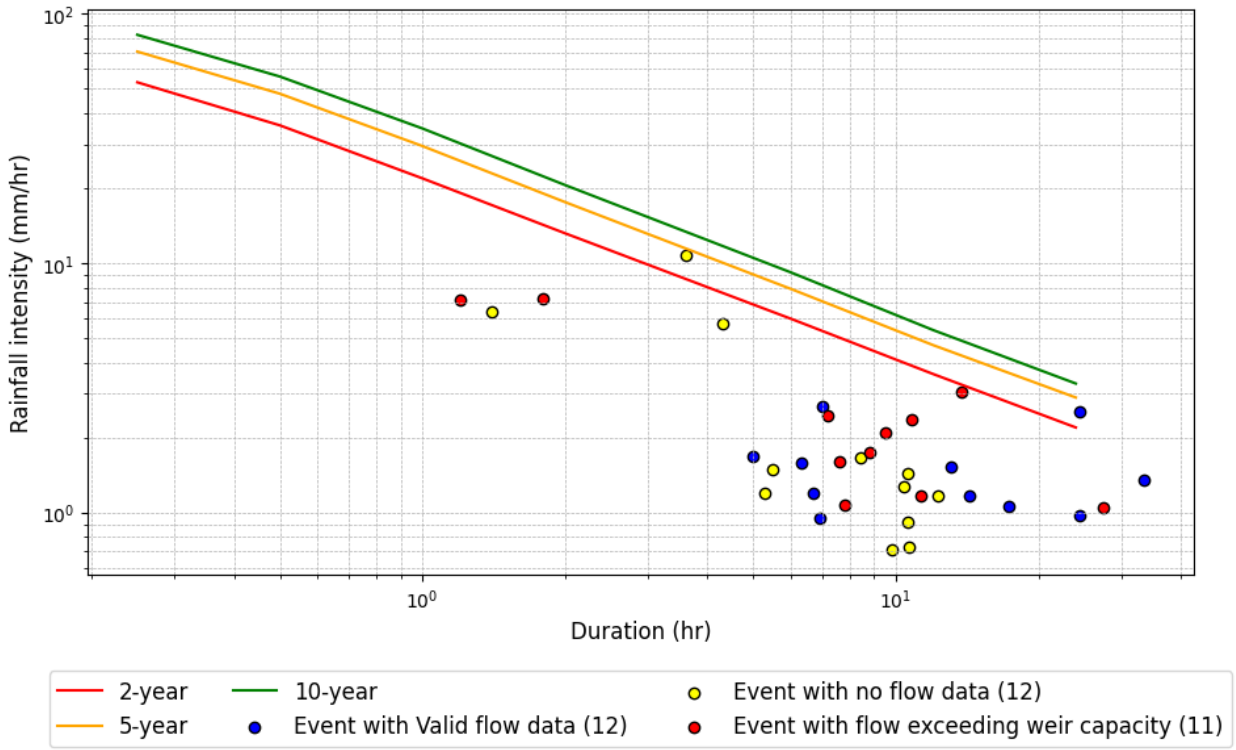

Figure 4-7 Rainfall intensity and duration of the recorded event at the study site, overlaid with 2-, 5- and 10-year IDF curves for Charlesbourg Parc-Orléans.

4.3.3 Evaluation of runoff volume and rate

Validated rainfall and flow data were used to evaluate the hydrological performance of the permeable zone in contrast to the impermeable one. For each rainfall event, the total volume of outflow was determined by integrating the discharge rate (Q, l/s) over the duration of the event. The flow duration was extended between 1 to 3 hours after the end of rainfall event (but without intermittent rain) until the minimum flowrate of the weir was stabilised to capture the complete runoff from the PA. To evaluate the performance of the two pavement types, both the total runoff volume and peak discharge were normalized by their respective drainage areas. Table 4.4 shows a summary of the rainfall events and their corresponding flow characteristics. Due to problems with one of the water level probes, the hydrological performance of the site could not be assessed for events #1 to #9, #21, #22, and #35. In the 2023 period, flows were measured at the outlet of the PA for events #13 and #14 (6.6 and 8.4 mm, respectively) which should normally have infiltrated. As a result, it was inferred that the PA was contributing surface runoff directly to the catch basin for which the flows were measured. A site visit conducted on August 30, 2023, confirmed that the PA surface was ponded during rainfall. Several field observations indicated that surface ponding and runoff generation were higher for events of higher intensity. For events

#10, #12, #13, #15, #19, #20, #25, #27, #29, #30, and #33, the water height in the outfall pipe of the CA exceeded the maximum height (99 mm) of the weir, which also happened on events #12, #15, #19, #20, #25, #27, #28, #30, and #33 for the weir collecting the PA outflows. As a result, it was not possible to determine the volume or flow rate for these events. The surface runoff on the PA, which occurred instead of infiltrating, was primarily caused by pavement surface clogging. Though the measured average IR of 148 mm/hr in 2023 should have been sufficient to infiltrate all rainfall events during the study period (maximum 5-minute intensity = 69.6 mm/hr), a portion of the pavement area had localised IR below 35 mm/hr, which is insufficient to infiltrate 12 out of the 35 rainfall events. As a result, runoff cascaded quickly from low permeable areas to the catch basin leading to high measured discharge rates and volumes. Indeed, this low infiltrating PA could only infiltrate rainfall from frequent low-intensity events when rainfall intensity was less than 10 mm/hr.

Two recommendations were made prior to the 2024 monitoring period to mitigate and monitor surface runoff: (a) intensify cleaning maintenance to restore the infiltration capacity, and (b) measure underdrain flow from PA. The former brought little improvement (see section 4.2) and was thus unable to correct the underlying problem. Additionally, no flow was measured from the underdrain of PA throughout the period when the flow meter was installed (from May 5, 2023 to August 9, 2024). Field observations consistently showed that puddling and runoff generation were more pronounced during high-intensity rainfall events, irrespective of total rainfall. Some infiltration does take place, but at very low rates and especially for low-intensity rainfall. Figures 4.7 and 4.8 show examples of data collected during rainfall events in 2024. In these figures, the green curve corresponds to the total flow measured at the outlet of the permeable zone, i.e. the sum of the flow from the underground drain and the flow over the surface of the pervious asphalt into the PU-1 catch basin by runoff. For the two events illustrated, since the flow rate measured at the drain outlet (yellow curve) is always zero, the green curve corresponds to the surface runoff flow rate.

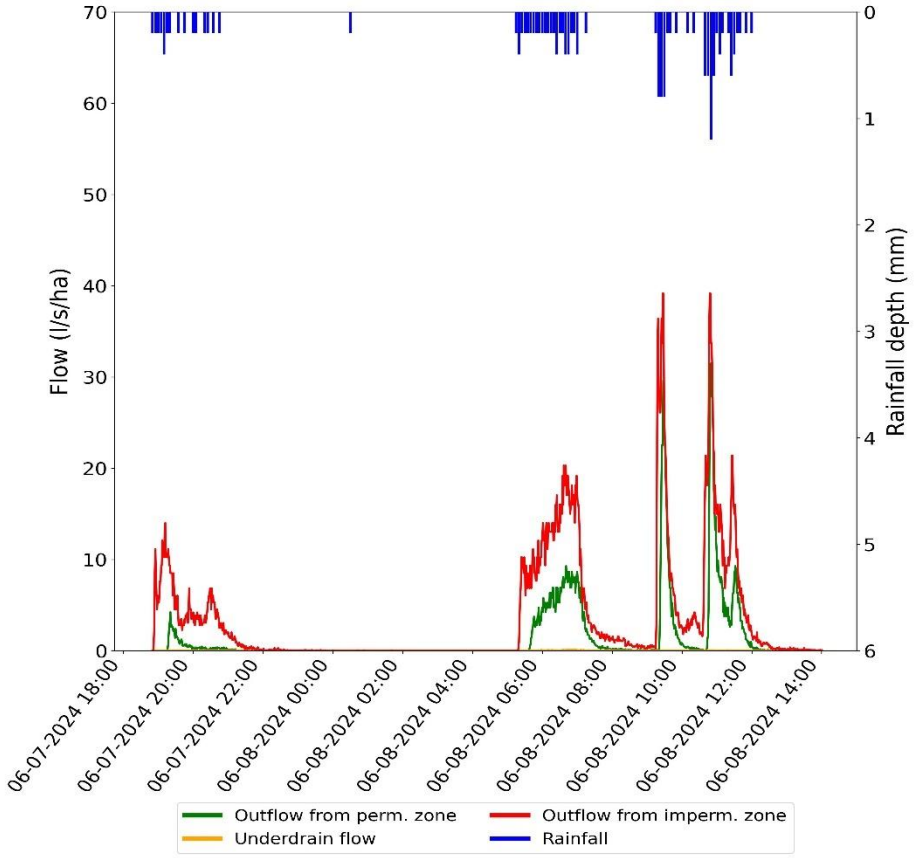

Figure 4-8 Hyetogram and hydrographs of the PA and CA zones for June 7-8, 2024 (total rainfall = 37 mm)

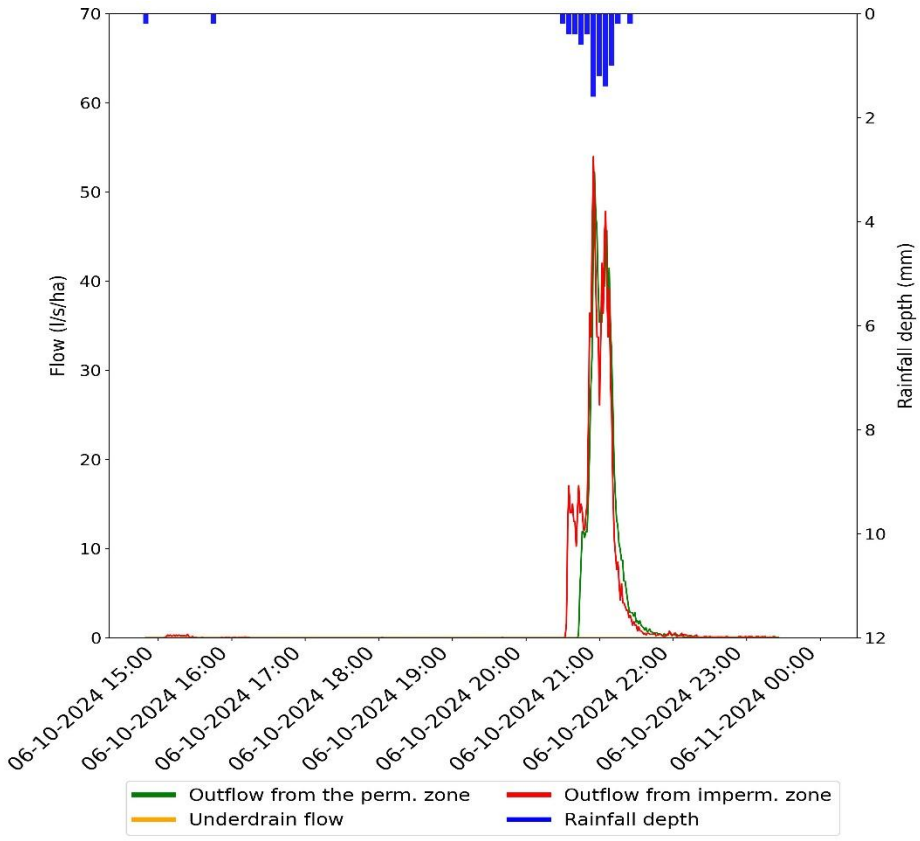

Figure 4-9 Hyetogram and hydrographs of the PA and CA zones for June 10, 2024 (total rainfall = 8.4 mm)

4.3.4 Reduction in volume and peak flow rate

Although the PA generated surface runoff, it attenuated flow during all recorded events. In general, the PA was able to reduce runoff volume by 9 % to 99 %, and runoff peak discharge by 2 % to 78 %. Drake et al. (2010) revealed that the reduction in runoff volume and rate of the PP depended on rainfall characteristics and antecedent dry periods. However, these relationships were not observed in this study for several events. For example, Drake et al. (2010) noted that a higher antecedent dry period is associated with a higher volume reduction for similar rainfall characteristics. Contrary to this study, the same volume reduction (62 %) was achieved here for events #23 and #24, with total rainfall depths of 18.6 and 18.4 mm, respectively, though event #23 had a longer antecedent dry period (224 h) than event #24 (8 h). A longer dry period normally leads to a lower moisture content of the reservoir layer, which should have helped to retain more water, thereby achieving a greater volume reduction. Event #32, which showed the greatest reduction in runoff volume (99 %), had a total rainfall depth of 7.8 mm and a maximum 5-minute intensity of 4.8 mm/hr. Event #26, with the lowest reduction in peak flow (2%) and runoff volume

(9 %), had also a low total rainfall depth (8.0 mm), but had a rather high maximum intensity over 5 minutes (19.2 mm/hr). Out of the 12 valid/estimated studied flow events, a peak reduction greater than 60 % was achieved for only four of them. Notably, all four events were characterized by low maximum 5-minute rainfall intensities: event #17 (9.6 mm/hr), event #18 (7.2 mm/hr), event #31 (7.2 mm/hr), and event #34 (12 mm/hr). This finding suggests that the studied PA underperformed during rainfall events with maximum intensity greater than 12 mm/hr irrespective of the rainfall depth. It is worth noticing that all studied rainfall events generated runoff from the PA surface. In contrast, Collins et al. (2008) evaluated the hydrological performance of four PP systems installed on poorly drained soils in eastern North Carolina. They observed that rainfalls below 6 mm did not produce any surface runoff.

The reduction in volume and peak flow observed from this studied PA were lower compared to many published studies. For instance, Roseen et al. (2009) reported that PA led to an 82 % reduction in maximum annual peak flow. Roseen et al. (2012) further examined the infiltration capability of a PA parking lot in coastal New Hampshire and observed runoff volume and peak flow reductions of 98 % and 80 %, respectively. A case study in Minnesota by Lebens & Troyer (2012) demonstrated that PA could decrease peak flow by up to 70 %. In contrast to these studies, research by Winston et al. (2016b) recorded stormwater volume reductions of 16 % and 32 % for two different rainfall events. However, this lower performance was attributed to the PA receiving runoff from catchment areas that were 7.2 and 2.2 times larger than the PP itself. Additionally, a study by Drake (2013) on partial infiltration PP systems over low-permeability soils found volume and peak flow reductions of 43 % and 91 %, respectively.

4.4 Water quality performance of the porous asphalt

Water quality from the PA was analysed to evaluate its contaminants concentrations including TSS, EC, petroleum hydrocarbons C_{10}-C_{50}, TP, TN, Zn, Cu, and heavy metals (total cations) compared to the runoff from the impermeable asphalt. Out of the 23 runoff events recorded at the PA outlet, water quality samples were collected for only three. The remaining events were not sampled because of unavailability of water at the sampling locations (underdrain and piezometer PZ-2). Table 4.9 represents the characteristics of the sampled rainfall events and sampling locations.

Figure 4-10 Sampling rainfall events characteristics and sampling locations

Event	Total rain depth (mm)	Max. 5-minute intensity (mm/hr)	Duration antecedent dry period (hr)	Rain duration (hr)	Sampling location	
					PA	CA
September 18, 2023	45.2	9.6	85	33.4	Underdrain	Outlet
June 23, 2024	42.0	9.6	220	13.8	PZ-2	Outlet
August 10, 2024	81.0	n.a.	80	19	Underdrain*	Outlet

*Sample taken from the stagnant water in the underdrain pipe

4.4.1 Total suspended solids

Variation in the results (Figure 4.10) are due to differences in sampling locations and the partial clogging of the draining asphalt. For instance, only one sample was collected in 2023, because the PA did not produce as much infiltration as expected. Indeed, on September 18, 2023, the TSS concentration was 72 % higher than that measured in the CA outflow. Following the unexpected lack of underdrain flow from the PA during the 2024 season, a sample collected from piezometer PZ-2 on June 23, 2024, showed a 86 % decrease in TSS concentration. However, on August 10, 2024, the TSS concentration increased by 40 %, echoing the trend observed in 2023. Results obtained from this study are inconsistent with the 65 % average reduction from Selbig & Buer (2018) and Huang et al. (2012), where TSS reductions were up to 94 %. Only TSS concentrations from the PA sampled on June 23, 2024 met the typical urban runoff water quality criteria of 30 mg/L provided by Quebec City (Ville de Québec, 2022; Canadian Council of Ministers of the Environment, 2017). Studies such as Legret et al. (1999) have found an average removal efficiency of 59 % by mass.

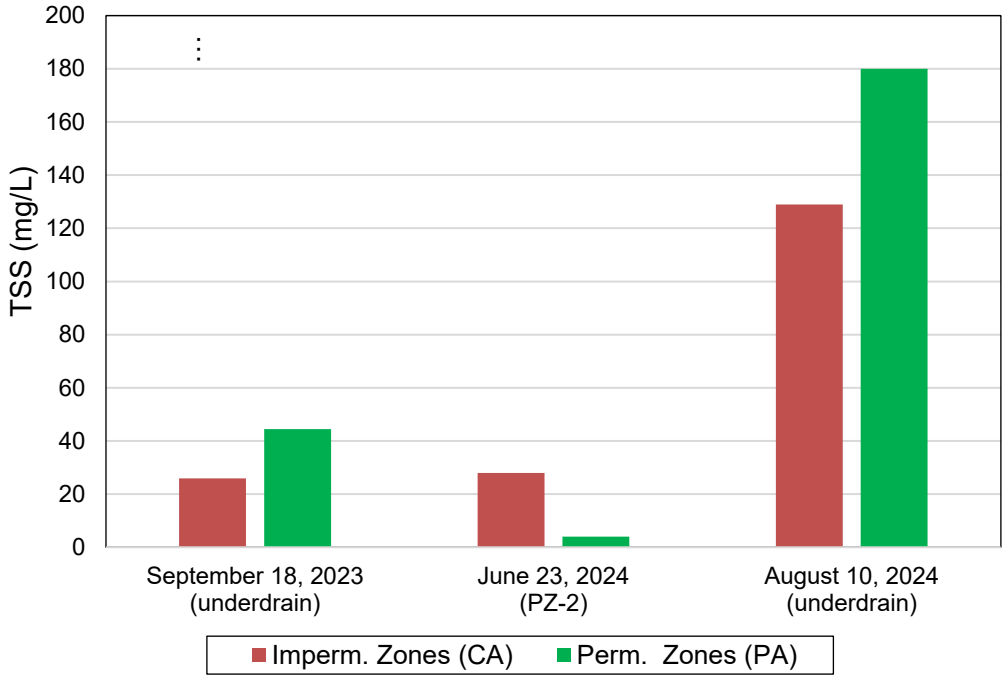

Figure 4-11 Total suspended solids concentrations for samples collected from impermeable and permeable zones during events on September 18, 2023, June 23, 2024, and August 10, 2024

In practice, TSS removal takes place through the asphalt porous layers, which act as a filter. However, in a condition where the porous media is partially clogged, higher TSS concentrations in the underdrain flow could be due to flushing of sediments trapped in the porous media or previously deposited in the underdrain pipe. It should be noted that, during the events on September 18, 2023, and August 10, 2024, water from the permeable zone was collected from the underdrain for the first time after 3-4 months of no flow, even for rainfall events greater than 30 mm. Consequently, these rainfall on September 18, 2023, and August 10, 2024 may have flushed sediments trapped in the pavement layers or the drainpipe. Even when less sand was applied on the PA, like in 2024, there was an increased in TSS concentrations compared to the impermeable zone on August 10, 2024. The rainfall on August 10, 2024 resulted in total rain depth of 81 mm which may have displaced clogged particles in the PA layers or underdrain pipe. Furthermore, some studies have found that vehicles appear to be the primary transport of contaminants, including sediments depositing on pavements (e.g. Drake et al., 2010). Therefore, the increased daily traffic on PA might explain this phenomenon. Fassman & Blackbourn (2010) conducted a three-year study on PICP in San Francisco, California, that revealed that sand from joints and bedding migrated into the drainpipe. Their research indicated that most of the

contaminants present in the water samples were derived from the sand from the joints and bedding itself rather than from surface sources. The sample on June 23, 2024, with a lower TSS concentration, was taken from the piezometer PZ-2, which is lined at the base with a geomembrane and vertically by a PVC pipe, therefore minimizing/preventing sediment transport from the porous media. Hence, results from this sample could represent the water quality performance of the PA, which remained at a high level in that case with a 86 % reduction.

4.4.2 Electrical conductivity

In Quebec, de-icing salts are commonly applied during winter months. When runoff water contains high levels of these salts, it can damage vegetation and degrade the water quality downstream. EC can be used as an indicator of the salinity in the runoff. Figure 4.11 presents the results of these measurements from the collected samples.

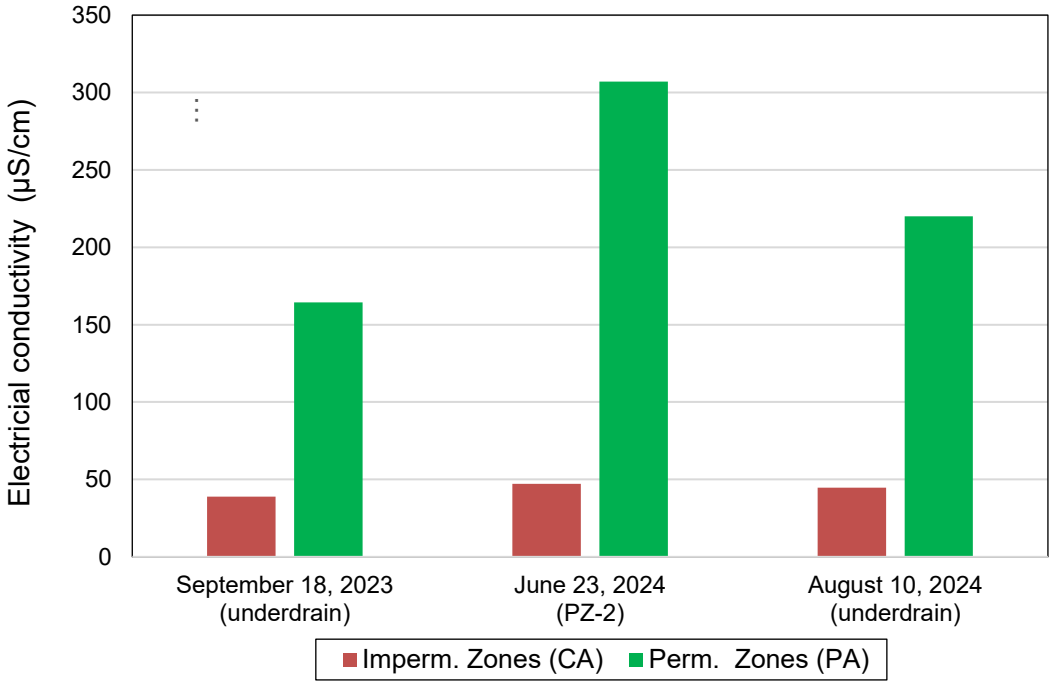

Figure 4-12. Electrical conductivity measurements for samples collected from impermeable and permeable zones during events on September 18, 2023, June 23, 2024, and August 10, 2024

Figure 4.11 shows that samples from the permeable zone consistently exhibit higher (324 % for date, 764 % for date, and 392 % for date) EC than those from the impermeable zone. This observation may be attributed either to the leaching of de-icing salts that have accumulated in the reservoir layer or to the release of dissolved ions from the asphalt aggregates (Fassman &

Blackbourn 2010). The maximal EC of 44.7 µS/cm (CA) and 307 µS/cm (PA) were recorded in June, indicating the release of road salts accumulated during the winter. As anticipated, these values gradually decreased during the year, suggesting that most road salts are flushed from the pavement layers during summer and fall storms. The lowest recorded values were 38.8 µS/cm (CA) and 164.4 µS/cm (PA), in September. This trend aligns with the findings of Borst & Brown (2014) and Winston et al. (2016a), which suggested that PPs can continue releasing winter de-icers into the spring and summer months. Since no de-icing agents were applied at the study site in winter 2023-2024, the June 2024 EC values were 26 % and 40 % lower in the permeable and impermeable zones, respectively, compared to those recorded during the same month in 2022 (Duchesne et al., 2022). Due to the limited number of samples collected in 2023-2024, only a few conclusions could be drawn. Continuous monitoring of the EC is recommended to assess the source of the ions.

EC and chlorides concentration do not have associated discharge limit (Ville de Quebec, 2022). However, the high EC (307 µS/cm) measured from the PA runoff needs to be monitored to ensure downstream water quality is not degraded. Roseen et al. (2012) observed that PP required less salt than conventional impermeable surfaces. Additionally, during winter thaw and rainfall periods, snowmelt infiltrates the PA layers, reducing the likelihood of ice formation during thaw-freeze cycles. Moreover, the textured surface of PA enhances friction, improving both vehicular and pedestrian safety. Therefore, further reductions in de-icing salt application compared to 2023 levels should enhance stormwater quality while maintaining safe usage.

4.4.3 Nutrients (total nitrogen and total phosphorus)

Elevated nutrient levels in stormwater can lead to eutrophication, negatively impacting surface water systems. By allowing stormwater to infiltrate through PA systems, particulate nutrients can be captured or filtered out, while certain nutrient species can undergo transformations. Figures 4.12 and 4.13 illustrate the system's performance for TN and TP.

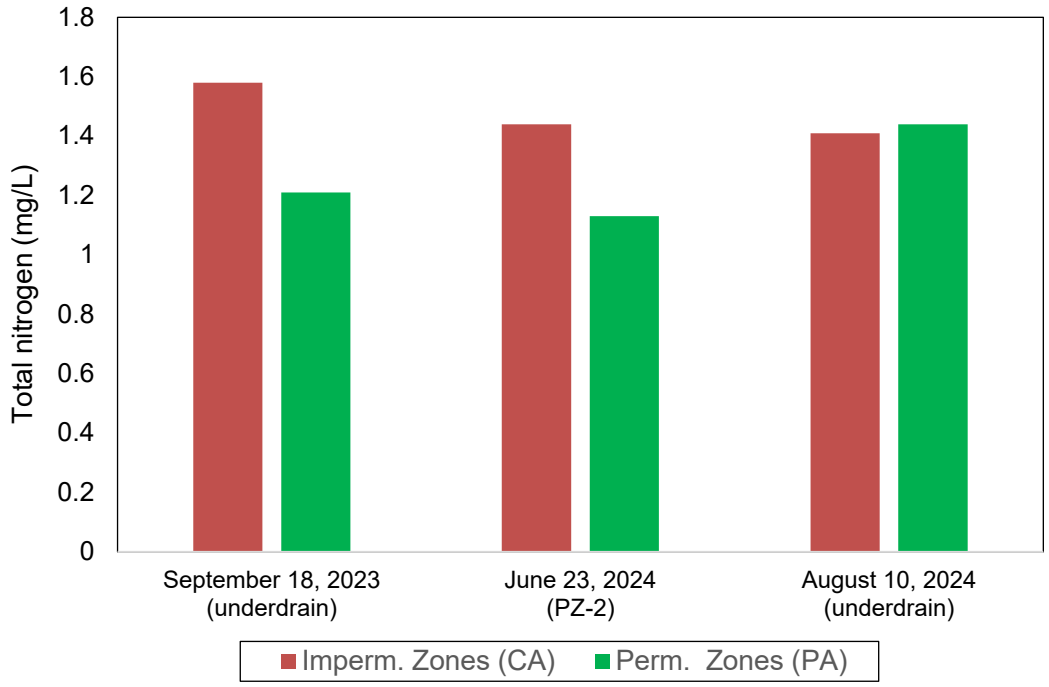

Figure 4-13 Concentration of total nitrogen for samples collected from impermeable and permeable zones during events on September 18, 2023, June 23, 2024, and August 10, 2024

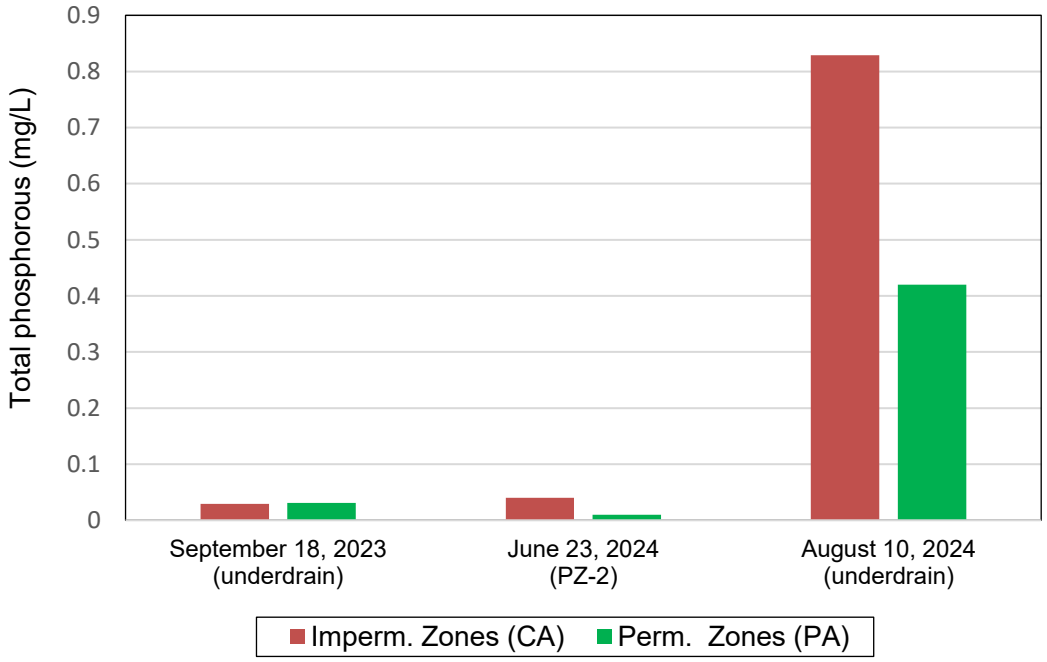

Figure 4-14 Concentration of total phosphorous for samples collected from impermeable and permeable zones during events on September 18, 2023, June 23, 2024, and August 10, 2024

The abatement efficiency for TN (Figure 4.12) was moderate, as CA concentrations (1.58 and 1.44 mg/L) were higher than those from PA (1.21 and 1.13 mg/L). However, during one storm event (August 10, 2024), no TN removal was observed, with a recorded removal rate of -2 %. The reduction of TN in PA effluent compared to impermeable runoff is likely attributed to the filtration of particulates, such as leaf litter or organic matter bound to suspended solids. Despite these findings, TN concentrations in both CA and PA remained within a similar range, which aligns with expectations since significant nutrient removal typically requires vegetated filtration (Roseen et al., 2006).

Like TN, TP removal (Figure 4.13) was generally effective, with removal rates of 75 % and 49 % observed for storm events on June 23 and August 10, 2024, respectively. However, during the September 18, 2023, event, PA concentrations were 7 % higher than those in CA. The average TP removal rate (18 %) was lower than the 20 % and 42 % reported by Selbig & Buer (2018) and Roseen et al. (2012), respectively. Overall, the results indicated that TN removal was minimal. The discrepancies in removal rates between TP and TN is likely due to differences in their removal mechanisms. TP removal appears to be primarily influenced by physical and chemical processes, whereas TN removal is dominated by biological processes (Huang et al., 2012; Collins et al., 2010).

4.4.4 Total hydrocarbons (C_{10}-C_{50})

Reduction of total hydrocarbons was effective across all samples (Figure 4.14). Notably, during the events on September 18, 2023, and June 23, 2024, C_{10}-C_{50} concentrations from the PA were below the detection limit (<50 µg/L). Even on August 10, 2024, when C_{10}-C_{50} was detected in PA runoff, its concentration was 47 % lower than that measured from CA; however, it exceeded the recommended guideline of 3.5 µg/L set by Quebec City (Ville de Quebec, 2022). Previous studies have consistently reported that solvent-extractable hydrocarbons (oil and grease) and petroleum hydrocarbons are often undetectable in PP systems (Drake, 2013; Boving et al., 2008; TRCA, 2008**;** Tota-Maharaj & Scholz, 2010). These findings reinforce the effectiveness of PA in reducing hydrocarbon concentrations.

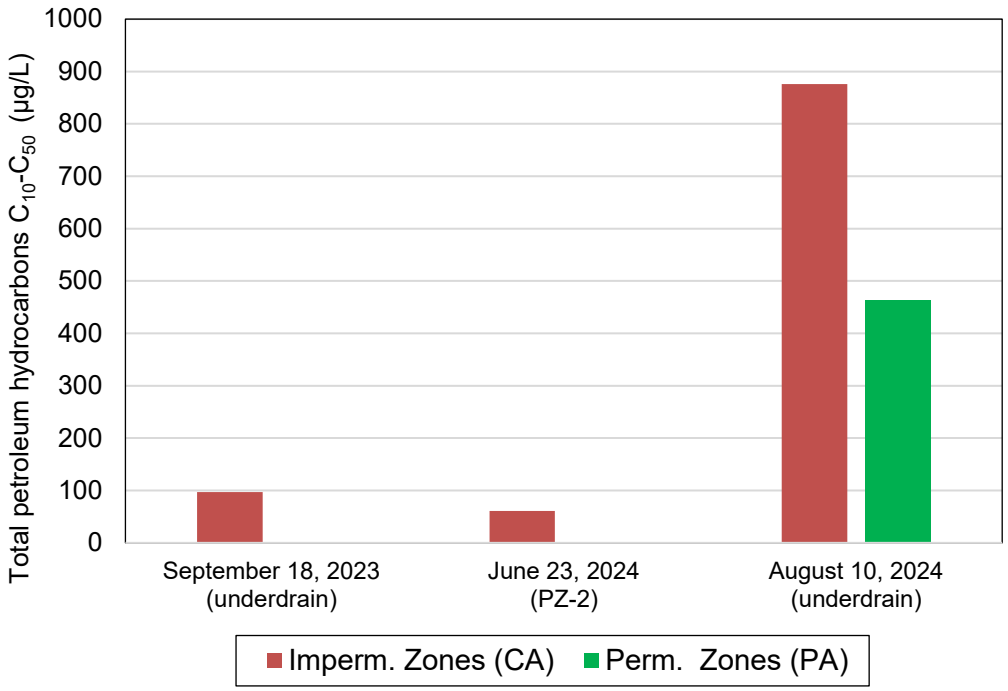

Figure 4-15 Concentration of total petroleum hydrocarbons C_{10}-C_{50} for samples collected from impermeable and permeable zones during events on September 18, 2023, June 23, 2024, and August 10, 2024

4.4.5 Heavy metals (total cations)

Table 4.5 presents the concentrations of total cations in samples collected from both permeable and impermeable zones.

Table 4.5 Water quality analysis results for total cations components

Parameters	September 18, 2023		June 23, 2024		August 10, 2024	
	Imperm. zone	Perm. zone (underdrain)	Imperm. Zone	Perm. zone (PZ-2)	Imperm. zone	Perm. zone (underdrain)
Al (mg/L)	0.165	0.112	0.028	0.054	0.579	0.628
As (mg/L)	< 0,005	< 0,005	< 0,003	< 0,003	< 0,003	< 0,003
Ba (mg/L)	0.0052	0.0096	0.0031	0.0086	0.0264	0.025
Ca (mg/L)	3.77	23.8	5.18	13.7	13	35.6
Cd (mg/L)	< 0,0007	< 0,0007	< 0,0004	< 0,0004	< 0,0004	< 0,0004
Co (mg/L)	< 0,002	< 0,002	< 0,001	< 0,001	< 0,001	< 0,001
Cr (mg/L)	< 0,0004	< 0,0004	< 0,0004	< 0,0004	0.0007	0.0009
Cu (mg/L)	0,003	< 0,002	0.0062	0.0022	0.049	0.0105
Fe (mg/L)	0.393	0.147	0.018	0.01	1.28	1.69
K (mg/L)	0.19	0.349	0.359	0.73	0.477	1.07
Mg (mg/L)	0.199	2.06	0.201	2.16	1.17	3.81
Mn (mg/L)	0.021	0.012	0.017	0.0004	0.077	0.046
Mo (mg/L)	< 0,0008	< 0,0008	< 0,0007	0,0026	0.0009	< 0,0007
Na (mg/L)	1.85	11.8	1.58	51.5	1.01	17.8
Ni (mg/L)	< 0,007	< 0,007	< 0,004	< 0,004	< 0,004	< 0,004
P (mg/L)	0.029	0.031	0.04	0.01	0.829	0.42
Pb (mg/L)	< 0,003	< 0,003	< 0,004	< 0,004	< 0,004	< 0,004
S (mg/L)	0.189	8.62	0.94	13.7	0.58	12.9
Sc (mg/L)	< 0,0003	< 0,0003	< 0,0005	< 0,0005	< 0,0005	< 0,0005
Se (mg/L)	< 0,008	< 0,008	< 0,006	< 0,006	< 0,006	< 0,006
Sr (mg/L)	0.028	0.319	0.041	0.29	0.068	0.441
Ti (mg/L)	0.014	0.004	< 0,0006	< 0,0006	0.059	0.108
V (mg/L)	0,0016	< 0,001	0,0027	< 0,0005	0.0038	0.0029
Zn (mg/L)	0.06	0.002	0.015	0.006	0.161	0.0508

Key

	CA conc. < PA conc.
	CA conc. > PA conc.

Results showed that, arsenic (As), cadmium (Cd), cobalt (Co), nickel (Ni), lead (Pb), scandium (Sc), and selenium (Se) were all below detection limits in every samples. Additionally, chromium (Cr) was undetectable in two out of three samples from both PA and CA. Similarly, Drake (2013) reported that over 50 % of PP samples showed non-detectable levels of As, Cd, Co, Ni, Se, and Cr, suggesting that these metals are not significant contaminants. Concentrations of Cd, Co, Mn, Mo, Pb and Se, from both pavement types were below the stormwater discharge standards set by the City of Quebec (Ville de Québec, 2022). Heavy metals such as As, Ba, Ca, Fe, K, Mg, Na, S, Sr, Ti, V, and Sc are not classified as contaminants of concern while Cr, Cu, Ni, and Zn are classified but without an associated concentration limit. Notably, the PA effluent contained detectable levels of molybdenum (Mo), which was absent in runoff from the impermeable surface on June 23, 2024.

Under the conditions tested, PA effluent had 97 %, 60 %, and 68 % lower concentrations of Zn, and 100 %, 65 %, and 79 % lower concentrations of Cu than the CA effluent for the events on September 18, 2023, June 23, 2024, and August 10, 2024 respectively This outcome is comparable in magnitude to the findings of Drake (2013) for a partially infiltrating PP, where Cu, Fe, Mn, and Zn removal rates ranged between 65 % and 93 %. Aluminum (Al) concentrations in PA outflow decreased by 32 % on September 18, 2023, but showed increases of 93 % and 8 % in the other two samples. Overall, heavy metal removal was moderate, with both positive and negative treatment efficiencies observed for different sampling events. Specifically, seven metals showed a reduction in concentration, while eight increased on September 18, 2023; six metals concentrations were reduced, while nine increased on June 23, 2024; and seven metals showed reductions in concentrations, while ten increased on August 10, 2024, as detailed in Table 4.5. This modest performance can be explained by the fact that the efficiency of heavy metal removal by PP depends on the form in which the metals exist in stormwater (Huang et al., 2012; Murakami et al., 2008; Brown et al., 2015b. Research on PP indicates that heavy metals in their free elemental state are primarily retained on the pavement surface, whereas those in ionic form are captured within the pavement base layer (Dierkes et al., 1999). A study by Brattebo & Booth (2003) on three types of PP in Renton, Washington, observed an increase in Zn concentrations in exfiltrated water, while Cu and Pb concentrations decreased.

4.4.6 Runoff water temperature

Figures 4.15 to 4.18 illustrate a comparison of water temperatures recorded at the downstream location (manhole RP-1) for pipes collecting water from both permeable and impermeable

pavement zones, as well as temperatures measured in piezometer PZ-1. These events were selected to reflect the two pavements (CA and PA) stormwater temperature responses for low depth-short duration rainfall (Figures 4.15 and 4.16) and high depth-long duration rainfall (Figures 4.17 and 4.18) events. Unlike many previous studies, which have predominantly compared underdrain or effluent temperatures from PA with those of impervious runoff, this current study compares the surface runoff from PA to CA, knowing that the PA surface runoff similarly affects water temperature. Despite the low infiltration capacity of the PA, which leads to water accumulation and surface runoff, water temperatures from the PA are always consistently lower than those observed from the impermeable surface for all rainfall events examined. In contrast to CA, the porous structure of PA retains water near its surface, which increases evaporation during the day and keeps the pavement cooler. The amount of heat absorbed by the pavement plays a key role in influencing runoff temperature (Drake, 2013). Moreover, the porous medium and water contained in the underlying reservoir layer of PA help reduce surface heat absorption and promote evaporative cooling (Qin, 2015). As a result, when rain contacts a PA surface, it receives less heat compared to CA, even though PA is partially sealed.

Because the PA underdrain does not contribute directly to the measured water temperatures, these readings are predominantly affected by the temperature at the PA's surface and a few millimeters beneath the surface. Selbig & Buer (2018) observed that temperature decreases with increasing depth through PA layers. For the four rainfall events illustrated in Figures 4.15 to 4.18, the averaged recorded runoff temperatures for PA (17.20, 17.79, 18.58, and 21.14 °C, respectively) were only about 0.69 to 1.09 °C cooler than those for CA (which were 18.02, 18.53, 19.27, and 22.23 °C, respectively). In addition, the maximum water temperatures from PA were found to be 1.43, 1.81, 0.96, and 0.96 °C cooler than those from CA, respectively, for the four illustrated rainfall events. Asaeda & Ca (2000) studied the surface temperature of impervious asphalt and PA during the summer in Kuki, Japan. They noted a surface temperature difference of 1 to 2 °C between PA and impervious asphalt types, providing further evidence that PA can help moderate runoff temperatures.

Differences between water temperatures could also be partially explained by the longer travel distance that water from the permeable zone must traverse through underground pipes before being measured, compared to water from the impermeable zone. After rainfall begins, water temperature in the impermeable zone rises more sharply and rapidly than in the permeable zone. Moreover, water temperatures recorded in PZ-1 remained constant during events #26, #31, and #33, and changed only gradually during event #28, possibly due to reduced infiltration capacity

or low rainfall amount reaching the reservoir layer, which delays the temperature response. Among the three monitored water locations, PZ-1 registered the lowest temperatures. Temperature of water from both asphalt types consistently decreased as rainfall progressed. However, the increase in water temperature observed in PZ-1 during certain stages of the rainfall (events #28 and #31) may indicate that heat absorbed at the surface is being transferred downward through the asphalt's void spaces, potentially aided by infiltration.

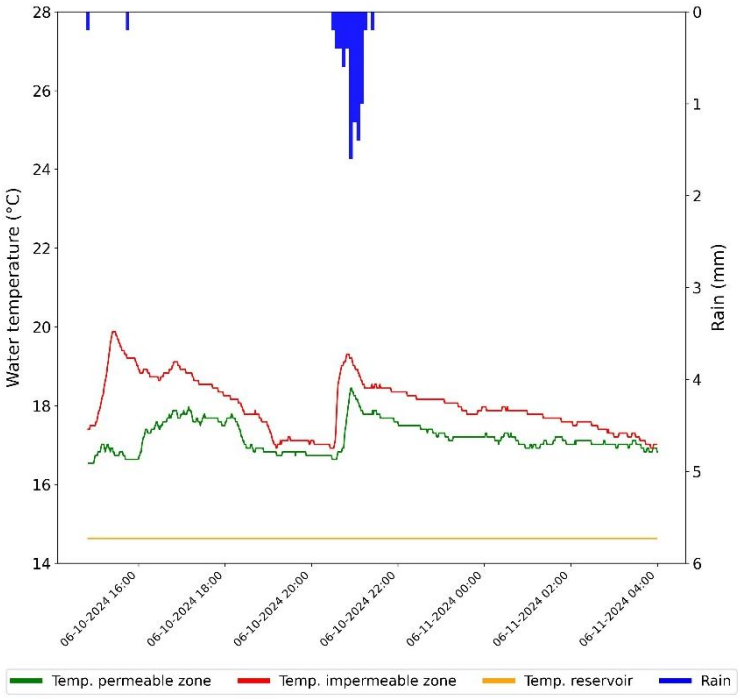

Figure 4-16 Hyetogram and water temperature of the PA lot (green) and the CA lot (red) for event #26

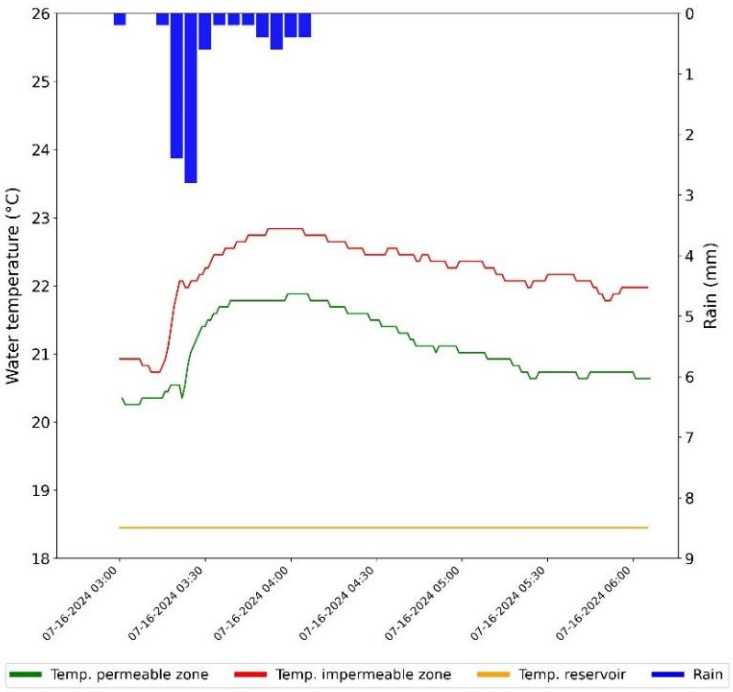

Figure 4-17 Hyetogram and water temperature of the PA lot (green) and the CA lot (red) for event #33

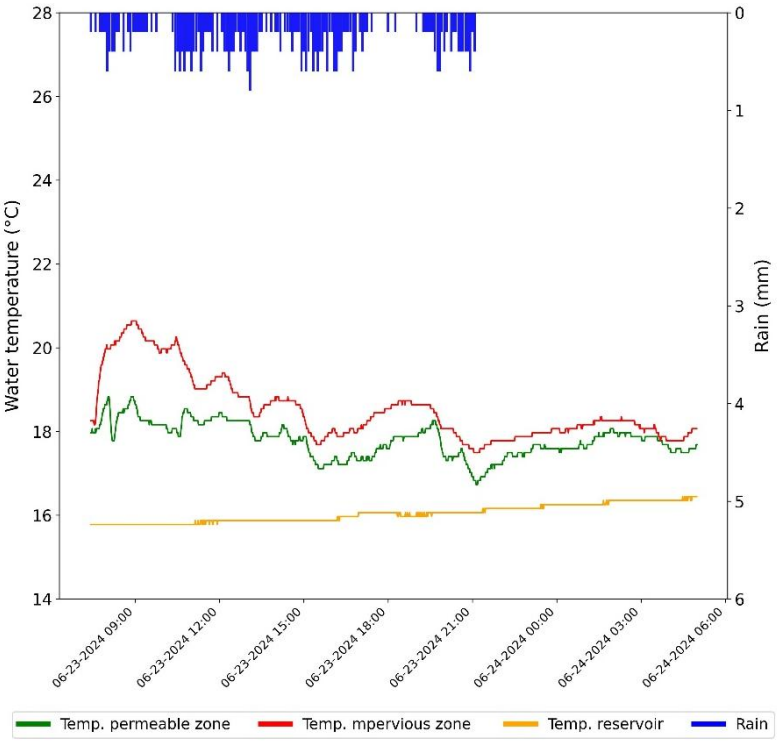

Figure 4-18 Hyetogram and water temperature of the PA lot (green) and the CA lot (red) for event #28

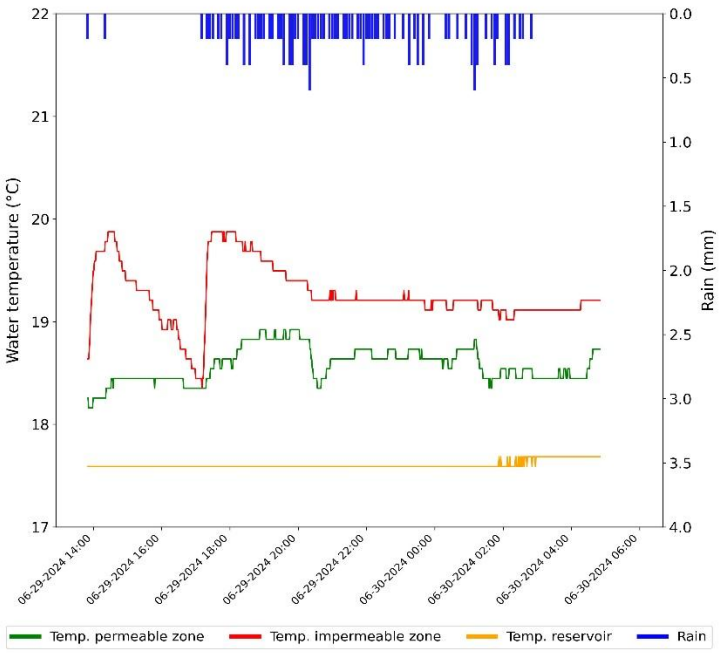

Figure 4-19 Hyetogram and water temperature of the PA lot (green) and the CA lot (red) for event #31

4.5 Calibration and validation of the SWMM model

This section presents the findings from the calibration and validation for each subcatchment. The model was calibrated to best represent the conditions of the study site. Table 4.6 presents the characteristics of the events used for calibration and validation of the pavement. The events were selected to cover a range of different rainfall characteristics. However, achieving a fully diverse distribution was challenging, as most rainfall events were intense enough to exceed the weir's capacity. Additionally, some events coincided with periods of missing flow data, as explained in Section 3.3.

Table 4.6 Characteristics of events used for the model calibration and validation processes

Start (date and time)	Total depth (mm)	Maximum intensity over 5 min (mm/hr)	Mean intensity (mm/hr)	Duration of antecedent dry period (hr)	Duration of rainfall (hr)
Conventional asphalt - calibration					
August 8, 2023 00:40:00	62.2	33.6	2.5	83.25	24.5
October 7, 2023 19:20:00	23.8	7.2	1	114.75	24.5
Conventional asphalt – validation					
September 18, 2023 09:55:00	45.2	9.6	1.4	85	33.42
Permeable asphalt - calibration					
August 30, 2023 10 :55 :00	10	24	1.6	12.58	6.33
June 7, 2024 18 :50 :00	18.4	14.4	1.1	8.25	17.25
Permeable asphalt - validation					
July 24, 2024 18 :50 :00	16.8	12	1.2	95.25	14.33

4.5.1 Calibration and validation of the model for the subcatchment

The final unknown (calibration parameter) values of the SWMM model for the CA are given in Table 4.7. A depression was noticed on certain areas of the CA catchment, majorly around manhole RP-1, which contributed to the high value of 5.07 mm obtained for the depression storage parameter (Dstore imperv). This was evident as sand accumulation was constantly present on these areas between every rainfall events. Moreover, part of the initial rainfall on the CA surface was lost through an opening on the manhole RP-1 without been measured as outflow. As such, the model may have attributed it as depression losses. This depression areas on the CA surface did not extend on the entire pavement, confirming the resulting calibration value of 48 %

for the portion of the impervious area without depression storage (Zero imperv area). The calibration value for the catchment slope was 1.79 %, which closely aligned with the average slope of 1.8 % estimated from the design plan provided by the MTTD. On the other hand, the Manning n of 0.03 obtained suggests a pavement surface with micro-texture and cracks as noticed on the site. This surface condition impeded surface flow. Once the model achieved satisfactory performance in calibration, the model was validated for the 18 September, 2023 event.

Table 4.7 Final parameter values from the calibration of the model for the conventional asphalt subcatchment

Parameter	Units	Value
Slope	%	1.79
Flow width	m	73.8
Manning coefficient (N imperv)	-	0.03
Depression storage depth (Dstore imperv)	mm	5.07
Percentage of impervious surface without depression (Zero imperv area)	%	48

Calibration and validation performance are shown in Table 4.8 and Figures 4.19 to 4.21. Calibration results, with NSE values of 0.79 and 0.88, can be considered excellent (Rossman, 2015). However, validation results, with an NSE of 0.66, can only be considered satisfactory (Rossman, 2015). This may be due to the model's difficulty in reproducing the response of the impermeable subcatchment to very low rainfall intensities, as shown in Figure 4.27. This difficulty may be linked to certain particularities of the site not considered in the model, such as, for example, part of the runoff bypassing through the two perforated holes located on the manhole RP-1 cover for low intensity rainfalls and its non-tightness. These conditions prevent the bypassed water from being measured by the flowmeter. Though measures were put in place to avoid this, the sealing objects were periodically removed by vehicle movement and neighbors who use the lot.

Table 4.8 Calibration and validation results of the model for conventional asphalt subcatchment

Event	Simulated volume (L)	Observed volume (L)	Nash Coefficient (NSE)
Calibration			
August 8, 2023 00:40:00	31,530	30,860	0.79
October 7, 2023 19:20:00	11,100	11,590	0.88
Validation			
September 18,2023 09:55:00	22,340	17,090	0.66

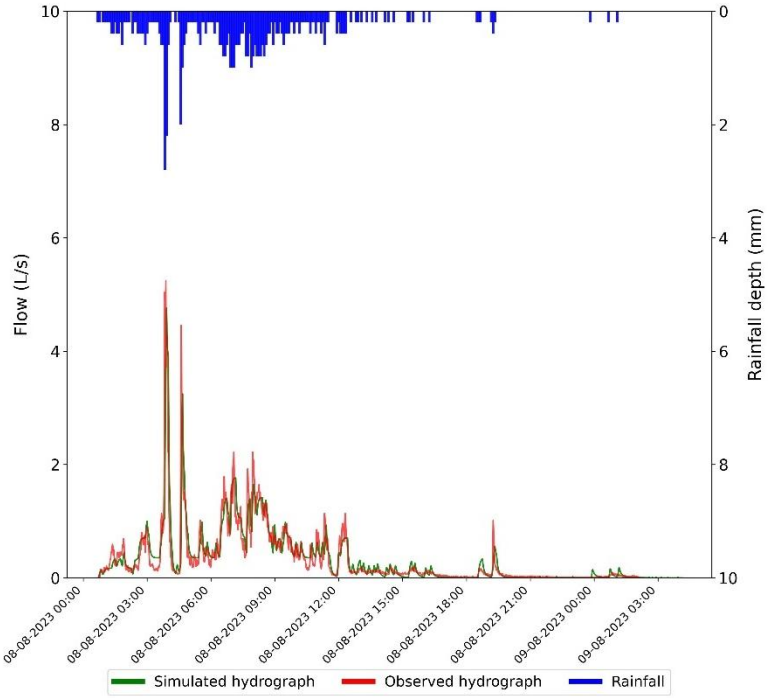

Figure 4-20 Calibration results for the event of August 8, 2023 (conventional asphalt)

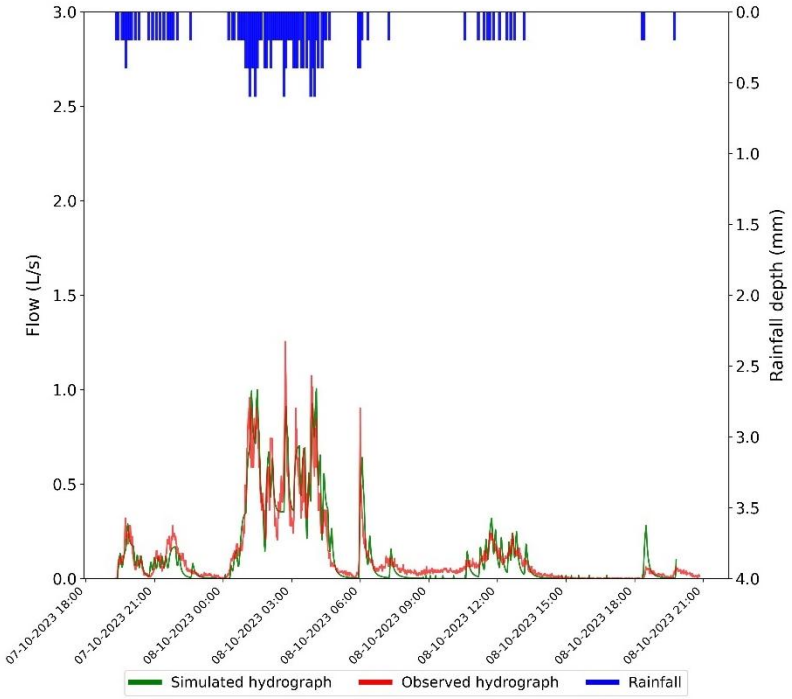

Figure 4-21 Calibration results for the event of October 7, 2023 (conventional asphalt)

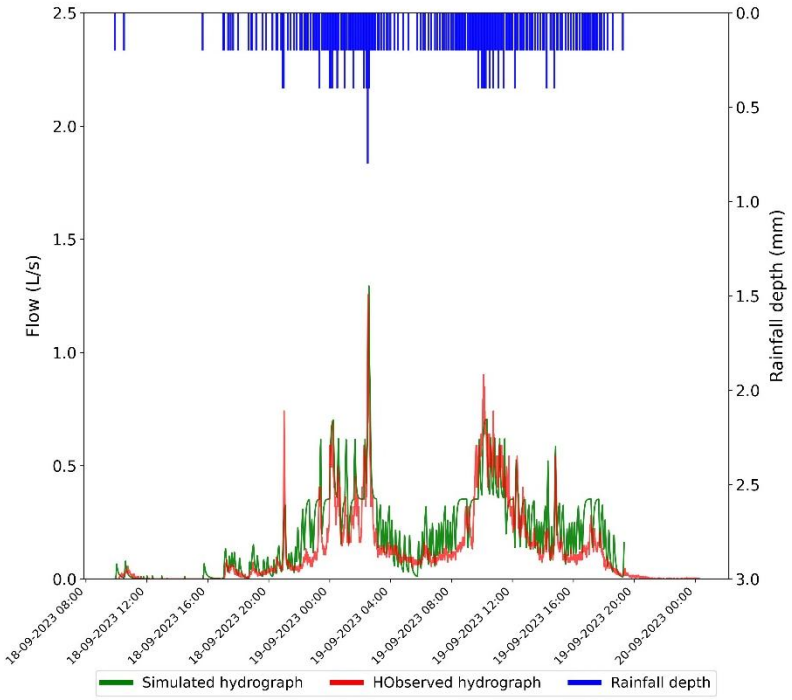

Figure 4-22 Validation results for the event of September 18, 2023 (conventional asphalt)

4.5.2 Calibration and validation of the model for the porous asphalt subcatchments

As explained in section 3.8.1, the observed flow from the PA was a combination of flow from the clogged subcatchment (a) and the underdrain of the pervious catchment (b). This means that two models needed to be calibrated: one for the clogged subcatchment and one for the pervious one. Accurate LID module calibration required having underdrain flow as a PA outflow. By fine-tuning the underdrain flow, key parameters like the wilting point and conductive slope were optimized to accurately represent their contribution to the PA outflow. This step ensured that the model closely reflected the physical behavior of the system, resulting in more reliable simulations. However, the decline in IR prevented underdrain flow for almost all the rain events in 2023 and 2024. Since the flow from the PA outlet was primarily from the clogged pavement, the calibration parameters were mainly the characteristics of the clogged subcatchment including slope, width, Manning roughness, depression storage, etc., and the IR of the pervious subcatchment. The final calibrated parameter values of the SWMM model for the clogged subcatchment of the PA are given in Table 4.9. For the pervious subcatchment, an IR of 24 mm/hr was optimal for the calibration.

Table 4.9 Final parameter values from the calibration for the clogged sub catchment of the porous asphalt

Parameter	Units	Value
Slope	%	2.67
Flow width	m	140
Manning's coefficient (N imper)	-	0.009
Depression storage depth (Dstore imperv)	mm	2
Percentage of impervious surface without depression (Zero imperv)	%	15

The calibrated depression storage depth of 2 mm can be attributed to the porous nature of the PA surface created during its construction. These depressions were noted to accumulate rainwater after each event. Furthermore, many of these depressions were clogged with fine particles (relative smoother surface than when new), aiding in the rapid movement of water across the pavement. As these fine sediments filled the pore spaces in the PA, the clogged surface

became smoother (less surface obstruction or friction), resulting in a lower Manning n of 0.009. The calibrated value of 15 % obtained for the percentage of impervious surface without depression shows that greater proportion of this catchment was clogged. Field estimates indicated a flow width of 124 m from the clogged area, compared to the calibrated value of 140 m; the clogged area was simplified to 584 m² in the model. However, site observations suggest that every part of the PA contributed runoff to catch basin PU-1, which could have increased the effective flow width. This discrepancy may be attributed to the model assumptions. Similarly, the calibrated slope of 2.67% exceeds the 1.9% average slope indicated in the PA site drawing plan from MTMD. Overall, accurately determining the catchment characteristics of the clogged area is challenging, as the estimated area of 584 m² used in the model can vary with rainfall characteristics and site conditions.

Calibration and validation results are shown in Table 4.10 and Figures 4.22 to 4.24. While calibration results can be considered good for the August 30, 2023, event (NSE = 0.76), calibration results for the June 7, 2024, event and the validation (July 24, 2024) event are barely satisfactory (NSE of 0.47 and 0.49 respectively). This is due to the difficulty of reproducing the hydrological functioning of a non-standard, non-uniformly disturbed site, such as this experimental site with SWMM. During high intensity rainfall events, the simulated hydrographs of the calibration and validation flows closely matched with the observed flow hydrographs, but it performed poorly during low intensity periods.

Table 4.10 Calibration and validation results for the porous asphalt

Event	Simulated volume (L)	Observed volume (L)	Nash coefficient (NSE)
Calibration			
August 30, 2023	1,911	1,610	0.76
June 7, 2024	3,911	8,113	0.47
Validation			
July 24, 2024	3,541	5,125	0.49

Limitations to modeling this site included high level of clogging over the entire surface of the PA, rendering it almost impermeable. As such, it was only by separating the PA catchment that a site

representative model could be produced. In addition, the imperfect levelling of the surface creates zones of water accumulation and preferential flow paths that are not represented in the model. Added to this is the fact that the spatial distribution of PA infiltration capacity evolves over time, making it difficult to model its hydrological functioning with the same parameter values for the 2023 and 2024 seasons, and using the same surface areas for the clogged and pervious subcatchment of the PA.

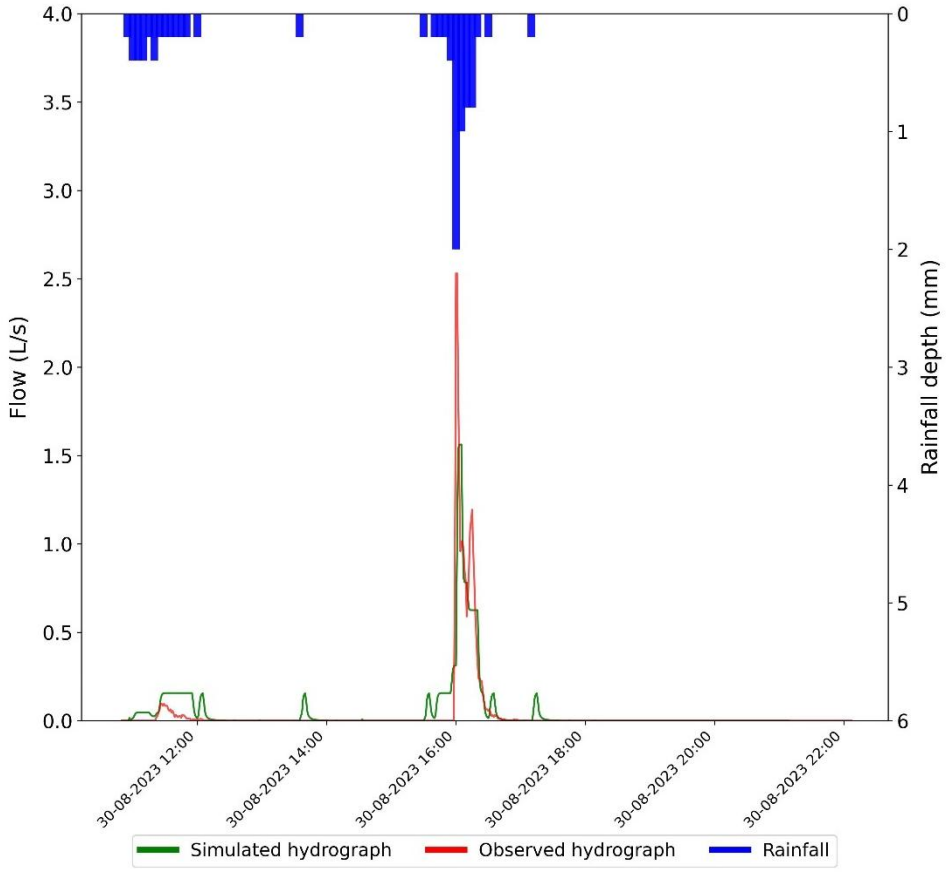

Figure 4-23 Calibration results for the event of August 30, 2023 (porous asphalt)

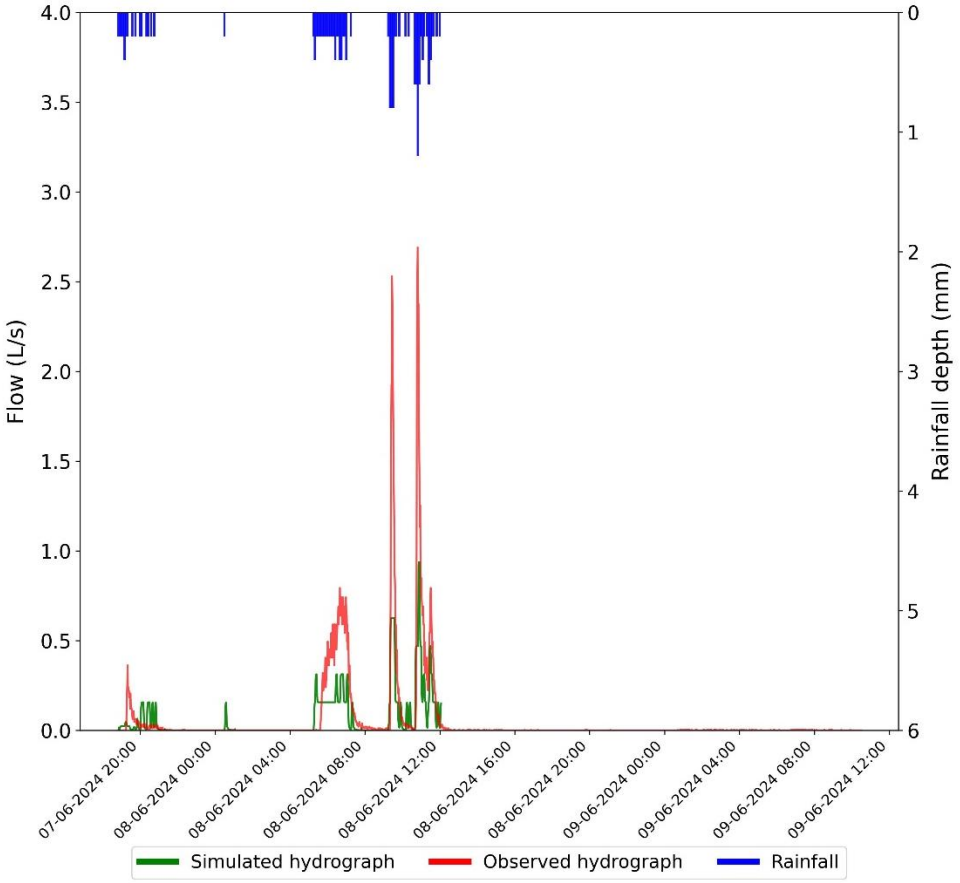

Figure 4-24 Calibration results for the event of June 7, 2024 (porous asphalt)

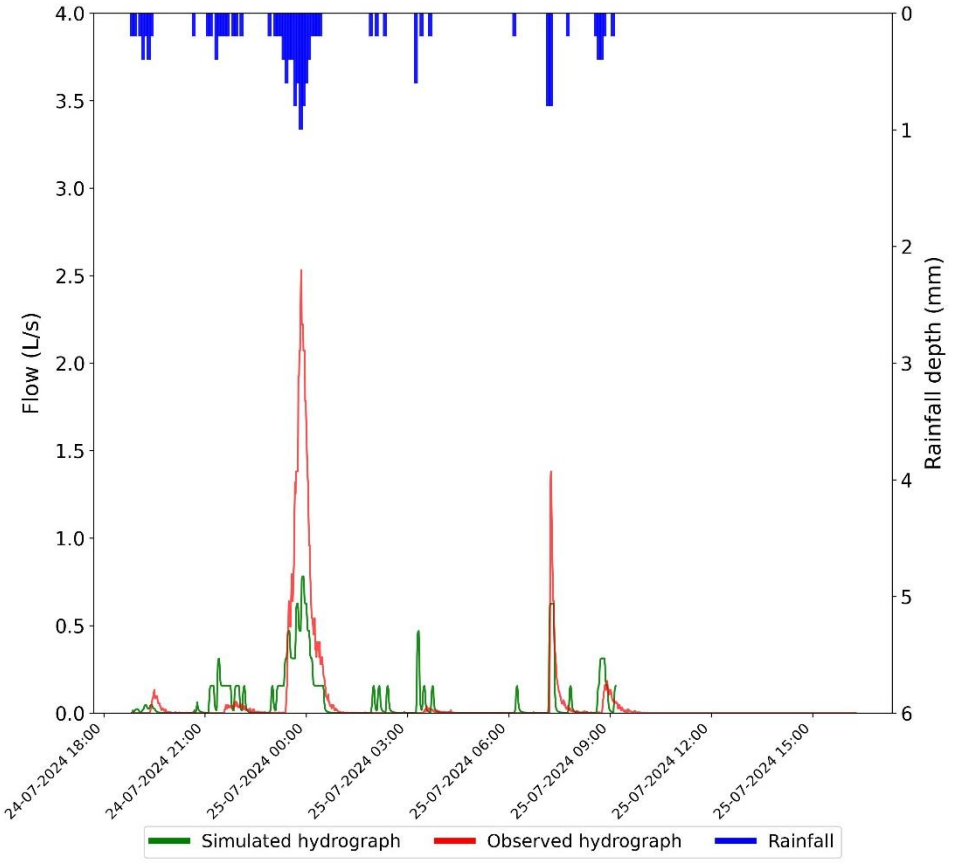

Figure 4-25 Validation results for the event of July 24, 2024 (porous asphalt)

5 CONCLUSION

This study examined the hydrological (in terms of runoff rate and volume reduction) and water quality performance of a porous asphalt (PA) as compared to an impervious conventional asphalt (CA) installed at the parking lot of the Le Tournesol library, in Quebec City. The studied PA was two years old at the beginning of this study, with a previous 18-month monitoring campaign carried out from October, 2019 to November, 2022. In the current study, monitoring of flow and water quality from the two asphalts was carried out from May to October in 2023 and 2024.

The infiltration rates (IR) of the PA measured at the end of each winter seasons were very low, with an average IR of 50 mm/hr on May 26, 2023, and 67 mm/hr on May 21, 2024. The use of winter abrasives on the parking lot may have resulted in the lost of IR as sand aggregates clog the pavement pore spaces. The spring cleaning on June 13, 2023, was only able to restore the average IR to 148 mm/hr. This represents a 98 % decline in the average IR from what was observed in June 11, 2021, which was 8460 mm/hr. In 2024, the restorative maintenance of the PA was carried out using three different cleaning trucks: CityFant 6000, Elgin Whirlwind, and Ravo 5, each deployed on separate sections of the area. The CityFant 6000 contributed to infiltration rate (IR) improvements of 137 %, 753 %, and 14 % at various test locations. The Elgin Whirlwind increased the IR by 85 % after cleaning, while the Ravo 5 resulted in a 153 % increase. Despite these improvements, the maintenance efforts were insufficient to fully restore infiltration capacity to a level that would significantly enhance stormwater infiltration, primarily due to the severe clogging before maintenance.

The decline in IR in the 2023 and 2024 monitoring periods led to a low to moderate performance in terms of peak runoff rate and volume reduction. Out of 23 studied rainfall events, the water height in the PA's outfall pipe exceeded the weir's capacity for 9 of them. Similarly, for the weir collecting CA outflows, the water height surpassed this limit during 11 events. As a result, for 11 of the 23 events, it was not possible to determine the volume or flow rate reductions. The hydrological analysis of the valid computed flows (12 events) revealed a volume reduction from 9 % to 99 % and peak flow reduction from 2 % to 78 %, depending on the rainfall event. These peak reductions were far below those observed in 2021 and 2022, which were between 91 % to 100 %. In fact, in the 2023 and 2024 seasons, out of the 12 estimated flow events, a peak reduction greater than 60 % was achieved for only four. Notably, all these four events were characterized by low maximum rainfall intensities measured over a 5-minute period (from 7.2 to

12.0 mm/hr). Similarly, the reductions in runoff volume were from 9 % to 99 % in 2023 and 2024, compared to 68 % to 100 % in 2021 and 2022. In the 2023-24 monitoring campaign, events which showed greater reductions in runoff volume had low total rain depth (less than 10 mm) and low maximal 5-minute intensity (less 9.6 mm/hr). Contrary, the event with the lowest reduction in peak flow (2 %) and runoff volume (9 %) had a total rain depth of 8.0 mm, but had a high maximal 5-minute intensity of 19.2 mm/hr. The PA underperformed during rainfall events with maximum 5-minute intensity greater than 12 mm/hr, irrespective of the rainfall depth. Surface runoff was generated on the PA for all the studied rainfall events.

Water samples were collected during three rainfall events. Analysis of the PA stormwater effluent indicated that, despite infiltration challenges, moderate performance in stormwater quality were achieved. These improvements were because the infiltration process still occur through the PA underlying aggregate layers, although at a lower rate than expected. Moreover, observations showed that in summer, water temperature at the outlet of the PA was lower than at the outlet of the CA, which may be explained by less heat accumulation by the PA than by the CA, or by a longer water path in the underground pipe before temperature measurement.

Although the study made significant contributions to understanding the hydrological and water quality performances of porous asphalt, certain limitations prevented a full capture of PA performance. This led to flows in monitoring pipes often exceeding the weir's capacity. The measurement setup led to incomplete data for 11 out of 35 observed rainfall events, thereby decreasing the number of events for which flow performance could be estimated. This sample size limited the statistical strength, especially when trying to generalize the hydrological performance under varied rainfall intensities. Additionally, the water quality was assessed during only three rainfall events at different sampling locations. Given the variability in stormwater contaminants loads with differing rainfall characteristics, the limited sampling restricted the robustness of the conclusions regarding water quality improvements.

The decline in IR during the studied period had a negative impact not only on the hydrological and water quality characterisations but, also, on how the PA catchment could be modeled in SWMM with its current hydrological condition. There was high level of clogging over the entire surface of the PA, rendering the surface almost impermeable. Added to this is the fact that the spatial distribution of PA infiltration capacity evolved over time, making it difficult to model its hydrological functioning with the same parameter values for the 2023 and 2024 seasons, and using the same surface areas for the clogged and pervious subcatchment of the PA. In terms of maintenance practices, the different cleaning trucks deployed achieved varying degrees of

improvement in IR. However, it was inconclusive to which truck could be utilised for future cleaning. It would have been better to deploy each truck on the entire PA at different years to be able to standardise their efficiencies.

Despite these limitations, the outcomes of this study underscore how site-specific factors, seasonal changes, and pavement age can influence the performance of PA systems by altering both hydrological and water quality (levels and type of contaminants). Therefore, further research is needed to evaluate how these variables affect the PA stormwater treatment performance. Although this study characterized the hydrological and water quality from a 4-year-old PA, ongoing monitoring is essential to understand the long-term behavior of the system, particularly after reducing the amount of de-icing salt and sand aggregate used on the PA site. The following additional recommendations are based on study findings and observations:

1. Vacuum cleaning was found to only partially restore infiltration capacity of the PA. Further tests of different techniques for removing clogged material in PA is needed.
2. Even though the vacuum cleaning did not produce a significant increase in surface IR, regular maintenance needs to be prioritised. A bi-annual cleaning of PA is recommended to increase the operational life and stormwater benefits.
3. The winter maintenance practices should be reviewed to eliminate the spreading of de-icing salts and sand on the PA. Further research is needed to evaluate how and whether the PA can maintain safe conditions for cars and pedestrians with lower salt and sand use than conventional pavements.
4. The conductivity of water discharged from the permeable zone following changes in de-icing salt application practices should be monitored, to better understand the accumulation and leaching of these salts.
5. A sample of the PA should be collected to study its current structure (depth of clogging) and to gain a better understanding of what may have led to its clogging.
6. Additional work should consider extended monitoring periods, improved instrumentation for capturing high-flow events, and more comprehensive water quality assessments.

6 BIBLIOGRAPHY

Ahmad, M., & Hafeez, I. (2021). Permeability of asphalt mixtures with bailey and conventional aggregate gradations. Arabian Journal for Science and Engineering, 46(11), 10869-10884.

Al-Rubaei, A. M., Stenglein, A. L., Viklander, M., & Blecken, G.-T. (2013). Long-Term Hydraulic Performance of Porous Asphalt Pavements in Northern Sweden. Journal of Irrigation and Drainage Engineering, 139(6), 499–505.

American Society of Civil Engineers (ASCE). (2015). Permeable Pavement. ASCE, Reston, VA, United States.

Asaeda, T., & Ca, V. T. (2000). Characteristics of permeable pavement during hot summer weather and impact on the thermal environment. Building and Environment, 35(4), 363-375.

Azad, A., Sheikh, M. N., & Hai, F. I. (2024). A critical review of the mechanisms, factors, and performance of pervious concrete to remove contaminants from stormwater runoff. Water Research, 251, 121101.

Barrett, M. (2008). Effects of a permeable friction course on highway runoff. Journal of Irrigation and Drainage Engineering, 134(5), 646-651.

Boving, T. B., Stolt, M. H., Augenstern, J., & Brosnan, B. (2008). Potential for localized groundwater contamination in a porous pavement parking lot setting in Rhode Island. Environmental Geology, 55(3), 571–582.

Borst, M., & Brown, R. A. (2014). Chloride released from three permeable pavement surfaces after winter salt application. JAWRA Journal of the American Water Resources Association, 50(1), 29-41.

Brattebo, B. O., & Booth, D. B. (2003). Long-term stormwater quantity and quality performance of permeable pavement systems. Water Research, 37(18), 4369–4376.

Brown, R.A., & Borst, M., (2015). Nutrient infiltrate concentrations from three permeable pavement types: Journal of Environmental Management, 164, 74–85.

Bruinsma, J., Smith, K., Peshkin, D., Ballou, L., Eisenberg, B., Lurie, C., ... & Haselbach, L. (2017). Guidance for usage of permeable pavement at airports. National Academies Press. Washington, United States (No. Project 02-64).

Cahill, T., Adams, M., & Marm, C. (2003). Porous asphalt: The right choice for porous

pavements. HMAT: Hot Mix Asphalt Technology, 8(5).

Canadian Council of Ministers of the Environment. (2017). Canadian water quality guidelines for the protection of aquatic life, User's Manual. Canada: Canadian Council of Ministers of the Environment.

Candra, A. I., Mudjanarko, S. W., Poernomo, Y. C. S., & Vitasmoro, P. (2020). Analysis of the ratio of coarse aggregate to porous asphalt mixture. In Journal of Physics: Conference Series (Vol. 1569, No. 4, p. 042029). IOP Publishing.

Chopra, M., Stuart, E., & Wanielista, M. (2010). Pervious pavement systems in Florida – research results. Low Impact Development 2010: Redefining Water in the City (pp. 193-206). San Fransico: American Society of Civil Engineers.

Collins, K. A., Hunt, W. F., & Hathaway, J. M. (2008). Hydrologic comparison of four types of permeable pavement and standard asphalt in eastern North Carolina. Journal of Hydrologic Engineering, 13(12), 1146-1157.

Collins, K. A., Hunt, W. F., & Hathaway, J. M. (2010). Side-by-side comparison of nitrogen species removal for four types of permeable pavement and standard asphalt in eastern North Carolina. Journal of Hydrologic Engineering, 15(6), 512-521.

Connolly, V., Légaré, S., Audet, B., Fournier, F. (2014). Bird conservation strategy for Bird Conservation Region 12 in Quebec: boreal hardwood transition. Environment Canada.

Credit Valley Conservation & Toronto Region Conservation Authority. (2010). Low Impact Development Stormwater Management Planning and Design Guide. Version 1.0. Toronto and Region Conservation Authority and Credit Valley Conservation Authority. Toronto, Canada.

Danz, M. E., Selbig, W. R., & Buer, N. H. (2020). Assessment of restorative maintenance practices on the infiltration capacity of permeable pavement. Water, 12(6), 1563.

Dempsey, B. A., & Swisher, D. M. (2004). Evaluation of porous pavement and infiltration in Centre County, PA. In World Water and Environmental Resources Congress 2003 (pp. 1-11).

Dierkes, C., Holte, A., & Geiger, W. F. (1999). Heavy metal retention within a porous pavement structure. In Proc. the Eighth International Conference on Urban Storm Drainage (Vol. 605).

Dierkes, C., Kuhlmann, L., Kandasamy, J., & Angelis, G. (2002). Pollution retention capability and maintenance of permeable pavements. Global Solutions for Urban Drainage, 1–13.

Dover, J.W. (2015). Green Infrastructure: Incorporating Plants and Enhancing Biodiversity in Buildings and Urban Environments (1st ed.). London, United Kingdom.

Drake, J. A. P. (2013). Performance and operation of partial infiltration permeable pavement systems in the Ontario climate (Doctoral dissertation, University of Guelph).

Drake, J., Bradford, A., & Van Seters, T. (2010). Performance of Permeable Pavements in Cold Climate Environments. Low Impact Development 2010, 1369–1378.

Drake, J., & Bradford, A. (2012). Assessing the potential for rehabilitation of surface permeability using regenerative air and vacuum-sweeping trucks. CHI Monograph, Guelph: Computational Hydraulics International.

Duchesne, S., K. Aglida et G. Pelletier (2022). Essai d'un enrobé drainant et d'une chaussée réservoir comme ouvrage de gestion des eaux pluviales pour un stationnement - Rapport final - Projet R839.1. INRS - Centre Eau Terre Environnement, Rapport de No R2135, Québec, Canada.

Environment and Climate Change Canada. (2025). Daily Data Report for January 2024 [Data set]. Government of Canada. Retrieved May 17, 2025, from https://climate.weather.gc.ca/climate_data/daily_data_e.html?hlyRange=2005-03-24%7C2023-08-30&dlyRange=1992-12-04%7C2023-08-29&mlyRange=1998-01-01%7C2016-03-01&StationID=26892&Prov=QC&urlExtension=_e.html&searchType=stnName&optLimit=yearRange&StartYear=1 . (Last visited on 13/05/2025)

Fassman, E. A., & Blackbourn, S. (2010). Permeable Pavement Performance over 3 Years of Monitoring. Low Impact Development 2010, 152–165.

Godé, B. (2018). Renovation of parking lots in the City of Quebec, 2018 (PEC 180732) Parking lot S3028 of Parc Paul-Émile-Beaulieu (530, rue Delage, Québec, QC), Québec, Canada.

Henderson, V., & Tighe, S. L. (2011). Evaluation of pervious concrete pavement permeability renewal maintenance methods at field sites in Canada. Canadian Journal of Civil Engineering, 38(12), 1404-1413.

Hu, N., Zhang, J., Xia, S., Han, R., Dai, Z., She, R., Cui, X., & Meng, B. (2020). A field performance evaluation of the periodic maintenance for pervious concrete pavement. Journal of Cleaner Production, 263, 121463.

Huang, J., Valeo, C., He, J., & Chu, A. (2012). Winter performance of inter-locking pavers — Stormwater quantity and quality. Water, 4(4), 995-1008.

Houle, J. J., Roseen, R. M., Ballestero, T. P., Puls, T. A., & Sherrard Jr, J. (2013). Comparison of maintenance cost, labor demands, and system performance for LID and conventional stormwater management. Journal of Environmental Engineering, 139(7), 932-938.

Interlocking Concrete Pavement Institute (ICPI). (2008). Permeable Interlocking Concrete Pavement: A Comprison Guide to Porous Asphalt and Pervious Concrete. [online], https://www.willowcreekpavingstones.com/resources/pdf/icpi-permeable-pavement-comparisons.pdf. (Last visited on 19/03/2025)

Kia, A., Wong, H. S., & Cheeseman, C. R. (2017). Clogging in permeable concrete: A review. Journal of Environmental Management, 193, 221–233.

Kwiatkowski, M., Welker, A. L., Traver, R. G., Vanacore, M., & Ladd, T. (2007). Evaluation of an infiltration best management practice utilizing pervious concrete. Journal of the American Water Ressources Association, 43(5), 1208-1222.

Lebens, M. A., & Troyer, B. (2012). Porous asphalt pavement performance in cold regions (Report No. MN/RC 2012-12). Minnesota Department of Transportation. Maplewood. MN,, United States.

Legret, M., Nicollet, M., Miloda, P., Colandini, V., & Raimbault, G. (1999). Simulation of heavy metal pollution from stormwater infiltration through a porous pavement with reservoir structure. Water Science and Technology, 39(2), 119-125.

Mailhot, A., & Talbot, G. (2025). IDF curves – Charlesbourg Parc-Orléan [Online]. https://www.agrometeo.org/atlas/idf_station/CHARLESBOURG_PARC_ORLEAN/Charlesbourg%20Parc-Orl%C3%A9an/7011309/false. (Last visited on 13/06/2025)

Minnesota Stormwater (2023) Operation and maintenance of permeable pavement - Minnesota Stormwater Manual. [online], https://stormwater.pca.state.mn.us/index.php/Operation_and_maintenance_of_permeable_pavement. (Last visited on 19/01/2025)

Montalto, F., Behr, C., Alfredo, K., Wolf, M., Arye, M., & Walsh, M. (2007). Rapid assessment of the cost-effectiveness of low impact development for CSO control. Landscape and urban planning, 82(3), 117-131.

Murakami, M., Nakajima, F., & Furumai, H. (2008). The sorption of heavy metal species by sediments in soakaways receiving urban road runoff. Chemosphere, 70(11), 2099–2109.

Muttuvelu, D. V., Wyke, S., & Vollertsen, J. (2024). Measuring Infiltration Rates in Permeable Asphalt Pavement in Urban Landscapes. KSCE Journal of Civil Engineering, 28(11), 5255-5265.

National Asphalt Pavement Association (NAPA). (2008). Porous Asphalt Pavements for Stormwater Management: Design, Construction, and Maintenance Guide (IS-131). Lanham, MD, United States.

National Ready Mix Concrete Association (NRMCA). (2004). Freeze Thaw Resistance of Pervious Concrete. National Ready Mixed Concrete Association. Silver Spring, Maryland, United States.

Ndon, U. J. (2017). Trends in the Application of Permeable Pavement as Sustainable Highway Storm Water Management Option for Safe-Use of Roadways. Journal of Civil and Environmental Engineering, 07(06).

Northern Virginia Regional Commission (NVRC). (2007). Low Impact Development Supplement to the Northern Virginia BMP Handbook. Fairfax, Virginia, United States.

Pratt, C. J., Mantle, J. D. G., & Schofield, P. A. (1995). UK research into the performance of permeable pavement, reservoir structures in controlling stormwater discharge quantity and quality. Water Science and Technology, 32(1), 63-69.

Qin, Y. (2015). A review on the development of cool pavements to mitigate urban heat island effect. Renewable and Sustainable Energy Reviews, 52, 445–459.

Rosa, D. J., Clausen, J. C., & Dietz, M. E. (2015). Calibration and Verification of SWMM for Low Impact Development. Journal of the American Water Resources Association, 51(3), 746–757.

Roseen, R. M., Ballestero, T. P., Houle, J. J., Avelleneda, P., Wildey, R., & Briggs, J. (2006). Storm water low-impact development, conventional structural, and manufactured treatment strategies for parking lot runoff: Performance evaluations under varied mass loading conditions. Transportation Research Record, 1984, 135–147.

Roseen, R. M., Ballestero, T. P., Houle, J. J., Avellaneda, P., Briggs, J., Fowler, G., & Wildey, R. (2009). Seasonal performance variations for storm-water management systems in cold climate conditions. Journal of Environmental Engineering, 135(3), 128-137.

Roseen, R. M., Ballestero, T. P., Houle, J. J., Briggs, J. F., & Houle, K. M. (2012). Water Quality and Hydrologic Performance of a Porous Asphalt Pavement as a Storm-Water Treatment Strategy in a Cold Climate. Journal of Environmental Engineering, 138(1), 81–89.

Rossman, L. (2015). Storm Water Management Model (SWMM) User' s Manual Version 5 .2.1. U.S. Environmental Protection Agency (EPA), September 1–353.

Rushton, B. T. (2001). Low-impact parking lot design reduces runoff and pollutant loads. Journal of Water Resources Planning and Management, 127(3), 172-179.

Schaefer, V. R., & Wang, K. (2006). Mix design development for pervious concrete in cold weather climates (No. 2006-01). Center for Transportation Research and Education, Iowa State University. Ames, Iowa, United States

Selbig, W. R., & Buer, N. (2018). Hydraulic, water-quality, and temperature performance of three types of permeable pavement under high sediment loading conditions (No. 2018-5037). US Geological Survey.

Shahed Behrouz, M., Zhu, Z., Matott, L. S., & Rabideau, A. J. (2020). A new tool for automatic calibration of the Storm Water Management Model (SWMM). Journal of Hydrology, 581.

Singer, M. N., Hamouda, M. A., El-Hassan, H., & Hinge, G. (2022). Permeable Pavement Systems for Effective Management of Stormwater Quantity and Quality: A Bibliometric Analysis and Highlights of Recent Advancements. Sustainability, 14(20), 13061.

Støvring, J., Dam, T., & Bergen Jensen, M. (2018). Surface sedimentation at permeable pavement systems: implications for planning and design. Urban Water Journal, 15(2), 124–131.

Tota-Maharaj, K., & Scholz, M. (2010). Efficiency of permeable pavement systems for the removal of urban runoff pollutants under varying environmental conditions. Environmental Progress and Sustainable Energy, 29(3), 358–369.

TRCA. (2008). Performance Evaluation of Permeable Pavement and a Bioretention Swale. Sustainable Technologies Evaluation Program. Toronto: Toronto and Region Conservation. Toronto, Canada.

Vaillancourt, C., Duchesne, S., & Pelletier, G. (2019). Hydrologic Performance of Permeable Pavement as an Adaptive Measure in Urban Areas: Case Studies near Montreal, Canada. Journal of Hydrologic Engineering, 24(8).

Van Duin, B., Brown, C., Chu, A., Marsalek, J., & Valeo, C. (2008). Characterization of long-term solids removal and clogging processes in two types of permeable pavement under cold climate conditions. In 11th International Conference on Urban Drainage (pp. 1-10).

Ville de Québec (2022). Règlement R.A.V.Q. 1124 - Règlement de l'agglomération sur les rejets dans les réseaux d'égout et sur l'inventaire des matières dangereuses entreposées sur le territoire. Ville de Québec, Service des affaires juridiques, Québec, Canada.

Virginia DEQ (Department of Environmental Quality). (2011). Stormwater design specification No. 7: Permeable pavement (Version 1.8). Richmond. Virginia, United States.

Wang, J., Wang, X., Xu, W., Xue, C., Li, H., Sun, Z., ... & Li, J. (2023). Characteristics of thermal pollution from stormwater runoff from impermeable/permeable pavement surfaces via a lab-scale experiment. Journal of Environmental Management, 325, 116484.

Water Environment Research Federation (WERF). (2005). Performance and Whole-life Costs of Best Management Practices and Sustainable Urban Drainage Systems. Alexandria, VA. United States.

Winston, R. J., Al-Rubaei, A. M., Blecken, G. T., & Hunt, W. F. (2016a). A Simple Infiltration Test for Determination of Permeable Pavement Maintenance Needs. Journal of Environmental Engineering, 142(10).

Winston, R. J., Al-Rubaei, A. M., Blecken, G. T., Viklander, M., & Hunt, W. F. (2016b). Maintenance measures for preservation and recovery of permeable pavement surface infiltration rate. Journal of Environmental Management, 169, 132–144.

Wisconsin Department of Natural Resources (WDNR). (2021). Technical Standard 1008: Permeable pavement (Tech. Std. 1008). Madison, Wisconsin, United States.

Xie, J., Chen, H., Liao, Z., Gu, X., Zhu, D., & Zhang, J. (2017). An integrated assessment of urban flooding mitigation strategies for robust decision making. Environmental Modelling and Software, 95, 143–155.

7 APPENDIX I

7.1 Results of infiltration rate tests

Table 7.1 Infiltration rate of the porous asphalt

Period	Test date	Location	Infiltration rate (mm/hr)
Before cleaning	May 26, 2023	1	9
		2	34
		3	106
After cleaning	June13, 2023	1	11
		2	174
		3	259
Before cleaning	May 21, 2024	1	22
		2	39
		3	36
		4	383
		5	10
		6	31
After cleaning	June 13, 2024	1	53
		2	99
		3	66
		4	n.a.*
		5	86
		6	36
Monthly monitoring (July)	June 17, 2024	1	3
		2	2
		3	13
		4	191
		5	8
		6	32
	August 27, 2024	1	3
		2	14

Period	Test date	Location	Infiltration rate (mm/hr)
Monthly monitoring (August)		3	10
		4	202
		5	7
		6	10

*No infiltration test was carried out at this point after cleaning, as the vacuum truck did not cover this area.

7.2 Water temperature

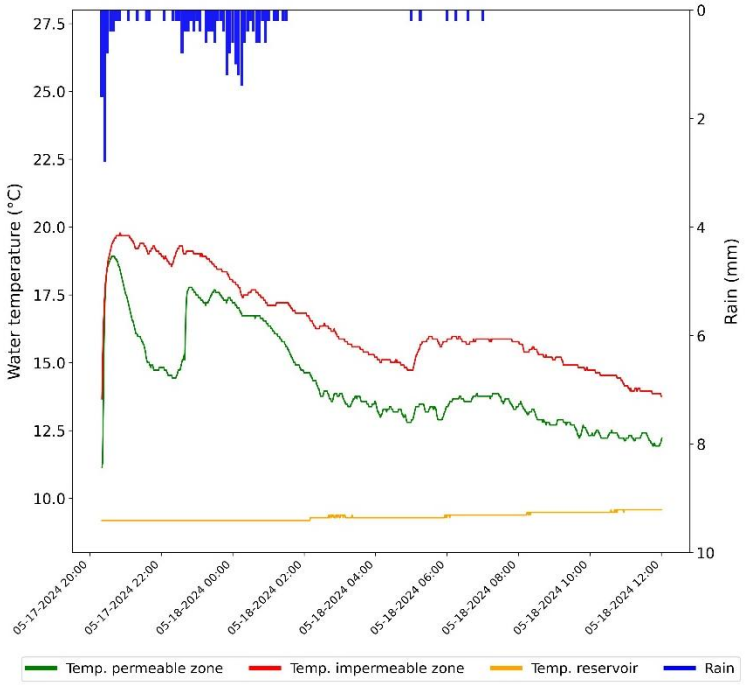

Figure 7-1 Hyetogram and water temperature of the PA (green) and the CA (red) for event #19

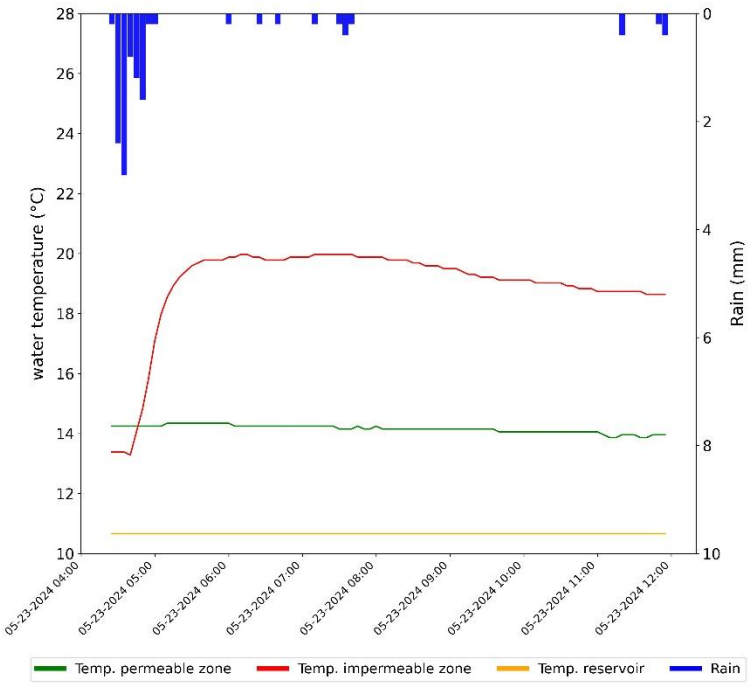

Figure 7-2 Hyetogram and water temperature of the PA (green) and the CA (red) for event #20

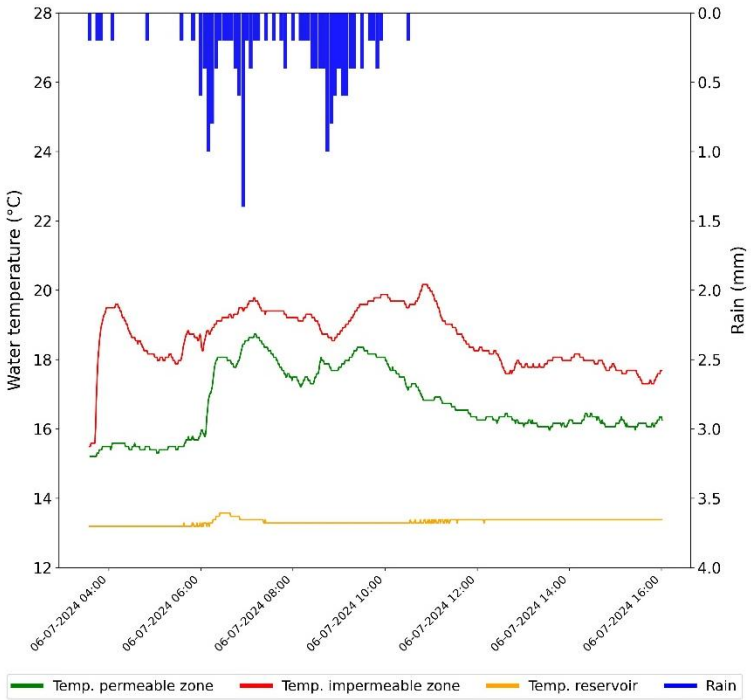

Figure 7-3 Hyetogram and water temperature of the PA (green) and the CA (red) for event #23

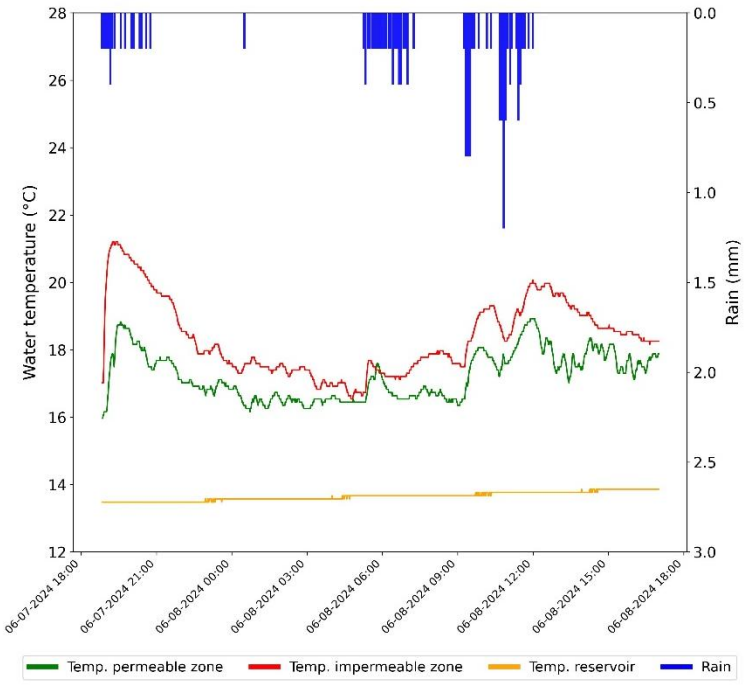

Figure 7-4 Hyetogram and water temperature of the PA (green) and the CA (red) for event #24

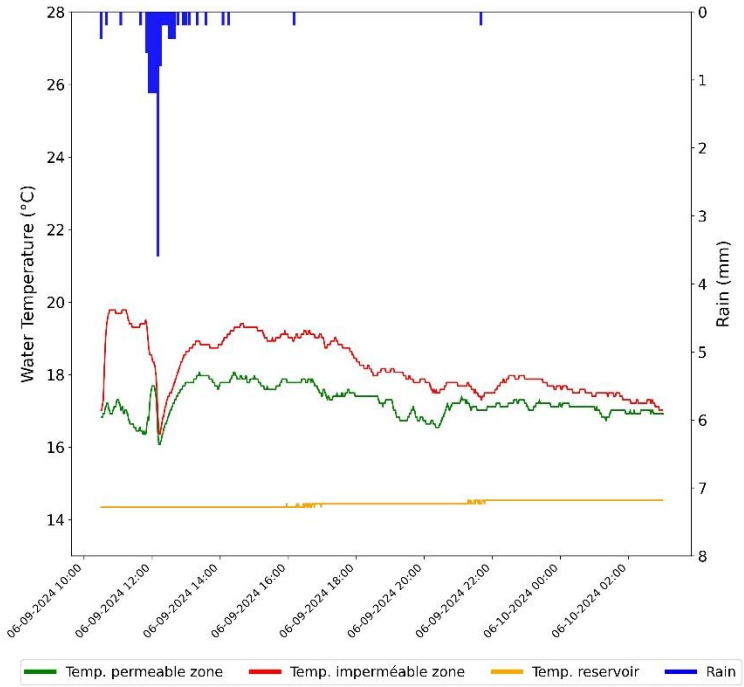

Figure 7-5 Hyetogram and water temperature of the PA (green) and the CA (red) for event #25

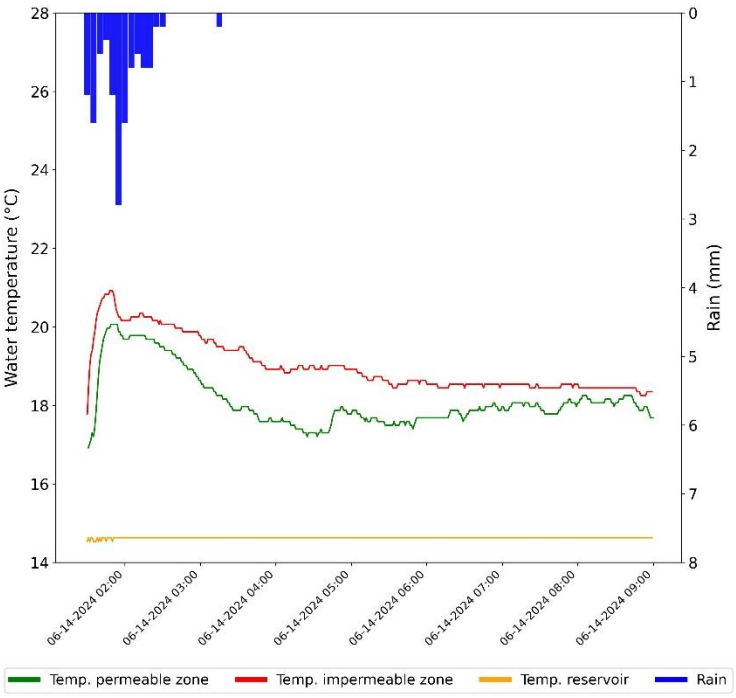

Figure 7-6 Hyetogram and water temperature of the PA (green) and the CA (red) for event #27

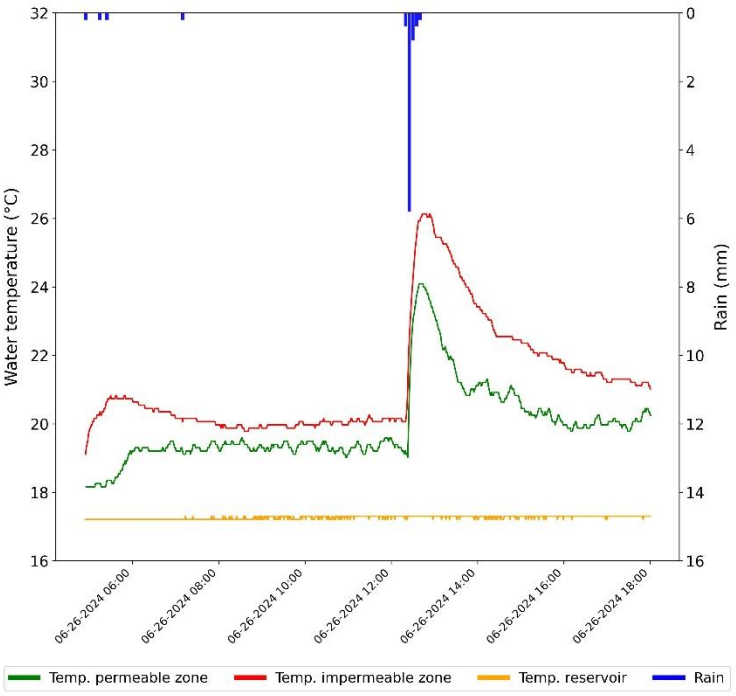

Figure 7-7 Hyetogram and water temperature of the PA (green) and the CA (red) for event #26

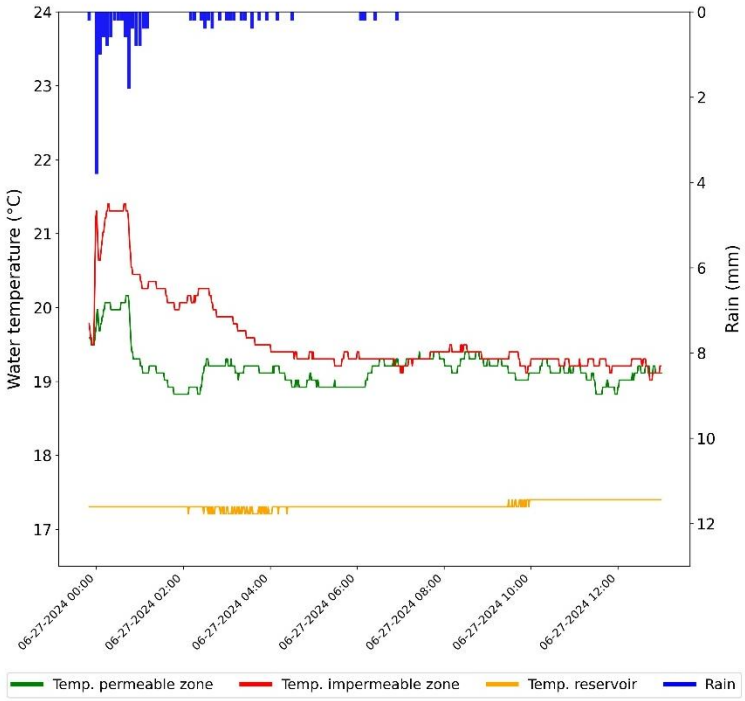

Figure 7-8 Hyetogram and water temperature of the PA (green) and the CA (red) for event #26